

The Nature of Massive Transition Galaxies in CANDELS, GAMA, and Cosmological Simulations

Viraj Pandya^{1,2,3}, Ryan Brennan², Rachel S. Somerville², Ena Choi², Guillermo Barro⁴, Stijn Wuyts⁵, Edward N. Taylor⁶, Peter Behroozi^{4,7}, Allison Kirkpatrick⁸, Sandra M. Faber³, Joel Primack⁹, David C. Koo³, Daniel H. McIntosh¹⁰, Dale Kocevski¹¹, Eric F. Bell¹², Avishai Dekel¹³, Jerome J. Fang^{3,14}, Henry C. Ferguson¹⁵, Norman Grogin¹⁵, Anton M. Koekemoer¹⁵, Yu Lu¹⁶, Kameswara Mantha¹⁰, Bahram Mobasher¹⁷, Jeffrey Newman¹⁸, Camilla Pacifici¹⁹, Casey Papovich²⁰, Arjen van der Wel²¹, Hassen M. Yesuf³

Affiliations are listed at the end of this paper.

Accepted ??? Received ??? in original form ???

ABSTRACT

It is common practice to speak of a “green valley” that hosts galaxies whose colors are intermediate relative to those in the “blue cloud” and the “red sequence.” In this study, we raise several questions about how galaxies might transition between the star-forming main sequence (SFMS) and varying “degrees of quiescence” from $z = 3$ to $z \sim 0$. We develop a physically and statistically motivated definition of “transition galaxies” based on their uniquely intermediate specific star formation rates, which relieves ambiguities associated with color-based selections and allows us to more cleanly compare observations to theoretical models. Our analysis is focused on galaxies with stellar mass $M_* > 10^{10} M_\odot$, and is enabled by GAMA and CANDELS observations, a semi-analytic model (SAM) of galaxy formation, and a hydrodynamical simulation with state-of-the-art mechanical AGN feedback. In both the observations and the SAM, transition galaxies tend to have intermediate Sérsic indices, half-light radii, and surface stellar mass densities compared to star-forming and quiescent galaxies. We place an observational upper limit on the average population transition timescale as a function of redshift, finding that the average high-redshift galaxy is on a “fast track” for quenching (~ 0.8 Gyr at $z \sim 2.5$) whereas the average low-redshift galaxy is on a “slow track” for quenching (~ 7 Gyr at $z \sim 0.5$). We identify four dominant evolutionary modes for star formation histories in the SAM: oscillations on the SFMS, slow quenching, fast quenching, and rejuvenation. Quenching timescales in both the SAM and the hydrodynamical simulation are not fast enough to reproduce the heavily quiescent population that we observe at $z \sim 3$. In the SAM, we do not find a clear-cut morphological dependence of quenching timescales, but we do predict that the mean stellar ages, cold gas fractions, SMBH masses, and halo masses of transition galaxies tend to be intermediate relative to those of star-forming and quiescent galaxies at $z < 3$.

Key words: galaxies: bulges, galaxies: evolution, galaxies: formation, galaxies: high-redshift, galaxies: star formation, galaxies: structure

1 INTRODUCTION

It is well known that there exists a bimodality in galaxy colors and star formation rates (SFRs) out to at least $z \approx 3$ (e.g., Strateva et al. 2001; Brinchmann et al. 2004; Bell et

al. 2004; Baldry et al. 2004; Faber et al. 2007; Wyder et al. 2007; Blanton & Moustakas 2009; Whitaker et al. 2011). In particular, the distribution of galaxy SFRs and colors splits into: (1) a “red sequence” of quiescent galaxies that host very little, if any, ongoing star formation and that are dominated

by an old stellar population, and (2) a “blue cloud” of star-forming galaxies that are actively forming new stars and are dominated by a young stellar population. Evidence suggests that these two populations’ typical SFRs, colors, and other properties change significantly as a function of cosmic time, implying evolution both within and between the two populations (e.g., see Madau & Dickinson 2014, and references therein). Furthermore, the fraction of all galaxies that are quiescent has increased with cosmic time, and this increase in the quiescent fraction happens earlier for more massive galaxies (this is known as “cosmic downsizing”; e.g., Cowie et al. 1996; Noeske et al. 2007b; Fontanot et al. 2009, and references therein).

It was thought since at least the 1970s that there may exist a third population of “transient” galaxies that are transitioning between what we now call the blue cloud and the red sequence, although such work was mostly restricted to dense environments such as clusters (e.g., van den Bergh 1976; Butcher & Oemler 1978). Chief among such galaxies are the classical post-starburst or “K+A” (or more restrictively, “E+A”) galaxies, which are predominantly old stellar systems that contain some A-type stars due to a recently truncated starburst (e.g., Dressler & Gunn 1983). However, such post-starburst galaxies were thought to be and are now confirmed to be rare, at least in the local Universe (e.g., Quintero et al. 2004; Wild et al. 2009; Yesuf et al. 2014; Pat-tarakijwanich et al. 2014; McIntosh et al. 2014). Despite the higher observed number densities of post-starburst galaxies at $z > 1$ (e.g., Whitaker et al. 2012), it is still not at all clear that this population can by itself account for the dramatic build-up of the red sequence across cosmic time (but see Wild et al. 2016, for an alternative view). Hints of a broad and general framework for the large-scale transition of galaxies between different populations did not clearly and explicitly begin to emerge until the early 2000s when statistical samples of galaxies became available through the advent of large astronomical surveys (e.g., Colless et al. 2001; Strateva et al. 2001; Strauss et al. 2002).

Bell et al. (2004) explicitly studied what they called the “gap” population (between the red sequence and blue cloud, defined using the classical color-magnitude diagram) and found that by turning off star formation in some small fraction of blue galaxies, such galaxies would fade across the gap, join the red sequence, and at least qualitatively explain the build-up of the red population since $z \sim 1$. Around the same time, Baldry et al. (2004) quantitatively studied the bimodal color-magnitude distribution of galaxies and found that, in the local Universe, the red and blue populations could be adequately modeled as the sum of two Gaussians, implying no need for such a “gap” population and therefore suggesting that all galaxies transition on extremely fast timescales. Like Bell et al. (2004), Faber et al. (2007) quantitatively demonstrated the build-up of the red sequence since $z \sim 0.7$ and qualitatively explored the different evolutionary pathways that galaxies could follow in order to become truly red-and-dead galaxies.

The idea of the classical “green valley” population was born and systematically explored in the seminal 2007 series of papers celebrating the advent of the ultraviolet *Galaxy Evolution Explorer (GALEX)* space-based telescope (Wyder et al. 2007; Martin et al. 2007; Schiminovich et al. 2007; Salim et al. 2007). Wyder et al. (2007) showed that the “gap”

population studied by Bell et al. (2004) became much more pronounced in the NUV-optical color-magnitude diagram (i.e., using $NUV-r$ color rather than $u-r$ or $g-r$ color) because the blackbody emission from young stars peaks in the NUV, allowing for much finer constraints on the recent star formation histories (SFHs) of galaxies. Martin et al. (2007) and Gonçalves et al. (2012) found that the recent SFHs of green valley galaxies, and their quenching timescales in particular, were indeed consistent with the build-up of the red sequence implied by the cosmic evolution of the blue and red galaxy luminosity functions.

The classical green valley population clearly has major implications for theories of galaxy evolution, but it is also subject to many possible caveats and uncertainties that have led to inconsistencies and confusion in the existing literature (see also the extensive discussions in Salim 2014; Schawinski et al. 2014). These caveats and uncertainties become even more pronounced as we attempt to undertake the daunting task of studying the green valley population out to ever higher redshifts. In particular, the empirically motivated definition of the low- and intermediate-redshift green valley (in terms of the minimum of the bimodal color distribution of galaxies) does not seem to be physically motivated enough for the high redshift Universe, where the red sequence is sparsely populated and still growing. It also does not help that intrinsic properties like dust attenuation and disk inclination can cause an otherwise blue star-forming galaxy to appear in the green valley or even in the red sequence; indeed, some studies have asserted that most green valley galaxies at higher redshifts are merely dusty star-forming galaxies (e.g., Brammer et al. 2009; Cardamone et al. 2010).

Perhaps the most interesting yet puzzling arguments stem from statistical modeling of the bimodal galaxy color distribution at low redshift. In particular, since the bimodal galaxy color distribution appears to be well fit by the sum of two Gaussians, it has been argued that galaxies must transition between the blue cloud and red sequence on universally fast timescales, so as to effectively prevent the existence of a green valley (e.g., Baldry et al. 2004; Taylor et al. 2015). Such a view may be tenable if galaxy evolution proceeds only in bursts of star formation and rapid quenching – and the prominence of such bursty SFHs is indeed an open question. However, it is not at all clear a priori that the full distribution of transition timescales must necessarily be so narrowly peaked at such fast values, nor is it clear that all physical mechanisms act on such fast timescales and that there is no redshift evolution in this distribution of transition timescales. It should also be emphasized that these arguments are typically made on the basis of global photometry or spatially-limited spectroscopy of galaxies, whereas what we need instead is a more fundamental understanding of the interrelationships between the many different sub-components of galaxies (e.g., central bulge growth versus extended disk fading; see Lackner & Gunn 2012; Fang et al. 2012).

All of the above caveats and uncertainties come together in the end to lend credence to the noteworthy diversity arguments. These arguments posit that even if the green valley is home to galaxies genuinely transitioning between populations, not all galaxies follow the same evolutionary pathway and therefore it might be extremely difficult to confidently disentangle the history of individual galaxies or even ensem-

bles of similar galaxies. Despite the inherent richness and complexity of the classical green valley, our current understanding of galaxy evolution demands that galaxies must transform from one type into another. We therefore begin with the assumption that the classical green valley population, at all redshifts, must consist of some combination of the following types of galaxies:

- (i) blue star-forming and red quiescent galaxies that were scattered into the green valley due to measurement uncertainties.
- (ii) galaxies that are genuinely transitioning from the blue cloud to the red sequence (i.e., quenching galaxies).
- (iii) galaxies that are genuinely transitioning from the red sequence to the blue cloud (i.e., rejuvenating galaxies).

Determining the relative contributions of these three possibilities is crucial for properly guiding and interpreting studies of galaxy evolution. If measurement uncertainties (interpretation one) are extremely high, then we may have no hope of disentangling the relative fraction of quenching versus rejuvenating galaxies because green valley galaxies would merely be scattered blue and red galaxies (e.g., due to dust correction uncertainties or high photometric measurement errors). In the ideal case where there is no such scattered population, and where we have deep spectroscopy of green valley galaxies, we might be able to non-parametrically constrain their recent SFHs and determine the relative contribution of interpretations two and three. It is widely thought that, at least at low redshift, rejuvenation evolutionary tracks are much less likely to be observed than quenching tracks because the timescale on which a galaxy's color becomes bluer (due to the birth of young massive stars) happens much more quickly than the subsequent reddening of the stellar population. This means that a rejuvenated galaxy is much more likely to be caught during its subsequent “re-fading” or “re-quenching” phase. Consequently, the fraction of all galaxies that are in the green valley should tell us something about quenching timescales, and that in turn provides clues about the underlying physical mechanisms responsible for quenching.

Presupposing that scattered blue and red galaxies (i.e., those consistent with interpretation one) have a minimal contamination effect in the green valley, one way to help unravel the history of galaxy evolution and disentangle the quenching and rejuvenation interpretations is to consider structural and morphological properties. We know that there are strong correlations between color and morphology (e.g., [Kauffmann et al. 2003](#)). Structural properties like size and morphology can provide important clues about galaxies' evolutionary histories and the physical processes that shape them. In the nearby Universe, the seminal *GALEx*-based study of [Schiminovich et al. \(2007\)](#) uncovered the tendency of green valley galaxies to have more concentrated light profiles and lower gas content than star-forming galaxies. At intermediate redshift ($0.4 < z < 1.2$), [Mendez et al. \(2011\)](#) found that the structural properties of green valley galaxies were indeed offset, and in fact intermediate, compared to those of the blue and red galaxy subsamples, and that this trend was statistically different from what would be expected of a “purple valley” population (i.e., scattered blue and red galaxies). Back at low redshift, [Schawinski et al. \(2014\)](#) used visual classifications from *Galaxy Zoo* and NUV-

optical colors to suggest that spheroid-dominated green valley galaxies universally quench faster than disk-dominated green valley galaxies. Building on the work of [Schawinski et al. \(2014\)](#), [Smethurst et al. \(2015\)](#) also used *Galaxy Zoo* visual classifications and multi-wavelength photometry of $z \sim 0.1$ galaxies within a Bayesian framework, and found that a diverse continuum of quenching timescales was plausible.

The previous low- and intermediate-redshift studies of the green valley (e.g., [Martin et al. 2007](#); [Salim & Rich 2010](#); [Mendez et al. 2011](#); [Fang et al. 2012](#); [Salim et al. 2012](#); [Gonçalves et al. 2012](#); [Pan et al. 2013, 2014](#); [Schawinski et al. 2014](#); [McIntosh et al. 2014](#); [Smethurst et al. 2015](#); [Haines et al. 2015](#)) help motivate our high redshift study because pushing out to ever higher redshifts is yet another way to test the evolutionary framework of the green valley. Unlike the rather “messy” low-redshift Universe in which the red sequence is already firmly established, the vast majority of galaxies at high redshift are actively forming new stars. And yet, the fact that there are still stragglers below the tight star-forming main sequence (SFMS; e.g., [Noeske et al. 2007a](#)) suggests that we may be able to more cleanly catch galaxies that are on the verge of quenching (or rejuvenating) at these earlier times. Previous studies of the green valley population were limited to low- and intermediate-redshift because it is only for these relatively nearby galaxies that there exists an abundance of spectroscopic and imaging data with relatively high physical resolution. Studying the structural and evolutionary properties of the green valley population out to high redshift has not been feasible until only recently – enabled by the wealth of new high spatial resolution data taken with the *Hubble Space Telescope* Wide Field Camera 3 (*HST*/WFC3) as part of the Cosmic Assembly Near-infrared Deep Extragalactic Legacy Survey (CANDELS; [Grogin et al. 2011](#); [Koekemoer et al. 2011](#)). However, previous studies at high redshift have split the galaxy population into only blue/star-forming and red/quiescent subpopulations using empirically-motivated cuts in color-mass, color-color, or SFR- M_* diagrams (with many also looking separately at the dusty and dust-free star-forming populations; e.g., [Brammer et al. 2011](#); [Wuyts et al. 2011b](#); [Bell et al. 2012](#); [Muzzin et al. 2013](#); [Barro et al. 2013](#); [Lang et al. 2014](#); [van der Wel et al. 2014](#); [Brennan et al. 2015](#); [Huertas-Company et al. 2016](#); [Straatman et al. 2016](#)).

In this paper, we will depart from classical definitions of the green valley in terms of the color-magnitude and color-mass diagrams. Instead, we will consider a more statistically and physically motivated but analogous definition involving uniquely intermediate specific SFRs ($\text{ssSFR} \equiv \text{SFR}/M_*$). Our definition of “transition galaxies” is motivated by the difficulty of using and interpreting empirical rest-frame color cuts across a large range of redshifts. Our analysis will be restricted to massive galaxies with $M_* > 10^{10} M_\odot$. Alongside the observations, we will simultaneously and self-consistently analyze predictions from a semi-analytic model of galaxy formation, which contains prescriptions (albeit schematic ones) for both quenching and morphological transformations. We will also compare our observational and semi-analytic results to those obtained from hydrodynamical simulations. These comparisons can help constrain the implementation of physical processes in models and moti-

value future studies of the transition galaxy population in a cosmological context.

This paper is organized as follows. In section 2, we describe the observations and in section 3 we describe the semi-analytic model. In section 4 we explain our methods, and in section 5 we present our results. After an observational discussion in section 6 and a theoretical discussion in section 7, we summarize in section 8. Throughout the paper, we assume $H_0 = 67.8 \text{ km s}^{-1} \text{ Mpc}^{-1}$, $\Omega_m = 0.307$, and $\Omega_\Lambda = 0.693$ following Planck Collaboration et al. (2014).

2 OBSERVATIONS

2.1 CANDELS

Our study is primarily based on *HST*/WFC3 observations taken as part of CANDELS (Grogin et al. 2011; Koekemoer et al. 2011). The CANDELS data span five different fields which collectively add up to $\sim 0.22 \text{ deg}^2$. This large area helps to minimize the effects of cosmic variance (e.g., see Somerville et al. 2004). The five CANDELS fields and their associated data description papers are: COSMOS (Nayyeri et al., in preparation), EGS (Stefanon et al., in preparation), GOODS-N (Barro et al., in preparation), GOODS-S (Guo et al. 2013), and UDS (Galametz et al. 2013).

A major advantage of CANDELS is that the galaxies are selected in the near-IR F160W (H) band. This allows us to probe the rest-frame UV-optical spatial and SED features of galaxies out to $z \sim 3$ with unprecedentedly high resolution. In what follows, we will briefly describe the derivation of the most relevant physical parameters in the CANDELS catalogs.¹ For in-depth details about the data processing and source catalog creation for each CANDELS field, we refer the reader to the five data description papers cited above. Our overview below applies uniformly to all five CANDELS fields.

First, the template-fitting method (TFIT; Lee et al. 2012; Laidler et al. 2007) was used to merge multi-wavelength (UV to near-IR) observations with significantly different spatial resolutions, and construct the observed-frame multi-wavelength photometric catalog. Photometric redshifts were derived using the Bayesian framework described in Dahlen et al. (2013); this method combines the posterior redshift probability distributions from several independent codes to improve precision and reduce outliers. Spectroscopic redshifts were used where available and reliable; *HST*/WFC3 grism redshifts from Morris et al. (2015) were used for GOODS-S.

Rest-frame UV-optical-NIR photometry was derived by fitting the observed-frame SED with a set of templates using the EAZY code (Brammer et al. 2008, and Kocevski et al., in preparation). The method for computing stellar masses is described in Santini et al. (2015), and a critical assessment of the method, including the possible contribution of nebular emission to stellar mass estimates, is given in Mobasher et al. (2015). Several independent codes (including FAST; Kriek et al. 2009) were used to derive stellar masses under

a set of fixed assumptions, but with room for some variation such as assumed SFH parameterizations. Although the underlying data are the same, the use of several different SED codes and assumptions allows one to test the impact of systematic errors and to analyze the precision of estimated stellar masses. For our study, we use physical properties that were derived assuming the following: Bruzual & Charlot (2003) stellar population synthesis models, Chabrier (2003) initial mass function (IMF), exponentially-declining SFHs, solar metallicity, and the Calzetti et al. (2000) dust attenuation law.

For galaxies that are detected at $24\mu\text{m}$ with *Spitzer*-MIPS, the total IR luminosity (L_{TIR}) was computed using the mapping from $24\mu\text{m}$ flux to L_{TIR} given in Elbaz et al. (2011). In some cases, galaxies detected at $24\mu\text{m}$ also have significantly detected (and deblended) counterparts in far-IR *Herschel*-SPIRE imaging at 250, 350 and 500 μm ; for these, we instead use their best-fitting IR templates to determine L_{TIR} (Pérez-González et al. 2010; Barro et al. 2011). Both of these techniques ($24\mu\text{m}$ -based mappings and IR template fitting) have two built-in assumptions: (1) there is minimal, if any, redshift evolution of the intrinsic IR SEDs of galaxies across a rather large redshift range (limited to $0 < z < 3$ for our study), and (2) emission from an obscured active galactic nucleus (AGN) does not contribute significantly to the $24\mu\text{m}$ flux (these topics are discussed extensively in Elbaz et al. 2011; Wuyts et al. 2011a; Barro et al. 2011). We will return to the impact of dust-obscured AGN near the end of this subsection.

SFRs were derived for galaxies according to a ladder of SFR indicators based on the prescriptions given in Wuyts et al. (2011a) and Barro et al. (2011). By default, every galaxy has an estimate of SFR_{UV} derived from its SED-based rest-frame NUV luminosity at 2800Å, L_{2800} . We correct this UV-based SFR for dust attenuation by assuming the Calzetti et al. (2000) dust attenuation curve:

$$\text{SFR}_{\text{UV,corr}} [\text{M}_\odot \text{ yr}^{-1}] = \text{SFR}_{\text{UV}} \times 10^{0.4 \times 1.8 \times A_V}, \quad (1)$$

where $\text{SFR}_{\text{UV}} = 3.6 \times 10^{-10} \times L_{2800}/L_\odot$ assuming a Chabrier (2003) IMF as in Wuyts et al. (2011a). In the exponent, A_V is the SED-based optical attenuation output by FAST (Kriek et al. 2009), and the factor of 1.8 corresponds to the Calzetti et al. (2000) attenuation curve value at 2800Å.

For galaxies that are also detected in mid-IR (and possibly far-IR) imaging and thus have L_{TIR} measurements as described above, we can alternatively compute the total SFR as the sum of the unobscured, non-dust-corrected SFR_{UV} and the obscured SFR_{IR} (as described in Wuyts et al. 2011a; Barro et al. 2011):

$$\text{SFR}_{\text{UV+IR}} [\text{M}_\odot \text{ yr}^{-1}] = \text{SFR}_{\text{UV}} + 1.09 \times 10^{-10} \times L_{\text{TIR}}/L_\odot. \quad (2)$$

We adopt SFR_{UV+IR} as our standard indicator for all galaxies that have L_{TIR} measurements, and SFR_{UV,corr} otherwise. It is very interesting to consider the impact of excluding mid- and far-IR contributions by instead using dust-corrected SFR_{UV,corr} only, even if SFR_{UV+IR} is available. If we re-run our entire analysis in this paper using only SFR_{UV,corr}, then our results are slightly perturbed but the main conclusions do not change. Similarly, we also re-ran our entire analysis using the UV-optical-NIR SED-based SFR_{SED} output by FAST (Kriek et al. 2009) for every galaxy; these fits

¹ All CANDELS catalogs are available at the Rainbow Database: http://arcoiris.ucolick.org/Rainbow_navigator_public/

do not use bandpasses beyond the $8\mu\text{m}$ channel of *Spitzer*-IRAC. Again, our exact quantitative results are perturbed but our conclusions do not change. Interestingly, the SFMS in the sSFR- M_* diagram is more negatively sloped when using SFR_{SED} compared to both SFR_{UV,corr} and SFR_{UV+IR}. However, when allowing this slope to be a free parameter, our results are insensitive to the choice of SFR indicator.

One potential issue with UV-based SFRs can arise when a galaxy is not detected in the observed frame filter corresponding to rest-frame 2800Å at its redshift (or in either of the two adjacent filters). EAZY (Brammer et al. 2008) may then extrapolate its NUV luminosity based on detections at significantly different wavelengths, leading to highly uncertain L_{2800} and thus unreliable SFR_{UV,corr} values. If the SFR_{UV,corr} values of intrinsically star-forming or transition galaxies are underestimated, then the fraction and number density of quiescent galaxies at high redshift might be artificially boosted. The inverse is not as much of a problem because upper limits on L_{2800} non-detections naturally set a floor on SFR_{UV,corr}, below which we cannot detect quiescent galaxies anyway. We verified that in each redshift slice for a given CANDELS field, the majority of galaxies (usually $> 90\%$, at worst $\sim 70\%$) that make it past our selection cuts are indeed detected in the rest-frame filter corresponding to 2800Å at their respective redshifts. For the minority of galaxies that are not detected at 2800Å, their SFR_{UV,corr} is rarely lower than the SFR_{UV,corr} of the average robustly NUV-detected galaxy. This means that it is unlikely that our quiescent fractions at high redshift are significantly overestimated due to rest-frame NUV non-detections.

On a related note, the presence of an obscured AGN may boost an otherwise quiescent galaxy's $24\mu\text{m}$ -based SFR_{IR} and cause that galaxy to instead become classified as a star-forming or transition galaxy. This can make it difficult to test whether the transition region might indeed be an evolutionary bridge between the SFMS and the quiescent region. We have used the procedure described in Kirkpatrick et al. (2013, 2015) to assign a mid-IR luminosity AGN contribution fraction to each CANDELS galaxy (based on the $8\mu\text{m}/3.6\mu\text{m}$ versus $250\mu\text{m}/24\mu\text{m}$ diagnostic diagram). We find that it is unlikely that obscured AGN are preferentially boosting the SFRs of transition and quiescent galaxies. A full analysis of the demographics of this obscured AGN population in the context of the transition region will be presented in Kirkpatrick et al. (in preparation).

Lastly, structural parameters were derived for every galaxy using GALFIT (Peng et al. 2002). The fits were done to the *HST*/WFC3 F160W (*H*-band) images (van der Wel et al. 2012) using a global Sérsic model. We emphasize that there is a difference between fitting structural properties to *H*-band light images instead of *H*-band mass images. In this work, we use half-light radii (i.e., the semi-major axis radius), as opposed to half-mass radii. Similarly, our Sérsic indices give information about the *H*-band light distribution rather than the stellar mass distribution for each galaxy. Although studies suggest that adopting mass-based rather than light-based structural parameters would not significantly change our results (e.g., Szomoru et al. 2013; Lang et al. 2014), in the future it will be important to revisit this claim. The original GALFIT measurements for Sérsic index were allowed to run from $n = 0$ to $n = 8$, where $n = 8$ corresponds to very compact light profiles; for ease of in-

terpretation, we set all $n > 4$ to the classic de Vaucouleurs index, $n = 4$.

Since our CANDELS observations span a large range in redshift and we wish to compare our results to those that we obtain from the low-redshift GAMA survey (see below), it is important to apply morphological k-corrections to the structural measurements of CANDELS galaxies. van der Wel et al. (2014) provide a formula for converting half-light radii from observed-frame *H*-band to rest-frame 5000Å. Intriguingly, we find that our results are not significantly affected by the conversion of van der Wel et al. (2014). Therefore, in this paper, we will show our results in terms of observed-frame *H*-band Sérsic indices and half-light radii. In the future, it will be important to revisit this non-trivial task of morphological k-corrections.

In order to ensure high sample completeness and robust structural measurements, we make the following selection cuts (see also Newman et al. 2012, for a discussion of CANDELS completeness limits): F160W apparent magnitude < 25 , stellar mass $M_* > 10^{10} M_\odot$, and F160W GALFIT quality flag = 0 (good fits only). The total fraction of galaxies cut out by requiring good GALFIT structural measurements is $< 15\%$; we verified that these discarded galaxies do not occupy a special limited subspace of the sSFR- M_* or *UVJ* diagrams.

2.2 GAMA

The volume of the CANDELS fields is extremely small below $z \sim 0.5$, so we cannot extend our CANDELS analysis much below this redshift. However, there are 3.5 Gyr between our CANDELS low redshift limit, $z = 0.5$, and the local Universe at $z \sim 0.01$. In order to connect our results from CANDELS at $0.5 < z < 3.0$ with the nearby Universe at $z \sim 0.01$, we augment our analysis with Data Release 2 (DR2) from the Galaxy And Mass Assembly survey (GAMA; Liske et al. 2015). GAMA is a large (144 sq. deg.) survey that builds on the legacy of the Sloan Digital Sky Survey (SDSS; York et al. 2000) and the Two-degree Field Galaxy Redshift Survey (2dF-GRS; Colless et al. 2001). The “main galaxy survey” component of GAMA goes two magnitudes deeper ($r < 19.8$ mag) than that of SDSS (Strauss et al. 2002) while maintaining very high ($\gtrsim 98\%$) spectroscopic completeness. Like CANDELS, GAMA has also inherited a rich supplementary multi-wavelength dataset running from 1 nm to 1 m (Liske et al. 2015). The backbone of GAMA is deep optical spectroscopy with the Anglo-Australian Telescope (AAT), and its multi-wavelength catalogs are bolstered by collaborations with several other independent surveys (for a review, see Driver et al. 2011).

Specifically, the GAMA DR2 public catalog contains 72,225 objects in three unique GAMA fields: two 48 sq. deg. fields with $r < 19.0$ mag limits, and one 48 sq. deg. field with an $r < 19.4$ mag limit. This gives a total survey volume of 144 sq. deg; see Baldry et al. (2010) for more information about survey target selection.

Here we give only a brief overview of the derivation of physical properties available in the GAMA DR2 public catalog. We adopt bulk flow-corrected redshifts (Baldry et al. 2012). The rest-frame photometry and stellar masses were derived from SED fitting as described in Taylor et al. (2011), though here we make use of the *VST* VIKING near-IR data

discussed in [Taylor et al. \(2015\)](#) as well. We applied aperture corrections to the stellar masses and rest-frame photometry, as suggested in [Taylor et al. \(2011\)](#), to account for the fraction of flux that falls outside the r -band aperture used for aperture-matched photometry in Source Extractor ([Bertin & Arnouts 1996](#)).

Unlike with CANDELS, GAMA's high spectroscopic completeness affords us $\text{H}\alpha$ -based star formation rates, $\text{SFR}_{\text{H}\alpha}$. The $\text{SFR}_{\text{H}\alpha}$ are based on extinction-corrected $\text{H}\alpha$ line luminosities ([Gunawardhana et al. 2013](#)). We converted the original $\text{SFR}_{\text{H}\alpha}$ from a Salpeter IMF normalization to a Chabrier IMF normalization to be consistent with CANDELS.

Structural properties of GAMA galaxies are provided via multi-band measurements using GALFIT ([Peng et al. 2002](#)), as described in [Kelvin et al. \(2012\)](#). We adopt the GAMA structural fits in the r -band; this has the advantage that, like CANDELS, we will be analyzing the structural properties of GAMA galaxies in the same band in which those galaxies were selected (namely, the r band). More importantly, since most of our H -band-selected CANDELS galaxies are at $z > 1$, we are measuring their structural parameters at rest-frame optical wavelengths, which should be rather consistent with the r -band structural measurements of GAMA galaxies.

We make the following selection cuts to ensure strong completeness and reliability of structural parameters. The GAMA survey's r -band target selection limits are $r < 19.0$ for two fields and $r < 19.4$ for the third field. We require stellar mass $M_* > 10^{10} M_\odot$ and r -band GALFIT quality flag = 0 (good fits only). Roughly 15% of all galaxies did not satisfy our GALFIT selection criterion, and we verified that these galaxies did not occupy a special region of the sSFR- M_* or UVJ diagrams. We do not split our GAMA sample into finer redshift or stellar mass bins for this study. Our GAMA redshift slice is restricted to $0.005 < z < 0.12$; the lower limit helps prevent contamination from foreground stars, and the higher limit helps us avoid completeness issues (in combination with our stellar mass cut; [Taylor et al. 2011, 2015](#)).

We derive completeness correction weights for every GAMA galaxy that satisfies our selection cuts using the $V_{\text{survey}}/V_{\max}$ method ([Schmidt 1968](#)). As expected from our selection cuts and the high spectroscopic completeness of GAMA, only $\sim 3\%$ of the GAMA galaxies that make it past our selection cuts have completeness correction weights $V_{\text{survey}}/V_{\max} > 1$, with the max value being ~ 35 . This confirms that our selection cuts are sufficient to make our sample complete down to $M_* = 10^{10} M_\odot$, and that we do not actually have to apply completeness correction weights to our measurements (just as with CANDELS).

3 SEMI-ANALYTIC MODEL

One of the main strengths of our study is that we will simultaneously and self-consistently analyze a semi-analytic model (SAM) of galaxy formation in the same way as the observations. Our SAM includes prescriptions for quenching, rejuvenation, and morphological transformations. Unlike the simple star formation histories frequently adopted in the literature, our SAM propagates effects from stochastic

events such as mergers, starbursts, and supermassive black hole (SMBH) feedback into the star formation histories of galaxies. This allows us to track the physical drivers behind galaxy transformations, in terms of both structure and star formation; these are directly relevant for tracing the origin and evolution of transition galaxies in a cosmological context.

Here we review only the most salient points of the “Santa Cruz” SAM used in this study. We refer the reader to the following sequence of papers for much greater detail about the physical prescriptions implemented in the SAM, and about the origin and evolution of the SAM itself: [Somerville & Primack \(1999\)](#), [Somerville et al. \(2001\)](#), [Somerville et al. \(2008a\)](#), [Somerville et al. \(2012\)](#), and [Porter et al. \(2014a\)](#). Our companion papers also have a more in-depth and very relevant discussion of the SAM: [Brennan et al. \(2015\)](#) and [Brennan et al. \(2016\)](#). Finally, we also recommend the recent review article by [Somerville & Davé \(2015\)](#) which discusses SAMs along with a general overview of physical models of galaxy formation and evolution.

We use the mock catalogs that were created for the CANDELS survey (Somerville et al., in preparation). These include lightcones that emulate the geometry of the five CANDELS fields, where the masses and positions of the root halos were drawn from the Bolshoi-Planck N-body simulations ([Rodríguez-Puebla et al. 2016a](#)). The Bolshoi-Planck simulations adopt cosmological parameters that are consistent with the Planck constraints ([Planck Collaboration et al. 2014](#)); $\Omega_m=0.307$, $\Omega_\Lambda=0.693$, $h=0.678$, with a baryon fraction of 0.1578. Merger trees for each halo in the light cone are constructed using the method of [Somerville & Kolatt \(1999\)](#), updated as described in [Somerville et al. \(2008a\)](#). We combine the five SAM mock catalogs corresponding to the five different CANDELS fields to achieve excellent number statistics, but we note that each SAM mock catalog is in general much larger than the corresponding observed CANDELS field. Since the CANDELS lightcones represent a very small volume at low redshift, we instead use a $z \sim 0.1$ snapshot drawn from Bolshoi-Planck for our lowest redshift slice.

As halos grow due to gravitational collapse, baryons are accreted into the halo. A standard spherically symmetric cooling flow model is adopted to track the rate at which gas can cool and collapse into the central galaxy (see [Somerville et al. 2008a](#), for details). Gas that has cooled and collapsed into a disk is considered available for star formation. The SAM has two prescriptions for star formation. The first prescription is applicable to isolated disks and adopts the Schmidt-Kennicutt relation ([Kennicutt 1998](#)) whereby only gas above a certain critical surface mass density can collapse to form new stars. The second prescription applies to starbursts and is triggered after a merger or an internal disk instability (see below). The efficiency and timescale of a starburst induced by a merger depends on the gas fraction and mass ratio of the progenitors (e.g., see [Hopkins et al. 2009](#)). We note that stars formed during a merger-induced starburst are added to the spheroidal component of the remnant galaxy. SFR estimates in the SAM have been averaged over 100 Myr to approximately replicate the timescale probed by UV and IR-based SFRs.

The SAM includes feedback from photoionization, stars and supernovae, as well as active black holes. Photoionization feedback is important only at mass scales much lower

than the ones we consider in this paper. In low mass galaxies ($M_* \lesssim 10^{10} M_\odot$), the mechanical and radiative feedback from supernovae and massive stars is primarily responsible for outflows of cold gas. Only some fraction (dependent on the halo circular velocity; Somerville et al. 2008a) of the outflows are deposited into the hot gas reservoir of the galaxy’s halo and allowed to cool again (thereby allowing for future gas inflows), while the rest is driven out of the halo completely, and falls back on a longer timescale. We note that each generation of stars produces heavy elements, which are also ejected from galaxies and deposited either in the ISM, hot halo, or intergalactic medium.

Feedback from AGN is very important in determining the properties of massive galaxies in these SAMs. Seed black holes are initially added to galaxies according to the prescription described in Hirschmann et al. (2012). Based on hydrodynamic simulations of galaxy mergers, our SAM assumes that galaxy mergers trigger rapid accretion onto the central BH (Hopkins et al. 2007). There are two “modes” of AGN feedback implemented in our SAM. In the “radiative mode” (sometimes called “bright mode” or “quasar mode”), radiatively efficient BH accretion can drive winds that remove cold gas from the galaxy, and eventually shut off the BH growth as well. In addition, hot halo gas can fuel radiatively inefficient BH accretion via Bondi-Hoyle accretion (Bondi 1952). This mode is associated with powerful radio jets that can heat the halo gas, suppressing or shutting off cooling. This latter mode is often referred to as “radio mode” or “jet mode.”

We note that mergers and disk instabilities (see below) cause the growth of a bulge and drive gas toward the center where the SMBH lives. This relationship between bulge growth and AGN activity in the SAM, along with the self-regulated BH growth, leads to final black hole masses and bulge masses that are consistent with the observed $M_{BH} - M_{\text{bulge}}$ relation (Somerville et al. 2008a; Hirschmann et al. 2012).

Initially all star formation is assumed to occur in disks. Bulge growth in our SAM occurs through two channels: mergers and disk instabilities. Mergers directly deposit a fraction of the pre-formed stars from the merging satellites into the bulge component, and also trigger starbursts. The stars formed in these merger-triggered bursts are also deposited in the bulge component. In addition, if the ratio of baryonic material in the disk relative to the mass of the dark matter halo becomes too large, we assume that the disk becomes unstable, and move disk material to the bulge until marginal stability is restored (for more details, see Porter et al. 2014a, and references therein). It was shown in Porter et al. (2014a) and in our companion paper (Brennan et al. 2015) that with our currently adopted recipes, our SAM does not produce enough bulge-dominated galaxies if bulges are allowed to grow only through mergers. We obtain much better agreement with the mass function and fraction of bulge-dominated galaxies when we include the disk instability channel for bulge growth. Note that galaxies that become bulge-dominated through a merger or disk instability can re-grow a new disk and become disk-dominated again through accretion of new gas (see Brennan et al. 2015, and our discussion in subsection 7.5).

One caveat of the SAM is that morphological transformations are treated as being instantaneous, i.e., following a

merger or disk instability the material is added to the bulge in a single timestep. As it is unlikely that morphological transformations act on timescales comparable to the cosmic times spanned by our redshift slices, we do not expect this to significantly affect our results.

We estimate the scale radius of our model disks based on the initial angular momentum of the gas, assuming the gas collapses to form an exponential disk. We include the contraction of the halo due to the self-gravity of the baryons (Blumenthal et al. 1986; Flores et al. 1993; Mo et al. 1998; Somerville et al. 2008b). The sizes of spheroids formed in either disk instabilities or mergers are estimated using the virial theorem and conservation of energy, including the dissipative effects of gas. Our modeling of spheroid sizes has been calibrated on numerical hydrodynamical simulations of binary galaxy mergers as described in Porter et al. (2014a), and has been shown in that work to reproduce the observed size evolution of spheroid-dominated galaxies since $z \sim 2$ (see also Somerville et al. in preparation).

The SAM produces a prediction for the joint distribution of ages and metallicities in each galaxy as described in Porter et al. (2014b). The predictions are consistent with the observed correlation between age, metallicity and stellar velocity dispersion, and the observed lack of radial trends in age and metallicity, for $z \sim 0$ elliptical galaxies (again, see Porter et al. 2014b, and references therein). We combine these age and metallicity predictions with stellar population synthesis models to obtain intrinsic (non-dust-attenuated) stellar energy distributions (SED) which may be convolved with any desired filter response functions. We use the stellar population synthesis models of Bruzual & Charlot (2003) with the Padova 1994 isochrones and a Chabrier IMF. Note that the synthetic SEDs currently do not include nebular emission. We optionally include attenuation of the light due to dust using an approach similar to that described in Somerville et al. (2012).

The existence of accurate size estimates for the disk and bulge components in our SAM allows us to do something novel. We can compute composite effective radii and Sérsic indices using a mapping derived by introducing fake galaxies that are composites of $n = 1$ (disk) and $n = 4$ (spheroid) components into images and then fitting them with a single Sérsic profile (see Lang et al. 2014; Brennan et al. 2015, for details). The Sérsic indices and effective radii that we derive here are light-weighted, in contrast with the stellar mass weighted quantities used in Brennan et al. (2015), and should provide a more accurate comparison to the Sérsic indices and sizes derived from light for our observed sample. However, we note that we do not attempt to include the effects of dust attenuation in our light-weighted quantities. These light-weighted quantities have also been used in Brennan et al. (2016), who showed that adopting light-rather than stellar mass-weighted quantities did not qualitatively change their results relative to Brennan et al. (2015), but it did result in a significantly better agreement between the models and the observations.

4 METHODS

4.1 Defining Transition Galaxies

We use a modified version of the method presented in our companion papers (Brennan et al. 2015, 2016) to split our sample of galaxies in each redshift slice into star-forming, transition, and quiescent subpopulations. Our splitting is done in sSFR- M_* space rather than color-color, color-mass, or color-magnitude space. In short, we find the normalization of the SFMS in each redshift slice using the average sSFRs of dwarf galaxies with $10^9 M_\odot < M_* < 10^{9.5} M_\odot$ (since these are known to be overwhelmingly star-forming objects; e.g., see Geha et al. 2012). We then fit a cubic polynomial to these normalizations as a function of the age of the Universe, which allows us to easily compute the time evolution of the SFMS normalization. We derive the slope of the SFMS just as described in Brennan et al. (2015): in a given redshift slice, the slope is calculated as the derivative with respect to stellar mass of the average sSFR of galaxies with $M_* \sim 10^9 M_\odot$ and $M_* \sim 10^{10} M_\odot$. Since allowing the slope to be a free parameter does not significantly change our results, we fix it to zero (but see subsection 4.2 for a description of how we control for stellar mass dependence).

Whereas Brennan et al. (2015) constructed one divisor in sSFR- M_* space (to split their sample into star-forming and quiescent galaxies), we construct two divisors based on the observed scatter of the SFMS. For all CANDELS redshift slices at $0.5 < z < 3.0$, we adopt a conservative value of 0.4 dex for the 1σ observed scatter in the SFMS (see also Kurczynski et al. 2016, for measurements of the ‘‘intrinsic scatter’’ of the SFMS). On the other hand, we find that the GAMA SFMS at $0.005 < z < 0.12$ appears to have a larger apparent width of 0.7 dex. This might be due to the fact that H α probes SFRs on shorter timescales ($\sim 10 - 20$ Myr) and thus could be sensitive to larger excursions of galaxies below the SFMS (see also Davies et al. 2016). We therefore adopt 0.7 dex for the width of the GAMA SFMS. For the SAM, we adopt 0.4 dex for the width of the SFMS for all redshift slices.

We then define the ‘‘transition region’’ to range from 1.5σ to 3.5σ below the SFMS (i.e., between 0.6 dex and 1.4 dex below the SFMS). The quiescent region comprises all galaxies further than 3.5σ (1.4 dex) below the SFMS. Assuming that the observed scatter of the SFMS follows a Gaussian distribution, our upper limit for the transition region of 1.5σ below the ‘‘mean’’ (i.e., SFMS normalization) suggests that $> 85\%$ of star-forming galaxies would lie above that line, and thus that the contamination in the transition region from star-forming galaxies would be $< 15\%$. Similarly, our upper limit for the quiescent region of 3.5σ below the SFMS normalization suggests that $> 99\%$ of star-forming galaxies should lie above that line, and thus that the contamination in the quiescent region from star-forming galaxies would be $< 1\%$. Note that these statistical arguments are weaker when applied to the GAMA redshift slice because its SFMS width is higher by 0.3 dex, and therefore its transition region boundaries are shifted down by 0.3 dex as well; this means that the upper and lower boundaries of the GAMA transition region are, respectively, 1.3σ and 2.4σ below the SFMS.

In Figure 1, we show the sSFR- M_* plane in each of our redshift slices for both the observations and the SAM.

We also show the redshift-dependent definition of the transition region for both the observations and the SAM. Our method captures the decreasing normalization of the SFMS toward low redshift. Since we define the transition region in each redshift slice relative to the SFMS in that same redshift slice, the normalization of the transition region also decreases toward low redshift. These features naturally account for the likely possibility that high redshift transition or quiescent galaxies might be considered star-forming galaxies if they were relocated to $z = 0$ (given that the sSFRs of high redshift galaxies are much higher than those of low redshift galaxies). In the SAM, the SFMS tends to have a lower normalization overall than in the observations; this is known to be a general issue in other models as well (e.g., see the discussions in Somerville & Davé 2015; Davé et al. 2016b). However, the crucial point is that our method is applied self-consistently and independently to the observations and to the SAM.

The above method of constructing the transition region naturally leads to the following physically and statistically motivated definition of transition galaxies. At a given M_* and redshift, galaxies that are offset downward by at least 1.4 dex compared to the sSFR of a typical SFMS galaxy are classified as quiescent (relative to the SFMS at their redshift). Similarly, at a given M_* and redshift, galaxies whose sSFRs are at most 0.6 dex below the SFMS at their redshift are classified as ‘‘still’’ star-forming. Lastly, at a given M_* and redshift, galaxies that are offset between 0.6 dex and 1.4 dex below the SFMS at their redshift are classified as transition galaxies. Therefore, by definition, a transition galaxy has an intermediate sSFR compared to other typical galaxies with a similar M_* and redshift, and it is the aim of this work to explore why the sSFRs of transition galaxies are not as heavily suppressed as those of quiescent galaxies.

4.1.1 On SFR Uncertainties and the Purple Valley

It is true that in the observations the width of the SFMS is not merely due to intrinsic scatter alone, but also additional measurement errors. For statistical samples of galaxies such as ours, a detailed uncertainty analysis of SFRs that takes into account our incomplete knowledge of stellar evolution, the IMF, and other topics is often infeasible (see our discussion of systematic errors in subsection 6.3). If we universally ascribe to each galaxy a conservative SFR measurement error of 0.3 dex (as is often done in studies like ours), then certainly galaxies from one subpopulation can also be consistent with belonging to another subpopulation. For example, star-forming galaxies that may otherwise lie at the intrinsic 1σ bottom tail of the SFMS (i.e., a distance of 0.4 dex below the SFMS fit) could be scattered further down by an additional 0.3 dex due to measurement errors (so 0.7 dex below the SFMS fit).

The simple exercise above illustrates that these star-forming galaxies would then also be consistent with a classification as transition galaxies. Although this is a concern, we have defined our transition region to span a wide enough range in sSFRs such that not all galaxies could be scattered into or out of it. While it is possible that the SFRs of some galaxies may be very poorly constrained (especially those with minimal ongoing star formation, far below the SFMS), the physically motivated methodology that we have devised

here should in principle be robust. However, in the future, it will be necessary to address just how bad the systematic errors in our SFR measurements of high-redshift transition and quiescent galaxies are because this ignorance is a shortcoming that all studies are subject to.

Now we briefly address the dual usage of the term “purple valley” in the literature. The term purple valley was first introduced in the study of Mendez et al. (2011), which asked whether the classical green valley might simply be a combination of blue cloud and red sequence galaxies that live in the tails of their parent populations. This includes intrinsically blue or red galaxies that were scattered into the green valley due to measurement uncertainties. Could the transition region merely be an analogous combination of intrinsically star-forming and quiescent galaxies that live in the “tails” of their parent populations? If the SFMS indeed has a physical basis, then this is unlikely for the following reason. We have effectively defined only two populations: (1) galaxies that are on the SFMS because they have maintained their equilibrium between gas inflows, gas outflows, star formation and stellar feedback, and (2) galaxies that have varying “degrees of quiescence” below the SFMS, in a continuous sense. As galaxies move further below the SFMS, it becomes less likely that they are maintaining their equilibrium like the average SFMS galaxy; instead, it becomes more likely that they were or are being subject to physical processes that are actively suppressing their star formation (see our theoretical discussion in section 7). As we will argue in this paper, the degree of quiescence of galaxies below the SFMS might reveal clues about the timescales on which their equilibrium was disrupted. In our companion paper by Brennan et al. (2016), we focus on the continuous approach. In the rest of this paper, we will show that there is also considerable value (both observationally and theoretically) in explicitly categorizing the transition population.

A second and more recent definition of the “purple valley” has been suggested by Dressler & Abramson (2015), who make use of the finding that composite bulge+disk systems dominate the classical green valley at low redshift (see also Lackner & Gunn 2012; Abramson et al. 2014). Given that a red bulge superimposed onto a blue disk can yield an intermediate color that is representative of the green valley, Dressler & Abramson (2015) argue that such purple composite systems are not necessarily in transition. This interpretation of the purple valley is conceptually quite different from the original definition put forward by Mendez et al. (2011). On some level, it is true that most galaxies in the classical green valley can be thought of as being “purple” (and in this paper we will suggest that this might also be the case for transition galaxies out to $z = 3$). However, this second interpretation of the purple valley does not adequately explain how the “superimposed” red bulges grew in the first place, and why they are preferentially hosted by galaxies in the green valley and the red sequence. Furthermore, even if these composite bulge+disk systems are universally the result of simple “fading” scenarios (as proposed by Schawinski et al. 2014; Dressler & Abramson 2015), it is still important to understand the contribution of this slow transition pathway to the overall growth of the quiescent population as a function of redshift.

Table 1. Coefficients for a cubic polynomial fit to the normalization of the SFMS as a function of the age of the Universe: $\log_{10}(SFMS(z)/\text{yr}^{-1}) = a_3t^3(z) + a_2t^2(z) + a_1t(z) + a_0$, where $t(z)$ is the age of the Universe at the redshift of interest. These coefficients are valid for t values between roughly 2.5 – 13 Gyr.

a_3	a_2	a_1	a_0	Sample
-0.0011	0.0233	-0.2766	-7.8597	GAMA+CANDELS
-0.0025	0.0787	-0.8940	-6.7503	SAM

4.2 Stellar Mass Matching

In principle, we should at least attempt to account for the dependence of global galactic structure on stellar mass. It is well known that more massive galaxies tend to be more bulge-dominated. In each of our redshift slices, the stellar mass distributions of our star-forming, transition, and quiescent galaxies are significantly different from each other. Therefore, it may not be appropriate to compare, e.g., a less massive star-forming galaxy to a more massive transition galaxy since the more massive transition galaxy will naturally have a more prominent bulge. We address this potential stellar mass dependence in three different ways.

Our default approach, which forms the basis for all results shown in this paper, is to perform “stellar mass-matching” for the transition galaxy subpopulation. Specifically, for each transition galaxy in a given redshift slice, we randomly picked three unique star-forming and three unique quiescent galaxies in the same redshift slice whose stellar masses were within a factor of two of the mass of the transition galaxy. In this way, we constructed “transition-mass-matched” samples of star-forming and quiescent galaxies whose structural parameters we could compare to those of transition galaxies. We note that our results are not sensitive to whether or not we apply this stellar mass-matching algorithm.

As one alternative to our stellar mass-matching approach, we re-did our entire analysis in three stellar mass bins: $10^{10}M_\odot < M_* < 10^{10.5}M_\odot$, $10^{10.5}M_\odot < M_* < 10^{11}M_\odot$, and $M_* > 10^{11}M_\odot$. Using this mass slice approach, we reproduced the main conclusions of this paper, although there is significantly more scatter in all measurements due to the smaller sample size in each mass bin. As another alternative to our stellar mass-matching algorithm, we re-did our entire analysis by allowing the slope of the SFMS in the sSFR- M_* plane to be a free parameter. Again, our exact quantitative results change slightly, but our conclusions do not.

In the future, it will be important to revisit the non-trivial question of the stellar mass dependence of our results, especially by extending our analysis to lower mass galaxies (see also Fang 2015). In particular, it will be insightful to consider the relative stellar mass growth of star-forming, transition and quiescent galaxies, assuming that they do indeed form an evolutionary sequence. A naive picture would be that star-forming galaxies should be more massive than their transition and quiescent galaxy descendants, since the latter are forming stars at significantly reduced rates. However, this view is too simplistic because galaxies can grow a significant fraction of their stellar mass through mergers and satellite accretion (e.g., Naab et al. 2007; Lackner et al. 2012), and because the most massive objects quench first

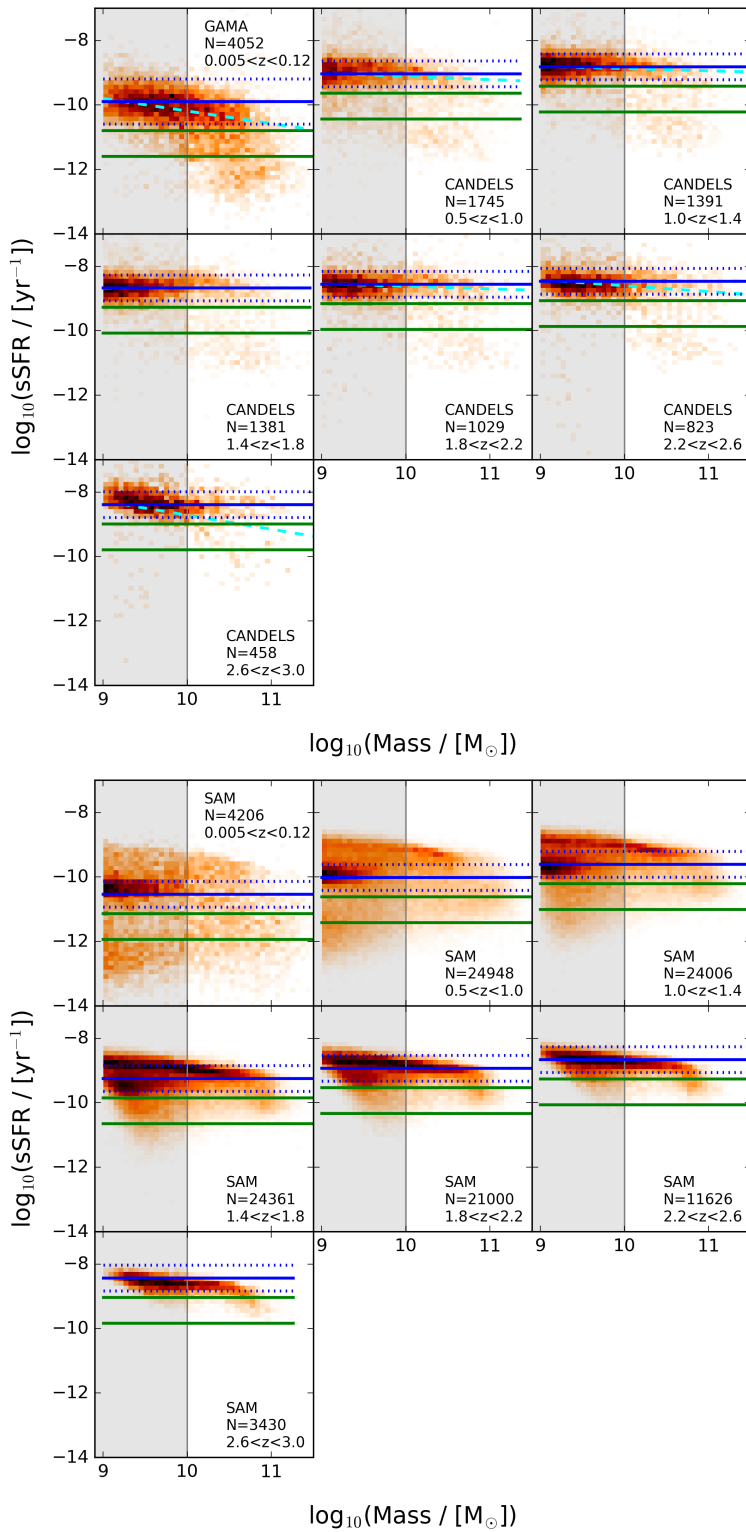


Figure 1. Defining transition galaxies in sSFR- M_* space for the observations (top) and for the SAM (bottom). In each panel, the solid blue line shows the SFMS fit (with slope fixed to zero), and the dotted blue lines mark the assumed conservative $0.4 \text{ dex } \pm 1\sigma$ width of the SFMS (0.7 dex for the $z \sim 0.1$ GAMA redshift slice; see text). The two green lines in each panel show the transition region, with the upper line being 0.6 dex (1.5σ) below the SFMS normalization and the lower line being 1.4 dex (3.5σ) below the SFMS normalization. The gray shaded region indicates the dwarf galaxy regime where most objects are star-forming; we use this region to self-consistently determine the SFMS normalization (but we do not include these lower mass galaxies in any subsequent analysis). In the observations, the cyan dashed line shows the SFMS fit if the slope is allowed to be a free parameter – our results and conclusions do not change significantly if we instead define a sloped transition region using the sloped SFMS fits (see subsection 4.2 for an extensive discussion of our stellar mass-matching techniques).

(e.g., [Fontanot et al. 2009](#)). A more detailed analysis of the stellar mass growth of individual galaxies as they move between the three different subpopulations is therefore deferred to future work.

5 RESULTS

5.1 UVJ Demographics of Transition Galaxies

In high-redshift studies, it is common practice to adopt empirically-motivated dividing lines in rest-frame color-color diagrams to separate quiescent systems from those that are still undergoing star formation. The rest-frame UVJ diagram in its modern incarnation was first proposed by the seminal studies of [Wuyts et al. \(2007\)](#) and [Williams et al. \(2009\)](#); the latter constructed an empirical “quiescent wedge” in order to distinguish truly “red and dead” systems from dusty star-forming galaxies and dust-free star-forming galaxies. Although several studies have shown that there is an “age sequence” for quiescent galaxies and a “dust sequence” for star-forming galaxies in the UVJ diagram (e.g., [Whitaker et al. 2010](#); [Brammer et al. 2011](#)), it is important to recognize that the UVJ diagram and its predecessors (e.g., [Labbé et al. 2005](#); [Shapley et al. 2005](#)) were never intended to allow easy selection of galaxies based on their varying degrees of quiescence below the SFMS. Instead, galaxies are either considered quiescent or some variant of star-forming (dusty or dust-free), and it then becomes unclear how transition galaxies might fit into this so-called “bimodal” picture (see also the insightful studies of [van Dokkum et al. 2015](#); [Fang 2015](#); [Kriek et al. 2015](#); [Whitaker et al. 2016](#); [Yano et al. 2016](#)). One of the main points of this paper is that the “degree of quiescence” of galaxies below the SFMS might reveal important clues about the timescales on which their quenching (and perhaps rejuvenation) occurred.

In [Figure 2](#), we show the demographics of our sSFR- M_* -defined star-forming, transition and quiescent galaxies in the UVJ color-color diagram, for the observations. The GAMA UVJ diagram is adapted from Figure 15 of [Taylor et al. \(2015\)](#). We also show the empirical boundaries for the quiescent wedge, for which the exact equations are adopted from [van Dokkum et al. \(2015\)](#). We recover the old results that: (1) quiescent galaxies generally live in the quiescent wedge, and (2) galaxies on the SFMS also span a “dust sequence” in this diagram, with dusty star-forming galaxies having higher rest-frame ($U - V$) and ($V - J$) colors compared to dust-free star-forming galaxies.

However, the galaxies that we cleanly categorized as “transition” using the sSFR- M_* diagram, as described in [subsection 4.1](#), do not all fall in a cleanly separated part of this diagram. In particular, they do not fall entirely in the quiescent region, and a non-negligible fraction of them would be considered dusty star-forming galaxies based on the empirical selection criteria of other studies. The reason that we were able to classify the latter objects as transition galaxies is because they did not end up on the SFMS after we corrected their UV-based SFRs for dust extinction using either infrared SFR indicators or the A_V output by SED fitting (see also Appendix A, where we show a version of [Figure 2](#) color-coded by A_V). We note that this lack of a clean separation in rest-frame UVJ space persists even if

we select transition galaxies using the UV-optical-NIR SED-based $sSFR_{SED}$, which is simultaneously constrained during the SED fitting process and is output alongside the ($U - V$), ($V - J$), and A_V values.

Overall, our finding that $sSFR$ - M_* -selected transition galaxies span the region in between the classical UVJ -based star-forming and quiescent galaxies suggests that the transition subpopulation might indeed represent some non-trivial evolutionary bridge between the quiescent and star-forming subpopulations. In particular, if there indeed exist “dusty transition galaxies,” then that might already be a clue that galaxies can follow a diversity of pathways toward quiescence. For example, our finding underscores the outstanding question about whether galaxies simply go from the SFMS into the transition region and end up as quiescent, or whether some fraction of these transitions must be preceded by a starburst (in some cases, perhaps leading to dusty post-starburst galaxies; e.g., [Yesuf et al. 2014](#); [Rowlands et al. 2015](#); [Belli et al. 2015](#); [Alatalo et al. 2016a](#)). On the other hand, those transition galaxies that do extend into the classical UVJ dusty star-forming region might also in the future offer important clues about potential systematic errors in dust correction methods (see our discussion in [subsection 6.3](#)).

5.2 The Transition Fraction Across Cosmic Time

In [Figure 3](#), we show how the fraction of all galaxies that are classified as star-forming, transition and quiescent evolves since $z = 3$. The fractions of star-forming, transition, and quiescent galaxies in each redshift slice for the observations and the SAM are respectively given in [Table 2](#) and [Table 3](#). We remind the reader that, in this paper, we are focusing only on massive galaxies with $M_* > 10^{10} M_\odot$. As has been known for some time (e.g., [Bell et al. 2004](#); [Faber et al. 2007](#)), the fraction of all massive galaxies that are quiescent has risen considerably while the fraction all massive galaxies that are star-forming has decreased. We see in [Figure 3](#) that this trend is reproduced since $z \sim 3$ even when explicitly defining a transition population. Interestingly, the transition fraction is relatively constant between $z = 3$ and $z = 0.5$; we will explore one possible theoretical reason for this in [subsection 7.3](#).

It is immediately apparent from [Figure 3](#) that at high redshift ($z > 1$), the SAM underproduces quiescent galaxies. This underproduction of quiescent galaxies at high redshift is very likely related to the overproduction of star-forming and transition galaxies at similar redshifts. However, the fact that by low redshift the quiescent fraction of the SAM agrees relatively well with that of the observations (down to a discrepancy of $\approx 5\%$) suggests that the overall rate at which galaxies begin to quench in the SAM is correct, but that the quenching timescales tend to be too long (we will explore this further in [section 7](#)). We note that if the transition and quiescent populations are grouped into one category (the classical idea of one “quenched fraction” for all galaxies below the SFMS), then we would find better agreement with observations, although still with hints that quenching is not efficient enough at high redshift in the SAM (see [Brennan et al. 2015](#), and references therein).

We point out that there is a roughly factor of two increase in the observed transition fraction at very low red-

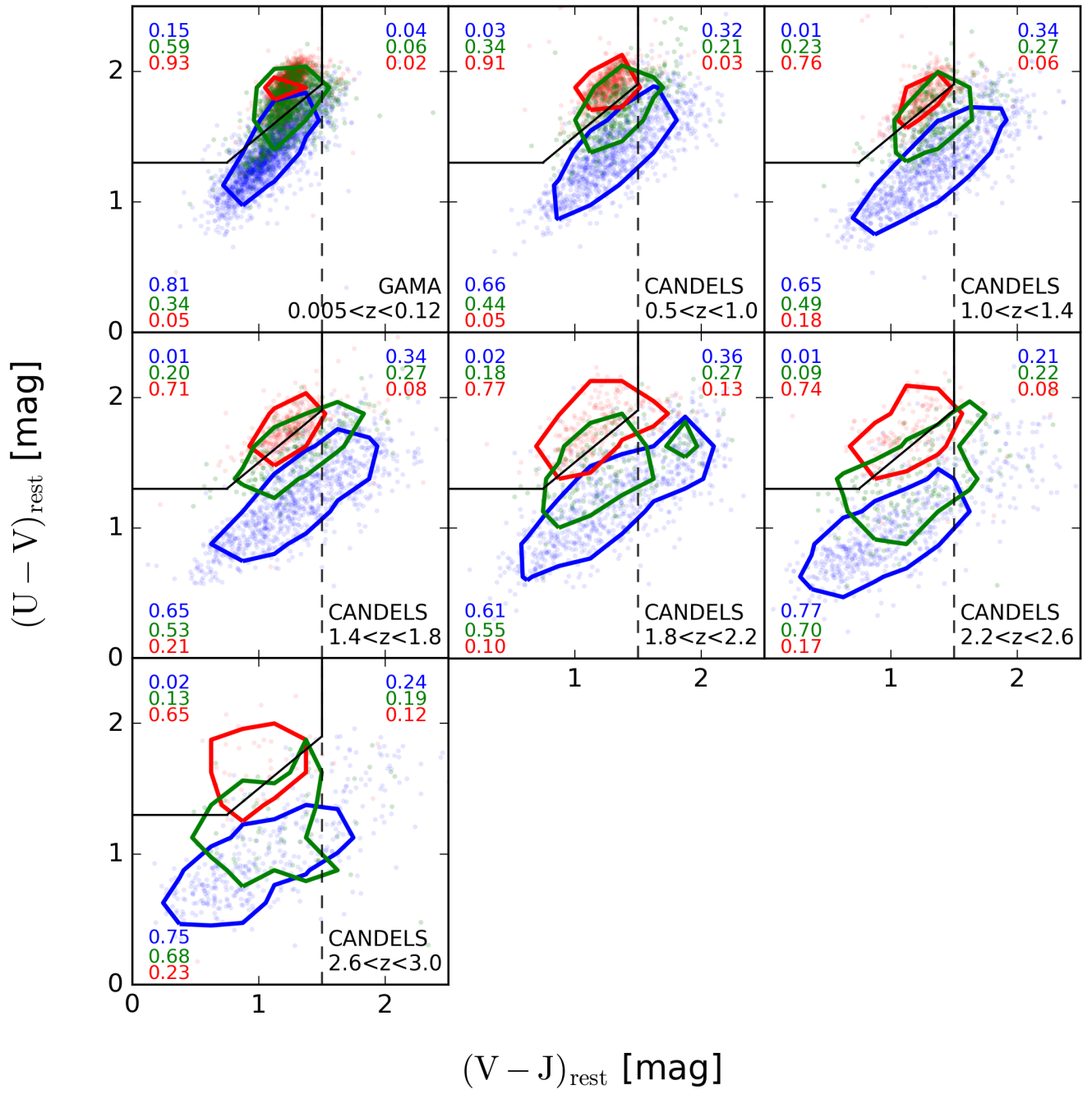


Figure 2. The UVJ color-color distribution of star-forming (blue points), transition (green points) and quiescent (red points) galaxies in GAMA+CANDELS observations. The color-coding of the points represents their classification using the sSFR- M_* diagram. The contours enclose 68% of each subpopulation. The GAMA UVJ diagram is adapted from Figure 15 of Taylor et al. (2015). In each panel, we write the fraction of each subpopulation that falls into the three classical UVJ regions (quiescent wedge, dust-free star-forming region, and dusty star-forming region). The quiescent wedge is marked by the polygon. Dusty star-forming galaxies are classically thought to have $(V - J) > 1.5$, as marked by the dashed vertical line. In Appendix A, we show a version of this diagram where the points are color-coded by the A_V that is output by SED fitting. Note how the transition population spans the region between the classical star-forming and quiescent populations, but also that: (1) it would not be as straightforward to identify the transition population using UVJ cuts, and (2) there is a non-negligible fraction of supposedly “dusty transition galaxies.”

shifts, and that no such rapid increase is seen in the SAM. This might be an artifact of our different SFR indicators for GAMA ($\text{H}\alpha$, which probes SFRs on 10 Myr timescales) and CANDELS (NUV, which probes SFRs on 100 Myr timescales). However, it is also entirely possible that the rise is real: our CANDELS observations end at $z = 0.5$ and our GAMA observations only go up to $z = 0.12$. In the ~ 3.5 Gyr that have elapsed between these two limiting redshifts, a large number of galaxies could have finally consumed their gas supply and fallen into the transition region. This is also sufficiently high redshifts that galaxies would still have time to undergo mergers. In the future, it will therefore be interesting to bridge our observational results from the CANDELS and GAMA surveys with observations of “intermediate-redshift” transition galaxies.

5.3 Structural Distinctness

In Figure 4, we show the redshift evolution of the Sérsic index, half-light radius², and surface stellar mass density³ for the three subsamples in both the observations and the SAM. In the observations, it is striking how well-separated the median structural properties of the three subsamples are across more than 10 Gyr of cosmic time. We remind the reader that the results shown here are for stellar mass-matched samples (see subsection 4.2); it is interesting to note that we obtain similar results even without our stellar mass matching algorithm. The cumulative distribution functions (CDFs) underlying Figure 4 as well as the statistical results of two-sample Kolmogorov-Smirnov tests are given in Appendix B.

In the observations, we reproduce the well known result that both star-forming and quiescent galaxies have grown in size since $z \sim 3$, and that quiescent galaxies are preferentially more compact than star-forming galaxies at all redshifts (e.g., Barro et al. 2013; van der Wel et al. 2014; van Dokkum et al. 2015). What is remarkable, yet also puzzling, is that the transition population seems to remain intermediate between these two populations in terms of Sérsic index and compactness over this entire interval. Disentangling the various physical processes that might give rise to this phenomenon and interpreting this observational finding is non-trivial. We will discuss this further in section 6.

Intriguingly, we see qualitatively the same trends in the SAM, although with a less pronounced separation between the three populations than what is seen in the observations, especially in the size and surface stellar mass density.

We have confirmed that the separation between the three subpopulations in the SAM, in terms of the Sérsic index, continues to be seen at all redshifts if we use B/T ratio (either light-weighted or mass-weighted). This suggests that the Sérsic index separation seen in the SAM is not

² Our half-light radii are semi-major axis radii rather than circularized radii ($r_{\text{hl,circ}} = \sqrt{q} \times r_{\text{hl}}$, where $q \equiv b/a$ is the axis ratio). The latter are more difficult to compare between galaxies since they depend on the shape of each galaxy. However, we also see the same separation between the three subpopulations if we use $r_{\text{hl,circ}}$ instead of r_{hl} .

³ The motivation for using $\Sigma_{1.5} \equiv M_* r_{\text{hl}}^{-1.5}$ is given in Barro et al. (2013). In the future, it will be interesting to redo this comparison using the stellar mass density within one kpc (i.e., Σ_1 ; see Cheung et al. 2012; Fang et al. 2013; Barro et al. 2015).

necessarily driven by our assumed mapping from bulge-disk radii and masses to a composite half-light radius and associated single-component Sérsic index (see section 3). Overall, understanding what gives rise to the trends in the SAM is complex and we will return to it in section 7.

We point out that in our SAM, galaxies tend to have much larger half-light radii than in the observations (especially quiescent galaxies at $z \sim 0$). While this is an important issue that will be addressed in future work, what is crucial for this paper is not the exact normalization of the size and compactness trends in Figure 4, but rather the qualitative separation between the three subpopulations.

6 DISCUSSION OF OBSERVATIONAL RESULTS

6.1 Origin of Structural Distinctness

It is not straightforward to interpret the observational trends seen in Figure 4 because there are many factors that can cause the observed structural distinctness of transition galaxies. If we assume that the transition population does indeed mostly consist of galaxies moving below the SFMS and toward quiescence (regardless of the timescale), then the range of possibilities is significantly narrowed down. Although naive, such an assumption has at least some basis in our theoretical understanding of galaxy evolution (see our extensive discussion in section 7) as well as the observational result that the fraction of all massive galaxies that are quiescent is increasing toward low redshift (see again Figure 3).

One picture is that galaxies experience “compaction” through a dissipative process such as a merger or disk instability. The resulting increase in central stellar density (i.e., bulge growth) is thought to be causally connected with the process that leads to quenching (e.g., AGN feedback). The expected sequence in this picture, in which structural and morphological transformation precedes quenching, seems to lead to a natural explanation of the observed trends (see also our theoretical discussion in subsection 7.5). The recent discovery by Barro et al. (2015) of a “structural main sequence” for observed galaxies, which relates compaction to subsequent quiescence, also lends credence to this interpretation. There are also many other findings, both observational and theoretical, that support this first “compaction” picture (e.g., see Wuyts et al. 2012; Nelson et al. 2012; Patel et al. 2013; Dekel & Burkert 2014; Zolotov et al. 2014; Tacchella et al. 2015; van Dokkum et al. 2015; Tacchella et al. 2016a,b; Nelson et al. 2016).

An alternative interpretation is afforded by the concept of “progenitor bias” (e.g., see van Dokkum & Franx 1996; Bezanson et al. 2015; van Dokkum et al. 2015; Lilly & Carollo 2016; Abramson & Morishita 2016). In this scenario, if star-forming galaxies increase in size over time, but cease to grow as much after they quench, then a natural consequence will be that transition and quiescent galaxies will be more compact than star-forming galaxies observed at the same epoch. In particular, if transition galaxies in a given redshift slice indeed began to quench more recently than quiescent galaxies in the same redshift slice, then we might expect the transition galaxies to be more extended than the quiescent

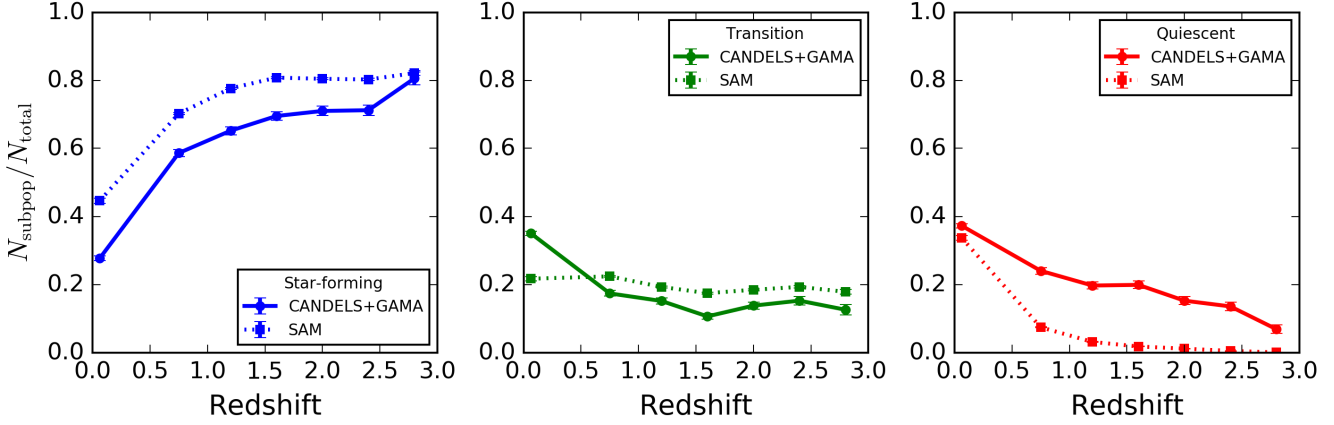


Figure 3. The redshift evolution of the fraction of galaxies in the three different subpopulations in the observations (solid lines) and the SAM (dotted lines). Star-forming galaxies are shown in blue (left panel), transition galaxies in green (middle panel), and quiescent galaxies in red (right panel). The errorbars were computed via bootstrapping of the sSFR- M_* diagram. The quiescent fraction builds up toward low redshift while the star-forming fraction decreases – for both the observations and the SAM. The transition fraction remains roughly constant at all redshifts in the SAM; this is also true for the observations except there is a significant increase from $z \sim 0.5$ to $z \sim 1.0$. The fact that the SAM quiescent fraction at $z \sim 0.1$ agrees well with the quiescent fraction of GAMA suggests that the rate at which galaxies are beginning to quench at high redshift in the SAM is correct. However, the deficit of high-redshift quiescent galaxies suggests that quenching timescales are too long in the SAM.

Redshift Slice	f_{SF}	f_T	f_Q	Sample
$0.005 < z < 0.12$	0.277 ± 0.007	0.350 ± 0.006	0.372 ± 0.006	GAMA
$0.5 < z < 1.0$	0.586 ± 0.011	0.174 ± 0.008	0.240 ± 0.010	CANDELS
$1.0 < z < 1.4$	0.652 ± 0.012	0.151 ± 0.009	0.197 ± 0.011	CANDELS
$1.4 < z < 1.8$	0.695 ± 0.012	0.106 ± 0.008	0.199 ± 0.011	CANDELS
$1.8 < z < 2.2$	0.710 ± 0.014	0.138 ± 0.010	0.152 ± 0.012	CANDELS
$2.2 < z < 2.6$	0.712 ± 0.015	0.152 ± 0.012	0.135 ± 0.012	CANDELS
$2.6 < z < 3.0$	0.806 ± 0.018	0.126 ± 0.015	0.069 ± 0.012	CANDELS

Table 2. The fraction of star-forming, transition, and quiescent galaxies in each redshift slice in the observations. The errorbars were computed via bootstrapping of the sSFR- M_* diagram.

Redshift Slice	f_{SF}	f_T	f_Q	Sample
$0.005 < z < 0.12$	0.446 ± 0.008	0.217 ± 0.006	0.337 ± 0.007	SAM
$0.5 < z < 1.0$	0.702 ± 0.003	0.224 ± 0.003	0.074 ± 0.002	SAM
$1.0 < z < 1.4$	0.776 ± 0.003	0.193 ± 0.003	0.031 ± 0.001	SAM
$1.4 < z < 1.8$	0.808 ± 0.003	0.174 ± 0.002	0.018 ± 0.001	SAM
$1.8 < z < 2.2$	0.804 ± 0.003	0.184 ± 0.003	0.011 ± 0.001	SAM
$2.2 < z < 2.6$	0.802 ± 0.004	0.193 ± 0.004	0.005 ± 0.001	SAM
$2.6 < z < 3.0$	0.821 ± 0.007	0.178 ± 0.007	0.000 ± 0.000	SAM

Table 3. The fraction of star-forming, transition, and quiescent galaxies in each redshift slice in the SAM. The errorbars were computed via bootstrapping of the sSFR- M_* diagram.

Redshift Slice	n^{SF}	n^T	n^Q	$r_{\text{hl}}^{\text{SF}}$ [kpc]	r_{hl}^T [kpc]	r_{hl}^Q [kpc]	$\Sigma_{1.5}^{\text{SF}}$ [log M $_{\odot}$ kpc $^{-1.5}$]	$\Sigma_{1.5}^T$ [log M $_{\odot}$ kpc $^{-1.5}$]	$\Sigma_{1.5}^Q$ [log M $_{\odot}$ kpc $^{-1.5}$]	Sample
$0.005 < z < 0.12$	$1.39^{+0.77}_{-0.39}$	$2.20^{+0.80}_{-0.66}$	$3.05^{+0.48}_{-0.65}$	$5.26^{+1.51}_{-1.39}$	$4.29^{+1.97}_{-1.34}$	$2.89^{+1.32}_{-1.00}$	$9.38^{+0.21}_{-0.21}$	$9.55^{+0.20}_{-0.21}$	$9.84^{+0.15}_{-0.17}$	GAMA
$0.5 < z < 1.0$	$1.52^{+0.42}_{-0.42}$	$2.57^{+0.61}_{-0.77}$	$2.95^{+0.51}_{-0.54}$	$4.49^{+1.00}_{-1.34}$	$3.09^{+0.60}_{-0.99}$	$1.71^{+0.65}_{-0.49}$	$9.50^{+0.20}_{-0.19}$	$9.80^{+0.25}_{-0.26}$	$10.15^{+0.18}_{-0.24}$	CANDELS
$1.0 < z < 1.4$	$1.27^{+0.66}_{-0.49}$	$2.51^{+0.69}_{-0.58}$	$2.75^{+0.71}_{-0.58}$	$3.99^{+1.27}_{-0.98}$	$2.55^{+1.57}_{-0.93}$	$1.41^{+0.60}_{-0.41}$	$9.60^{+0.24}_{-0.25}$	$9.93^{+0.28}_{-0.30}$	$10.36^{+0.15}_{-0.19}$	CANDELS
$1.4 < z < 1.8$	$1.06^{+0.63}_{-0.32}$	$2.28^{+0.55}_{-0.92}$	$2.62^{+0.55}_{-0.60}$	$3.88^{+1.00}_{-1.11}$	$2.18^{+1.02}_{-0.96}$	$1.37^{+0.62}_{-0.53}$	$9.55^{+0.25}_{-0.25}$	$10.01^{+0.35}_{-0.35}$	$10.36^{+0.14}_{-0.43}$	CANDELS
$1.8 < z < 2.2$	$1.00^{+0.74}_{-0.36}$	$1.98^{+1.06}_{-0.97}$	$2.25^{+0.50}_{-0.61}$	$3.57^{+1.49}_{-0.96}$	$2.63^{+1.54}_{-0.96}$	$1.21^{+0.81}_{-0.81}$	$9.62^{+0.29}_{-0.29}$	$9.82^{+0.38}_{-0.32}$	$10.46^{+0.28}_{-0.52}$	CANDELS
$2.2 < z < 2.6$	$1.14^{+0.73}_{-0.50}$	$1.80^{+0.56}_{-0.68}$	$2.26^{+0.49}_{-0.69}$	$3.19^{+1.07}_{-0.97}$	$2.40^{+1.89}_{-1.89}$	$1.23^{+0.53}_{-0.52}$	$9.66^{+0.28}_{-0.28}$	$9.88^{+0.46}_{-0.31}$	$10.45^{+0.30}_{-0.50}$	CANDELS
$2.6 < z < 3.0$	$1.16^{+0.62}_{-0.50}$	$1.12^{+0.98}_{-0.49}$	$1.86^{+0.69}_{-0.53}$	$3.12^{+0.97}_{-0.98}$	$2.77^{+1.25}_{-1.02}$	$1.20^{+0.48}_{-0.48}$	$9.62^{+0.26}_{-0.25}$	$9.77^{+0.33}_{-0.30}$	$10.47^{+0.34}_{-1.01}$	CANDELS

Table 4. Redshift evolution of the structural properties of star-forming, transition and quiescent galaxies in the observations. This table corresponds to what is shown in Figure 4. Each entry in the table gives the median and the 25th and 75th percentile values relative to that median.

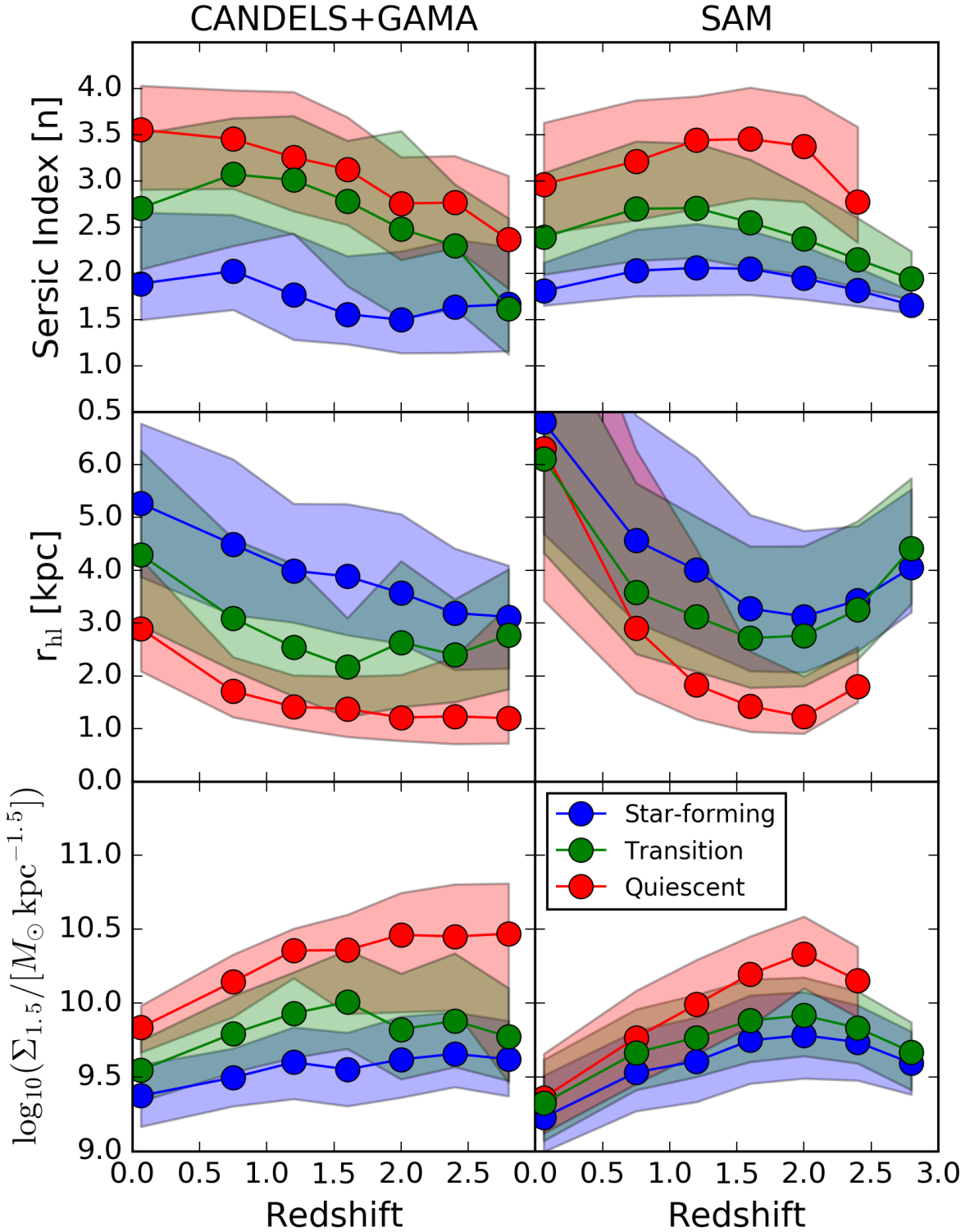


Figure 4. The redshift evolution of the Sérsic index (top row), half-light radius (middle row), and surface stellar mass density (bottom row) for transition galaxies (green), star-forming galaxies (blue), and quiescent galaxies (red). The observations are on the left and the SAM predictions are on the right. The shaded regions span the 25th to 75th percentiles of each distribution, whereas the symbols and lines represent the medians of those distributions. See subsection 4.2 for how the star-forming and quiescent subpopulations were stellar mass-matched to the transition subpopulation in each redshift slice. The quiescent predictions from the SAM have been truncated at $z = 2.6$ due to the low number of quiescent galaxies in the highest SAM redshift slice. The transition population tends to have intermediate values of these three structural properties relative to the star-forming and quiescent populations in both the observations and the SAM.

Redshift Slice	n^{SF}	n^{T}	n^{Q}	$r_{\text{hl}}^{\text{SF}}$ [kpc]	r_{hl}^{T} [kpc]	r_{hl}^{Q} [kpc]	$\Sigma_{1.5}^{\text{SF}}$ [log M_{\odot} kpc $^{-1.5}$]	$\Sigma_{1.5}^{\text{T}}$ [log M_{\odot} kpc $^{-1.5}$]	$\Sigma_{1.5}^{\text{Q}}$ [log M_{\odot} kpc $^{-1.5}$]	Sample
–	–	–	–	–	–	–	–	–	–	–
$0.005 < z < 0.12$	$1.31^{+0.31}_{-0.16}$	$1.89^{+0.70}_{-0.49}$	$2.46^{+0.67}_{-0.54}$	$6.81^{+3.51}_{-2.12}$	$6.11^{+2.75}_{-1.78}$	$6.30^{+4.59}_{-2.87}$	$9.23^{+0.28}_{-0.23}$	$9.32^{+0.29}_{-0.25}$	$9.36^{+0.30}_{-0.24}$	SAM
$0.5 < z < 1.0$	$1.53^{+0.28}_{-0.23}$	$2.20^{+0.56}_{-0.53}$	$2.71^{+0.66}_{-0.64}$	$4.56^{+1.55}_{-1.55}$	$3.58^{+2.07}_{-1.16}$	$2.90^{+1.88}_{-1.21}$	$9.53^{+0.26}_{-0.26}$	$9.67^{+0.29}_{-0.25}$	$9.77^{+0.31}_{-0.31}$	SAM
$1.0 < z < 1.4$	$1.56^{+0.48}_{-0.30}$	$2.20^{+0.70}_{-0.66}$	$2.94^{+0.47}_{-0.74}$	$4.00^{+2.13}_{-1.47}$	$3.12^{+1.89}_{-1.04}$	$1.83^{+2.58}_{-1.04}$	$9.61^{+0.30}_{-0.28}$	$9.77^{+0.29}_{-0.29}$	$9.99^{+0.30}_{-0.34}$	SAM
$1.4 < z < 1.8$	$1.55^{+0.41}_{-0.38}$	$2.05^{+0.68}_{-0.65}$	$2.95^{+0.56}_{-0.56}$	$3.27^{+1.74}_{-1.18}$	$2.72^{+1.69}_{-1.04}$	$1.43^{+1.04}_{-0.76}$	$9.75^{+0.28}_{-0.28}$	$9.88^{+0.28}_{-0.28}$	$10.20^{+0.26}_{-0.26}$	SAM
$1.8 < z < 2.2$	$1.44^{+0.34}_{-0.23}$	$1.87^{+0.56}_{-0.39}$	$2.87^{+0.60}_{-0.60}$	$3.12^{+1.62}_{-1.06}$	$2.76^{+1.69}_{-0.96}$	$1.23^{+0.76}_{-0.32}$	$9.78^{+0.29}_{-0.29}$	$9.92^{+0.26}_{-0.27}$	$10.34^{+0.25}_{-0.23}$	SAM
$2.2 < z < 2.6$	$1.31^{+0.25}_{-0.15}$	$1.65^{+0.45}_{-0.30}$	$2.27^{+0.44}_{-0.44}$	$3.43^{+1.68}_{-0.95}$	$3.25^{+1.68}_{-0.94}$	$1.80^{+0.75}_{-0.30}$	$9.74^{+0.25}_{-0.29}$	$9.83^{+0.25}_{-0.24}$	$10.16^{+0.23}_{-0.25}$	SAM
$2.6 < z < 3.0$	$1.15^{+0.15}_{-0.09}$	$1.44^{+0.30}_{-0.22}$	–	$4.05^{+0.49}_{-0.49}$	$4.42^{+1.03}_{-1.05}$	–	$9.60^{+0.20}_{-0.21}$	$9.67^{+0.24}_{-0.26}$	–	SAM

Table 5. Same as Table 4 but for the SAM. Since there are so few quiescent galaxies in the SAM at $2.6 < z < 3.0$, we do not measure the distribution of structural properties for quiescent galaxies in that redshift bin.

galaxies. It is important to note that in this picture, there is no need for “compaction” – transition and quiescent galaxies are more compact than star-forming galaxies not because any mass was transferred toward or grown in their centers, but rather simply because they stopped increasing in size at an earlier epoch, when all galaxies were smaller.

It seems likely that “progenitor bias” plays some role in explaining the structural distinctness of star-forming, transition, and quiescent galaxies. However, it is still unclear whether it alone can account for all of the observed effect. It is quite possible that both the “progenitor bias” picture and the “compaction” picture are at play in the Universe. We also refer the reader to section 6.2.3 of our companion paper (Brennan et al. 2016), which directly addresses the contribution of progenitor bias in our SAM.

6.2 Average Population Transition Timescale as a Function of Redshift

We are in a unique position to place an upper limit on the average population transition timescale out to $z = 3$, by explicitly using the transition population that we have defined in the observations. To do this, we need to make the extreme assumption that transition galaxies observed at any given epoch are all moving from the SFMS toward quiescence, and that they will only make this transition once (i.e., no rejuvenation events). In the future, it will be necessary to re-examine this extreme assumption after we have more constraints on the following: the full distribution of possible quenching and rejuvenation timescales, the redshift evolution of these timescale distributions, the relative frequency of quenching and rejuvenation events as a function of redshift, and the fraction of galaxies that are merely undergoing large “oscillatory excursions” below the SFMS rather than genuinely moving toward quiescence (see also section 7 for our theoretical discussion of these topics).

In Appendix C, we show cubic polynomial fits to the observed number densities of star-forming, transition and quiescent galaxies as a function of redshift. We can use our smooth fits and the redshift-age relation to compute the average population transition timescale as a function of redshift with the following equation:

$$\langle t_{\text{transition}} \rangle_{z_1, z_2} = \langle n_{\text{transition}} \rangle_{z_1, z_2} \times \left(\frac{dn_{\text{quiescent}}}{dt} \right)_{z_1, z_2}^{-1}. \quad (3)$$

Here, $\langle t_{\text{transition}} \rangle_{z_1, z_2}$ is the average population transition timescale between two closely spaced redshifts z_1 and z_2 , $\langle n_{\text{transition}} \rangle_{z_1, z_2}$ is the average number density of transition

galaxies within those two redshifts, and $\left(\frac{dn_{\text{quiescent}}}{dt} \right)_{z_1, z_2}$ is the change in the number density of quiescent galaxies with respect to the age of the Universe elapsed between those two redshifts. We remind the reader that, in this paper, we focus only on massive galaxies with $M_* > 10^{10} M_{\odot}$.

The results of our calculation are shown in Figure 5. It is immediately apparent that $\langle t_{\text{transition}} \rangle_{z_1, z_2}$ rises smoothly from $z = 3$ toward $z = 0$. This finding explicitly quantifies the notion that, on average, galaxies at high-redshift are on a “fast track” for quenching (~ 0.8 Gyr at $z \sim 2.5$) whereas galaxies at low-redshift are on a “slow track” for quenching (~ 7 Gyr at $z \sim 0.5$), as schematically described in Barro et al. (2013). Note that our upper limit on the average population transition timescale is below the age-redshift relation, particularly at high redshift. This is a natural consequence of the apparent existence of highly quiescent galaxies far below the SFMS at these high redshifts, and it suggests that star-forming galaxies are able to make the transition to quiescence faster than the growing age of the Universe at these very early times. Note that if galaxies go through the transition region multiple times due to rejuvenation events, then our measurements can also be interpreted as quantifying the average total time spent in the transition region (i.e., the sum of all such transits). This effect likely plays some role in the longer average population transition timescale at low redshift (since galaxies have had more time to undergo rejuvenation events by then). On the other hand, the steep rise in the GAMA transition fraction that we discussed in subsection 5.2 could also be playing a role.

We emphasize that these calculations and conclusions pertain to the average population at each redshift. We simply do not yet have the necessary observational constraints to comment meaningfully on the statistical diversity of individual galaxies’ transition timescales, but explicitly studying the transition timescale of the average galaxy observed at each redshift is an important first step (e.g., Behroozi et al. 2013). Furthermore, since our SAM does not yet reproduce enough heavily quiescent galaxies at high redshift, we are unable to place a meaningful constraint on the average population transition timescale as a function of redshift for the SAM as we did for the observations. The existence of so few heavily quiescent galaxies at $z \sim 2.5$ and their very slow build-up toward $z \sim 1$ (see Figure 3) means that Equation 3 would necessarily return large values at $z \geq 1$ for the SAM. However, in the future, our results and the methodology presented here can be adopted to tune such models to bring them into better agreement, on average, with the observations.

As we continue to learn more about the full distribu-

tions of possible quenching and rejuvenation timescales and their dependence on other galaxy properties, Equation 3 can be modified and Figure 5 can be decomposed based on various attributes (e.g., morphology, environment, and gas content). This is tremendously difficult to do at present because we do not completely understand the interrelationships between, e.g., SFHs and bulge formation histories (but see our theoretical discussion of this in subsection 7.5). For instance, it is highly non-trivial to account for the fact that galaxies may not preserve their morphological class as they undergo SFH transitions. Quiescent disk-dominated galaxies can undergo dry mergers and become quiescent bulge-dominated galaxies, whereas transition disk-dominated galaxies might themselves undergo secular physical processes that transform them into transition bulge-dominated systems (see also Brennan et al. 2015).

It is necessary to briefly comment on post-starburst galaxies, which have inferred fast quenching timescales and short observability timescales at all redshifts.⁴ Wild et al. (2016) recently identified post-starburst galaxies at $0.5 < z < 2$ using a novel SED fitting technique based on principal component analysis, and then employed a simple scaling argument to match the stellar mass functions of the quiescent and post-starburst populations. Their simple scaling argument suggests that the relatively rare population of post-starburst galaxies can account for the majority (up to one hundred percent) of massive red sequence galaxies formed over the past several Gyr. However, the simple scaling argument of Wild et al. (2016) does not seem to account for the spread in the sSFR distribution of galaxies below the SFMS. As we have suggested in this paper, the observed spread in the degree of quiescence of galaxies below the SFMS might already be a clue that galaxies have a diversity of quenching and rejuvenation timescales. While post-starburst galaxies may indeed account for a significant fraction of the growth of the quiescent population across cosmic time, additional work is needed in order to disentangle the relative contributions of the slow quenching, fast quenching, rejuvenating, and post-starburst transition pathways (see our theoretical discussion in section 7; and also, e.g., Dressler et al. 2013; Belli et al. 2015).

6.3 Beyond Average Trends, and Using the Transition Population to Probe Systematic Uncertainties

In population studies such as ours, we are inherently drawn to make statements about average trends rather than the diversity of individual objects. For example, much of our analysis of structural properties was based tightly around the median: Figure 4 shows the 25–75th percentiles of each

⁴ We emphasize that, just like for our more broadly defined transition population, it is also not straightforward to observationally define post-starburst galaxies, with there being a slew of definitions adopted in the literature (this issue is discussed in, e.g., Pattrakijwanich et al. 2014; Yesuf et al. 2014; Haines et al. 2015; Alatalo et al. 2016c). In particular, it is a non-trivial task to observationally constrain the properties of the immediate progenitors of post-starburst galaxies, including for how long their starburst was sustained before finally being recently truncated (e.g., see the insightful discussion in section 4.2 of Wild et al. 2016).

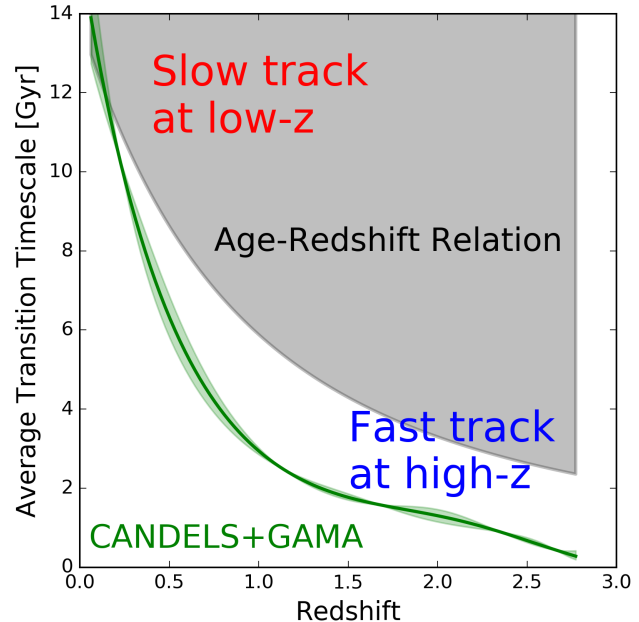


Figure 5. Observational upper limit on the average population transition timescale as a function of redshift (solid green line). The green shaded area reflects the 1σ uncertainty in our polynomial fits to the number densities of transition and quiescent galaxies as a function of redshift, as shown in Figure C1. The gray shaded area reflects transition timescales that would be greater than the age of the Universe at that redshift (i.e., the age-redshift relation). Our measurements are below the age-redshift relation because we do observe quiescent galaxies (even at high-redshift), meaning that they have had enough time at early epochs to make the transition to quiescence. Note how the average population transition timescale is consistent with “fast track” quenching at high redshift but “slow track” quenching at low redshift. These calculations are based on massive galaxies only, with $M_* > 10^{10} M_\odot$.

structural property distribution. In that respect, we are focusing on the “typical” star-forming, transition and quiescent galaxies in each epoch (this is not entirely unlike how some studies might choose to focus only on the evolution of “compact” galaxies; e.g., Barro et al. 2014; Wellons et al. 2015; van Dokkum et al. 2015). However, there certainly exist atypical galaxies such as star-forming spheroid-dominated galaxies (e.g., Schawinski et al. 2009; Kaviraj 2010; McIntosh et al. 2014; Haines et al. 2015) and quiescent disk-dominated galaxies (e.g., Masters et al. 2010a,b; Bundy et al. 2010), which live in the tails of their parent populations (see also Vulcani et al. 2015; Brennan et al. 2015). These atypical galaxies might be intimately related to transition galaxies, and they suggest that there is a great diversity in the set of all evolutionary pathways. In other words, the existence of atypical galaxies already supports the argument that not all transition galaxies must necessarily be on the same evolutionary track between the SFMS and the quiescent region (see also our theoretical discussion in section 7).

We are only now beginning to observationally constrain the individual SFHs and structural evolutionary histories of a handful of objects at $z \gtrsim 2$ (e.g., Barro et al. 2016a) and a statistical number of objects at $z \sim 1$ (e.g., Dressler et al. 2016; van der Wel et al. 2016). The constraints on individual

SFs have been made possible due to the availability of very deep spectroscopy with relatively high spectral resolution, to which we can robustly fit stellar population synthesis models and derive non-parametric SFHs (e.g., [Pacifici et al. 2012](#); [Leja et al. 2016](#)). Future large-scale deep spectroscopic campaigns and the construction of even more densely-sampled panchromatic SEDs than are available in the CANDELS and GAMA datasets should allow for much finer constraints on the SFHs of individual transition galaxies as a function of redshift, mass, and morphology (e.g., [Takada et al. 2014](#); [Domínguez Sánchez et al. 2016](#); [Fumagalli et al. 2016](#); [van der Wel et al. 2016](#)).

While it is indeed promising and compelling that models are beginning to at least qualitatively reproduce observational results derived from statistical samples of galaxies (see [Somerville & Davé 2015](#)), it is sobering to realize just how many basic questions arise when we try to explicitly define and study this so-called “transition” population, which we believe must exist in one form or another. A major issue is that we want to study rest-frame colors, relatively “instantaneous” SFRs, and ultimately the full SFHs of galaxies, but all of these are based onx fundamental assumptions made during the SED fitting process (which, in the end, relies critically on getting the redshift correct). If there are any fundamental flaws in our SED fitting assumptions (e.g., universal IMF, universal dust attenuation law, simple SFH parameterizations, assumed light profiles for bulge-disk decompositions, and so on), future attempts at defining and characterizing the transition population may reveal important clues about those problems. Here we briefly comment on potential future improvements on the work we have presented in this paper.

On the observational side, it will be crucial to obtain a sharper view of [Figure 4](#), which suggests that bulges directly trace the evolution of galaxies as they fall below the SFMS. The structural measurements that we have used in this paper are based on single-component Sérsic profile fits ([van der Wel et al. 2012](#)). Although there are considerable uncertainties associated with bulge-disk decompositions and non-parametric approaches, these are additional tools with which we can observationally probe the relationship between morphological change timescales and transition timescales (e.g., [Lackner & Gunn 2012](#); [Conselice 2014](#); [Bruce et al. 2014](#); [Lang et al. 2014](#); [Peth et al. 2016](#); [Margalef-Bentabol et al. 2016](#)). Fitting and comparing structural profiles across the full suite of available multi-wavelength imaging (e.g., [Häußler et al. 2013](#); [Vika et al. 2013](#)), studying spatial gradients (e.g., [Haines et al. 2015](#); [Liu et al. 2016](#)), and deriving the full posterior distributions of structural properties of individual galaxies using a Bayesian framework (e.g., [Yoon et al. 2011](#)) may also yield physical insights. In particular, such improvements to structural measurements may allow us to distinguish “globally quiescent” galaxies from those that are still undergoing star formation outside of the bulge/core component (either inside-out quenching or residual star formation on the outskirts; e.g., [Fang et al. 2012](#); [Salim et al. 2012](#); [Wuyts et al. 2012](#); [Nelson et al. 2012](#); [Patel et al. 2013](#); [Abramson et al. 2014](#); [Tacchella et al. 2015, 2016b](#); [Nelson et al. 2016](#)).

On the theoretical side, we have argued that it is better to use SFRs than colors to define the transition population, especially at high redshift. This is because SFRs are rela-

tively “instantaneous” indicators (10-100 Myr timescales), whereas galaxy colors (depending on the adopted bandpasses) tend to probe the sum of several different stellar populations that may have formed at a variety of redshifts, and can be more sensitive to treatments of dust and metallicity. Nevertheless, SFRs can still be highly uncertain for galaxies that are not actively and continuously forming stars (i.e., galaxies below the SFMS). We know that severe systematic uncertainties in SFRs and stellar masses can arise if underlying assumptions such as a [Chabrier \(2003\)](#) IMF or a [Calzetti et al. \(2000\)](#) dust reddening law are invalid (e.g., see [Conroy et al. 2009](#); [Treu et al. 2010](#); [Conroy et al. 2010](#); [Conroy & van Dokkum 2012](#); [Conroy 2013](#); [Cappellari et al. 2012](#); [Reddy et al. 2015](#); [Salmon et al. 2016](#)). Uncertainties in the calibration of stellar population synthesis models (e.g., [Bruzual & Charlot 2003](#)) and failure to account for the impact of rare but important stellar populations (e.g., thermally-pulsating asymptotic giant branch stars; [Maraston et al. 2006](#); [Rosenfield et al. 2014](#); [Fumagalli et al. 2014](#); [Villaume et al. 2015](#)) on galaxy SEDs can also increase systematic uncertainties on observationally-derived physical parameters. These systematic errors are then hard to quantify in large statistical studies that are based on SED fitting, such as ours.

7 THEORETICAL DISCUSSION

7.1 Physical Significance of Transition Galaxies

Our current understanding of galaxy evolution – based on both observations and theory – demands that galaxies must flow between the SFMS and varying degrees of quiescence. As is well known, star-forming galaxies occupy a tight sequence in the sSFR- M_* diagram but quiescent galaxies are more diffusely distributed. This is different from classical color-magnitude diagrams, in which it is the quiescent galaxies that form a tight “red sequence.” It is difficult to use this red sequence to theoretically probe the diverse formation histories of quiescent galaxies because: (1) its normalization is due to the physics of stellar evolution, whereby stellar populations approach a maximally red color as they age, and (2) its intrinsic scatter is thought to be due to a degeneracy between age, dust, and metallicity for producing red colors, which has historically been a difficult phenomenon to disentangle both theoretically and observationally. Luckily, the tightness of the SFMS in the sSFR- M_* plane is thought to be due to self-regulation of star formation by stellar-scale feedback processes (e.g. [Somerville & Davé 2015](#); [Hopkins et al. 2014](#); [Sparre et al. 2015](#); [Hayward & Hopkins 2015](#); [Rodríguez-Puebla et al. 2016b](#)).⁵ In both sophisticated hydrodynamical simulations and simpler SAMs, galaxies tend to remain close to an “equilibrium” condition, in which the net inflow of gas is approximately balanced by outflows and

⁵ See [Kelson \(2014\)](#) for an alternative view about the tight scatter and correlation of the SFMS being due to the central limit theorem. It is still unclear how this interpretation would be affected by the fact that the observed stellar masses of galaxies need not be due entirely to their *in situ* star formation rates, but that they can also be grown through mergers and accretion of satellites (e.g., [Naab et al. 2007](#); [Lackner et al. 2012](#)).

the consumption of gas by star formation (see discussion in Somerville & Davé 2015, and references therein). When this equilibrium is disrupted by shutting off the inflow of new gas, galaxies naturally drop below the SFMS as they consume their remaining gas.

This highlights how much information transition galaxies potentially carry about the physical cause of the disruption of equilibrium and its timescale. A variety of processes have been suggested in the literature as possible ways to quench galaxies, including gravitational heating of the hot gas halo (sometimes called “halo quenching”; Birnboim & Dekel 2003; Dekel & Birnboim 2006), morphological quenching (Martig et al. 2009), tidal and ram pressure stripping (e.g., Kang & van den Bosch 2008), and radiative and jet mode AGN feedback (see Somerville & Davé 2015, and references therein). It is worth noting that quenching processes may be “ejective” (quenching is caused by removal of the ISM, usually on rapid timescales), “preventive” (quenching begins after gas inflows are shutdown and the galaxy consumes its existing gas supply), or “sterilizing” (gas remains present in the galaxy, but is rendered unable to form stars efficiently for some reason). These different types of processes should have distinct signatures in terms of the morphology, gas content, and large scale environment of transition galaxies. However, the issue is complicated by the fact that the “same” process, broadly construed (e.g., AGN feedback), can manifest in ways that are ejective, preventive, and sterilizing. For example, AGN are known to drive powerful outflows (ejective), cause heating of the extended diffuse gas in halos (preventive), and their hard radiation field may photo-dissociate molecules leading to inefficient star formation (sterilizing).

On the one hand, the qualitative reproduction of the observational trends by the SAM suggests a possible general picture for interpreting the observations. On the other hand, the quantitative discrepancies between the SAM predictions and the observational results may tell us something about the limitations of these models, or revisions that should be made to physical processes within them. The SAMs reproduce the observed trend that quiescent galaxies have the highest, star-forming galaxies have the lowest, and transition galaxies have intermediate Sérsic index values at all redshifts. In the models, this is a direct result of the connection between the main quenching mechanism (AGN feedback) and the growth of a central bulge (see the extensive discussion in Brennan et al. 2016). In contrast, the SAM clearly does not produce enough quiescent galaxies at high redshift (Figure 3). This is due to some combination of the following factors in the SAM: (1) the overall rate at which star-forming galaxies begin to quench is too low, (2) quenching galaxies take too long to go through the transition region, or (3) quiescent galaxies are rejuvenating too much. We will argue below that the main culprit is that the quenching timescales at high redshift are too long.

For the purposes of this section, we have run twenty SAM realizations of 100 different halo masses, leading to 2000 halos whose masses span $10^{10} M_\odot < M_h < 10^{15} M_\odot$ at $z = 0$. For simplicity, we will restrict the following discussions only to the central galaxies of these halos, and exclude all the satellites since they are subject to additional physical processes that we will not focus on here (e.g., tidal stripping). We will further require $M_* > 10^{10} M_\odot$ at $z = 0$, which

leaves us with ~ 1300 massive central galaxies. We note that the galaxy histories that we have pulled out of the SAM for this section are quite general, and that our aim is partly to motivate future studies using cosmologically representative sets of $z = 0$ halos.

7.2 The Diversity of Transition Pathways

Even in population studies, we can learn a lot by first studying the diverse evolutionary histories of individual galaxies (e.g., see Brennan et al. 2015; Wellons et al. 2015; Trayford et al. 2016). In this section, we will ask: how do galaxies move in sSFR- M_* space and what does the diversity of transition pathways tell us about the underlying physics that governs galaxy evolution? We have identified four dominant evolutionary modes for SFHs in our SAM: oscillations on the SFMS, slow quenching, fast quenching, and rejuvenation of quiescent galaxies. In Figure 6, we show twenty representative SFHs from the SAM; these SFHs were chosen to illustrate the four main evolutionary modes that repeatedly occur for galaxies in the SAM. We use the colorbar as a third dimension to show how the stellar mass-weighted B/T ratio evolves alongside each SFH. The bottom row of Figure 6 shows five additional SFHs that were pulled from a state-of-the-art hydrodynamical simulation with mechanical AGN feedback (Choi et al. 2016); these will be discussed in subsection 7.4.

For reference, in each panel we also show the time evolution of the transition region as defined for the SAM in this paper. The decreasing normalization of the transition region toward low redshift reflects the fact that a galaxy classified as transition at high-redshift would be considered star-forming if it were relocated to $z \sim 0$ (based on its sSFR). We also show the time evolution of the SFMS and its $\pm 1\sigma$ scatter as predicted by the independent Stellar-Halo Accretion Rate Coevolution model (SHARC; Rodríguez-Puebla et al. 2016b), in which the SFR of central galaxies is determined by the overall halo mass accretion rate. The SFMS of the SAM shows remarkable agreement with the SHARC prediction.

The first evolutionary mode for SFHs is that of oscillations on the SFMS (top row of Figure 6). These oscillations are due to some combination of variations in a galaxy’s gas accretion rate, and the interplay between star formation and stellar-scale feedback processes. The overall halo mass accretion rate can also play a role: when the mass accretion rate of a halo drops faster than that of an average halo, the decline in the sSFR of the central galaxy has a steeper slope than the decreasing normalization of the SFMS with redshift (this occurs for halos that assembled their mass earlier than average). In general, these oscillations are consistent with the 1σ scatter of the SFMS (see also the SHARC model; Rodríguez-Puebla et al. 2016b). Galaxies tend to remain disk-dominated ($B/T < 0.5$) during their oscillations, but this is expected given that they are undergoing continuous star formation. Similar oscillatory behavior is seen in the hydrodynamical simulations discussed by Dekel & Burkert (2014); Zolotov et al. (2014); Tacchella et al. (2016a). An intriguing implication of this first evolutionary mode is that star-forming galaxies can dip into the transition region briefly and then ascend back onto the SFMS. Two notable examples are shown in Figure 6: both T754 and Q787

have quite large excursions and dominant bulges. If such oscillation-induced dips into the transition region are accompanied by significant bulge growth and culminate in quiescence at high redshift, then such galaxies observed during their transition phase may be the so-called “green nuggets,” the direct descendants of compact star-forming galaxies and immediate progenitors of compact quiescent galaxies observed at $z \sim 2$ (Zolotov et al. 2014; Dekel & Burkert 2014; Barro et al. 2016a). On the other hand, this first mode can also include rare cases like SF816 and SF772, in which the galaxy has “lived high” on the SFMS for its whole life (effectively maintaining a constant SFH since $z \sim 3$). It is far above the SFMS at $z = 0$ not because it is experiencing a classical starburst, but simply because its halo mass accretion rate (and therefore gas accretion rate) was higher than that of an average SFMS galaxy.

In the second evolutionary mode for SFHs, galaxies undergo “slow quenching” that can lead to extremely long times spent in the transition region (second from top row in Figure 6). This is driven mainly by mergers and the SMBH accretion rate, but is also affected on some level by the halo mass accretion history. We emphasize the diversity of morphological evolutionary histories accompanying this slow quenching pathway: all five representative galaxies shown for this mode in Figure 6 underwent a merger (which appears to initiate all slow quenching events in the SAM), but not all of them developed a dominant bulge (e.g., Q1083 would be considered a “disk-dominated” quiescent galaxy at $z = 0$; see also our discussion in subsection 7.5). It has long been noted that many galaxies that are observed to live in the classical green valley do not show any obvious signs of recent or ongoing violent star formation suppression mechanisms like AGN feedback; two prominent examples, at least in terms of the classical green valley, are the Milky Way (Bland-Hawthorn & Gerhard 2016) and M31 (Mutch et al. 2011; Williams et al. 2015). Resolved stellar population studies of M31 might teach us a lot about this “slow quenching” mode. Williams et al. (2015) used the Panchromatic Hubble Andromeda Treasury (PHAT; Dalcanton et al. 2012) to determine that a major global star formation event occurred in M31 roughly 2–4 Gyr ago. Although the cause of the event is unknown, the main proposed scenarios invoke tidal interactions with M32 and/or M33, or a major merger with another galaxy that became part of what we now call M31 (see section 4 of Williams et al. 2015, and references therein). Detailed bulge-disk-halo-nucleus decompositions of M31’s light reveal complex structures even though on a global scale the galaxy would be considered merely “disk-dominated”; namely, that a massive bulge dominates within ~ 1.5 kpc, and that the stellar halo exhibits intricate streams (Courteau et al. 2011; Dorman et al. 2013, and references therein). It is clear that whatever happened to M31, a violent quenching event did not rapidly drive the entire galaxy toward a state of heavy quiescence and heavy “bulge dominance” – regardless of whether the SMBH was fed or whether the bulge grew in mass and size.

The third evolutionary mode for SFHs involves rapidly quenching galaxies with radiatively efficient AGN feedback that is triggered by mergers (middle row in Figure 6). Recall that in the SAM shown here, there are two modes of AGN feedback: (1) radiation pressure-driven winds that correspond to the rapid accretion phase of the black hole and

quickly remove the cold gas, and (2) the jet mode feedback which can act as a “maintenance mode” and prevent hot halo gas from further cooling and accreting into the galaxy. The significant bulge growth associated with major mergers and the subsequent “ejective” feedback associated with radiative mode are crucial in our SAM for producing the bulge-dominated quiescent galaxies that we observe in CANDELS at very early times ($z \sim 3$). However, Figure 6 reveals that not all fast quenching events act at early times (e.g., Q972), and that not all such events lead to “pure bulge” (elliptical) remnants (e.g., Q880 and Q1495 have roughly intermediate B/T for roughly half the age of the Universe). Furthermore, some “fast quenching” pathways like Q1941 take ~ 2 Gyr to get through the transition region at $z \sim 3$, but that is a very large fraction of the age of the Universe at those early times. In subsection 7.4, we will explore high-redshift quenching timescales using state-of-the-art hydrodynamical simulations with mechanical AGN feedback (from Choi et al. 2016).

In some cases, the “maintenance mode” of AGN feedback fails to fully do its job of keeping the halo gas hot, and so the gas manages to cool and reignite star formation in the galaxy. This leads to the fourth evolutionary mode for SFHs in the SAM: rejuvenation (second from bottom row in Figure 6). Mergers can also bring in gas, causing brief rejuvenation events before the galaxy drops into quiescence once again. It is important to clarify that rejuvenation consists of two phases that occur on very different timescales. First, the galaxy’s sSFR jumps many orders of magnitude from quiescence back onto the SFMS (or perhaps into the transition region). Then, the galaxy will at some point begin to “refade”; this can certainly be sped up with quenching events as described above. The actual rejuvenation event occurs on a much faster timescale than the subsequent “re-fading” phase. The reason for this is that a galaxy’s color will become bluer due to the appearance of newly-born young stars on a much faster timescale compared to the subsequent reddening of the stellar population. This means that, in general, galaxies in the transition region will be caught during their declining sSFR phase rather than their increasing sSFR phase. With that said, it might still be interesting to speculate about the possible existence of “slow rejuvenation” tracks (e.g., due to a steady sequence of very minor star formation episodes). Constraining the physical mechanisms that could give rise to such “slow rejuvenation” tracks, and identifying their corresponding observables, might help place firm limits on the fraction of galaxies in the transition region that are actively rejuvenating rather than once again moving toward quiescence.

All of this begs the question: how do we observationally identify which galaxies in the transition region are merely undergoing large oscillations on the SFMS, very slowly fading towards quiescence, or rapidly being quenched? In addition to the costly method (especially at high redshift) of constructing non-parametric SFHs using spectroscopy, one way to proceed might be to attempt to link the four evolutionary modes for SFHs that we have identified in the SAM to the many other histories of galaxies (structural, dynamical/kinematical, and so on). Another way is to explore the predicted range of transition timescales for each of the four modes and their associated physical processes. Ultimately, we would want to understand the relative frequency with

which each of the four evolutionary modes occurs in a cosmological context (i.e., their dependence on redshift, stellar mass, halo mass, and so on). Many of these questions are beyond the scope of this paper, but in the remaining subsections, we will briefly explore these topics.

7.3 Transition Region Occupation Timescales

In the previous subsection, we showed representative SFHs and identified four dominant modes for how galaxies evolve in the sSFR- M_* diagram in our SAM. We will now present a statistical analysis of our ~ 1300 SFHs and use the transition population to diagnose why the SAM is under-predicting the quiescent fraction at high-redshift relative to the observations (see Figure 3). Specifically, for galaxies classified as star-forming, transition or quiescent at $z = 0$, we can study how much time they have collectively spent in the SFMS, transition region and quiescent region since $z = 3$. To do this, we simply trace each galaxy’s SFH back to $z = 3$ and count up the total time that it has spent in the three different regions of the sSFR- M_* diagram (while accounting for the fact that the normalizations of these three regions increase smoothly toward high redshift). It is crucial that we do not assume some parameterization for the SFH (e.g., exponentially decaying single- τ models) since many such parameterizations may not accurately capture the bursty, stochastic, and non-monotonic nature of our SFHs (see also our morphology-related discussion in subsection 7.5 and, e.g., Pacifici et al. 2015). To get a cleaner estimate of the transition region occupation timescale (as a diagnostic of the quenching timescale), we can discard galaxies that have rejuvenating SFHs (i.e., galaxies which have traversed the transition region multiple times). We identify galaxies with rejuvenating SFHs by applying a crude threshold of at most five timesteps since $z = 3$ in which: (1) a $z = 0$ star-forming galaxy can be quiescent in its history, (2) a $z = 0$ transition galaxy can be quiescent in its history, and (3) a $z = 0$ quiescent galaxy can be star-forming or transition after the first time in its history that it became quiescent.

In the SAM, we find that 13% of $z = 0$ star-forming galaxies, 25% of $z = 0$ transition galaxies, and 31% of $z = 0$ quiescent galaxies have experienced rejuvenation events since $z = 3$. Because the time spent on the upward rejuvenation track is far shorter than the time spent on the subsequent re-fading track, we do not expect the upward portion of rejuvenation tracks to significantly contaminate the transition region occupation timescale distribution. However, since the downward portion of rejuvenation tracks (i.e., the “re-fading” phase) can significantly increase a galaxy’s total time spent in the transition region, we restrict the following analysis to galaxies that have non-rejuvenating SFHs. We note, however, that including the rejuvenating SFHs does not alter our conclusions because only a minority of our ~ 1300 SFHs have significant rejuvenation events.

In Figure 7, we show cumulative distribution functions of the SFMS occupation timescale, transition region occupation timescale, and quiescent region occupation timescale. Each of these CDFs is split into three categories based on the classifications of galaxies at $z = 0$ as star-forming, transition or quiescent. The CDFs extend up to a maximum timescale of 12 Gyr (roughly the time elapsed since $z = 3$). We will

now consider the CDFs for each of the three different regions in turn.

7.3.1 Total Time on the SFMS

Galaxies classified as star-forming at $z = 0$ have a median SFMS occupation timescale of ~ 11 Gyr since $z = 3$, which implies that they have led rather quiet lives in terms of their SFHs. The very small tail toward lower SFMS occupation timescales identifies galaxies that underwent significant oscillations into the transition region, which would naturally lower their total time spent on the SFMS since $z = 3$. We remind the reader that this analysis is restricted to non-rejuvenating SFHs, which means that we do not consider galaxies that are classified as star-forming at $z = 0$ but that underwent very deep oscillations into the quiescent region at earlier times (e.g., Q787 in Figure 6). Broadly considered, our conclusions in this paragraph are not affected by such deep oscillatory SFHs or by bona fide rejuvenation cases (i.e., where a galaxy undergoes slow/fast quenching, becomes quiescent, and then re-joins the SFMS at a later time) because only $\sim 13\%$ of $z = 0$ SFMS galaxies have rejuvenating SFHs.

Galaxies that are classified as transition at $z = 0$ have a median SFMS occupation timescale of ~ 8 Gyr since $z = 3$. At first, this might suggest that the average $z = 0$ transition galaxy stayed on the SFMS for 8 Gyr and therefore did not enter the transition region until $z \sim 0.3$ (the redshift corresponding to 8 Gyr after $z = 3$). However, such long times spent on the SFMS could be the result of either oscillatory behavior, a fast quenching event at late times, or a slow quenching event at intermediate/late times. For example, T754 (shown in Figure 6) has been undergoing large oscillations on the SFMS for many Gyr, and it just happened to be caught in the transition region at $z = 0$. In contrast, the sSFR of T1537 was smoothly declining like that of the average SFMS galaxy, but then at $z \sim 0.6$, it underwent a slow quenching event which finally brought it into the transition region at $z \sim 0.01$ (due to a combination of merger history, halo mass accretion history, and eventual gas exhaustion).

There is a sharp drop-off toward lower values in the distribution of SFMS occupation timescales for $z = 0$ transition galaxies. Effectively none of them have spent less than 2 Gyr since $z = 3$ in the SFMS. This lack of very low times spent in the SFMS tells us that it is rare for a galaxy to start a slow quenching event close to $z = 3$ and still remain in the transition region by $z = 0$; many of these will in fact become quiescent by $z = 0$ (see below). Cases like T1478 (see Figure 6) are extremely rare in the SAM: this galaxy spent ~ 2 Gyr since $z = 3$ on the SFMS, underwent slow quenching for the next ~ 9 Gyr, and still remained in the transition region at $z = 0$. Interestingly, this galaxy ended up with intermediate B/T at $z = 0$; see our morphology-related discussion in subsection 7.5. In some cases, a galaxy undergoes a slow quenching event at high redshift, enters the transition region, but then undergoes a gas-rich merger that brings it back onto the SFMS. Thus, the process of slow/fast quenching is initiated all over again. Note that since the galaxy never became quiescent, this is not considered a classical “rejuvenation” event; its overall effect on the SFH is similar to that of oscillations on the SFMS.

Ultimately, the interplay between all of the possibilities

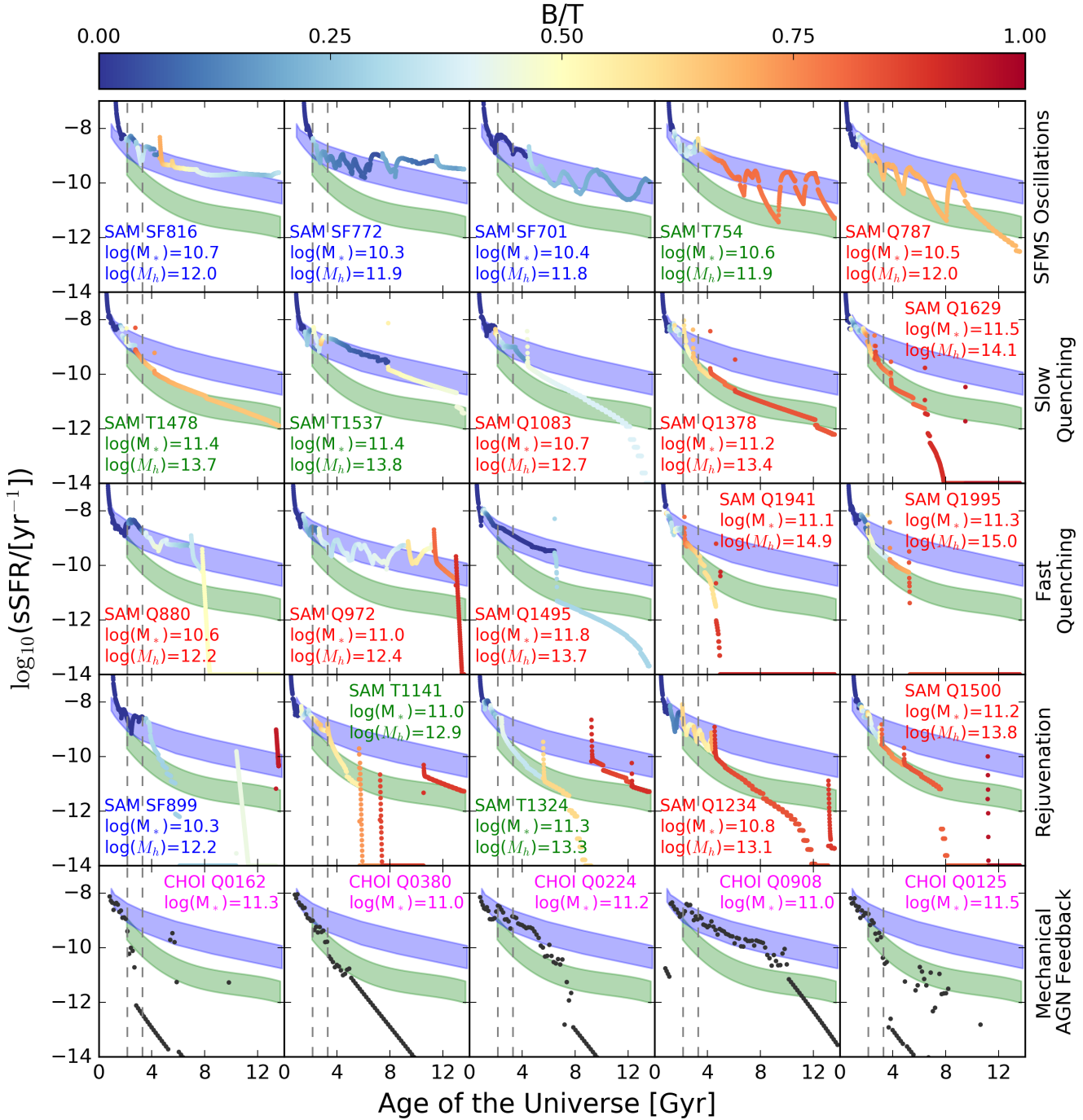


Figure 6. Representative SFHs for central galaxies in the SAM, grouped into the four dominant modes of evolution in sSFR- M_* space that we have identified: oscillations on the SFMS (top row), slow quenching (second from top row), fast quenching (middle row), and rejuvenation (second from bottom row). The label for each galaxy is color-coded according to its classification at $z = 0$ as star-forming (blue), transition (green), or quiescent (red). Also shown on the bottom row are SFHs of galaxies from the hydrodynamical simulations of Choi et al. (2016), which are all quiescent at $z = 0$ and include a state-of-the-art implementation of mechanical AGN feedback (magenta labels). Only for the SAM, the colorbar is used to show how the B/T value of the galaxy varies alongside its SFH. The two dashed vertical lines mark $z = 3$ (left) and $z = 2$ (right). The blue shaded region is the time evolution of the SFMS and its $\pm 1\sigma$ scatter from the independent SHARC model (Rodríguez-Puebla et al. 2016b), with which the SAM SFMS shows remarkable agreement. The green shaded region is the time evolution of the SAM transition region as defined in this paper. The decreasing normalization of the transition region toward low-redshift accounts for the fact that a high-redshift transition galaxy would be considered a star-forming galaxy if it was relocated to $z = 0$. Note the diversity and non-monotonicity of pathways through the transition region and how the effects from stochastic events like mergers and disk instabilities are propagated onto the SFHs and morphological evolutionary histories of SAM galaxies.

discussed in this and the previous paragraph gives rise to the constant transition fraction for the SAM seen in [Figure 3](#) – galaxies are constantly moving into and out of the transition region on a variety of timescales, with the average transition galaxy being of the slow quenching variety (see below about the average transition region occupation timescale). It is intriguing to wonder whether the constant transition fraction in the observations might also be due to the fact that the transition region is a highway of sorts for galaxy evolution.

Galaxies that are classified as quiescent at $z = 0$ spent a median time of only ~ 2 Gyr since $z = 3$ on the SFMS. Since we are only considering non-rejuvenating SFHs, this means that the average $z = 0$ quiescent galaxy began its slow or fast quenching event no later than $z \sim 1.5$ (the redshift corresponding to 2 Gyr after $z = 3$). Roughly 20% of these galaxies spent close to no time at all on the SFMS since $z = 3$, which means that their slow or fast quenching event was already underway by $z = 3$ (since by then they were already in either the transition or quiescent region). On the other hand, there is a long tail toward high SFMS occupation timescales: $\sim 20\%$ of these galaxies have remained on the SFMS for more than 4 Gyr since $z = 3$, which means that they did not begin their slow or fast quenching event until $z < 1$.

7.3.2 Total Time in Transition and Quiescence

We can gain more physical insight by looking at the CDF of transition region occupation timescales (middle panel of [Figure 7](#)). The most salient feature here is that a large fraction of $z = 0$ transition and quiescent galaxies have spent several Gyr since $z = 3$ in the transition region. The median transition timescale for $z = 0$ quiescent galaxies is ~ 2.5 Gyr since $z = 3$. In the previous section, we found that the average $z = 0$ quiescent galaxy started its slow or fast quenching event no later than $z \sim 1.5$. Combined with the ~ 2.5 Gyr median transition timescale, this means that the average $z = 0$ quiescent galaxy first joined the quiescent population by $z \sim 0.8$. This explains the rapid upturn in the SAM’s quiescent fraction starting at $z \sim 1$ as shown in [Figure 3](#). On the other hand, it is not as straightforward to interpret the median transition timescale for $z = 0$ transition galaxies because, as we discussed above, galaxies move into and out of the transition region on a variety of timescales (leading to the constant transition fraction seen in [Figure 3](#)). But, in general, the average transition galaxy would tend to be of the slow quenching variety, with a median transition timescale of ~ 3 Gyr. In the future, it will be interesting to decompose the distribution of transition region occupation timescales for $z = 0$ transition galaxies as a function of stellar and/or halo mass (we will address morphology in subsection 7.5).

To complete the circle, we can include rejuvenating SFHs and ask: how long do SAM galaxies actually remain quiescent after their quenching is complete? The total time in quiescence is shown in the right panel of [Figure 7](#). We know from above that 31% of quiescent galaxies in the SAM have experienced at least one significant rejuvenation event since $z = 3$. We also found that the average $z = 0$ quiescent galaxy first joined the quiescent population at $z \sim 0.8$ in the SAM. The time elapsed between $z = 0$ and $z = 0.8$ is ~ 7 Gyr, but the median time spent in the quiescent region for

$z = 0$ quiescent galaxies is ~ 6 Gyr. This suggests that the average $z = 0$ quiescent galaxy in the SAM spends ~ 1 Gyr in the SFMS or transition region after first becoming quiescent (this is the sum of all such rejuvenations since $z = 3$).

7.3.3 SAM Diagnosis and Comparisons to Other Models

All of the above points primarily to the quenching timescales in the SAM being too slow. A second-order effect is that not enough high-redshift star-forming galaxies are experiencing a bona fide quenching event, regardless of whether it is slow or fast (see the excess of star-forming and transition galaxies, relative to the observations, in [Figure 3](#)). Instead, many of them are undergoing oscillations on the SFMS, or if they do experience a slow quenching event, then during their transition phase they are kicked back up onto the SFMS due to a gas-rich merger. The most fundamental problem, however, is that many of the fast quenching events are not beginning early enough (or acting quickly enough), so that even the fastest quenching galaxies (e.g., Q1941 in [Figure 6](#)) are still in the SFMS or the transition region at $z = 3$ and do not reach the quiescent region until $z \sim 1.5$. In the next subsection, we will consider whether state-of-the-art mechanical AGN feedback in the recent hydrodynamical simulations of [Choi et al. \(2016\)](#) helps to alleviate this fundamental problem of the SAM.

It is imperative to comment on the possibility that the deficit of quiescent galaxies in our SAM might also apply to other models, both semi-analytic and hydrodynamic. The extensive study of [Lu et al. \(2014\)](#) found remarkable agreement between three independent SAMs, one of which was the “Santa Cruz” SAM considered in this paper. Although we did not present a comprehensive study of these other SAMs in this paper, we have verified that a similar issue related to the underproduction of the transition and quiescent populations at high-redshift exists in at least one more SAM examined by [Lu et al. \(2014\)](#).

On the hydrodynamical side, [Trayford et al. \(2016\)](#) carried out a comprehensive analysis of the EAGLE cosmological simulation ([Schaye et al. 2015](#)), and found that their $z \sim 0$ red galaxies spent a median time of ~ 2 Gyr in the classical green valley since $z = 2$ (see their Figure 10). They interpreted this to mean that their galaxies do not stay in the green valley for long, but their median timescale is not so different from the median transition timescale of our $z = 0$ quiescent galaxies (~ 2.5 Gyr since $z = 3$). On the other hand, [Feldmann et al. \(2016\)](#) recently found that the ultra-high resolution FIRE simulations ([Hopkins et al. 2014](#)) are unable to reproduce the “reddest” massive quiescent galaxies observed at $z = 2$ (based on rest-frame UVJ color selection criteria). Similarly, [Bluck et al. \(2016\)](#) also recently suggested that quenching might not be efficient enough in the Illustris cosmological hydrodynamical simulation ([Genel et al. 2014; Vogelsberger et al. 2014](#)), based partially on an analysis of the $z = 0$ transition population in SDSS and Illustris.

Interestingly, in the hydrodynamical simulations of [Cen \(2014\)](#), most galaxies that are in the red sequence at $z = 0.62$ (the computational redshift limit of their simulations) spent only 300 ± 150 Myr in the classical green valley. However, they also find that a whopping 40% of their massive galaxies that are in the green valley at $z \sim 1$ do not actually become

red by $z = 0.62$. In other words, even in the promising simulations of Cen (2014), there are a startling number of galaxies that linger in the green valley for ~ 2 Gyr (the age difference between $z = 1$ and $z = 0.62$), and this timescale would likely only increase if they could extend their simulations down to $z = 0$ (an additional 6 Gyr since their computational limit of $z = 0.62$).

Even these few qualitative comparisons between our SAM and other simulations stress the need to ask why this problem is only now beginning to be noticed in high redshift studies. One simple possibility is the splitting of a sample into only two subpopulations of star-forming and “quiescent” galaxies. In such a scenario, the modeled “quiescent” fraction can be boosted by including transition galaxies and perhaps also galaxies in the lower tail of the SFMS. This is one reason that our physically and statistically motivated approach described in subsection 4.1 is insightful. Two alternative ways forward, instead of explicitly categorizing the transition population as in our paper, are to: (1) check whether simulations reproduce the full observed spread in the “degree of quiescence” below the tight SFMS, in a continuous sense (see our companion paper; Brennan et al. 2016), and (2) construct and compare “sSFR functions” (see Davé et al. 2016a).

7.4 Quenching Timescales in Hydrodynamical Simulations

Although the SAM includes radiation pressure-driven winds from AGN, the implementation is based on an earlier generation of hydrodynamical simulations. We therefore examine recent high-resolution hydrodynamical simulations with a more detailed and physical implementation of AGN driven winds (Choi et al. 2016). In these simulations, both the thermal energy and the momentum arising from radiation pressure in the unresolved broad line region are injected into the gas surrounding the accreting black hole. As shown by Choi et al. (2015, 2016), this mechanical feedback from AGN drives powerful galaxy-wide outflows that not only sweep the ISM out of the galaxy, but also shock-heat the surrounding hot gas halo leading to strong quenching over long timescales.

In the bottom row of Figure 6, we show representative SFHs from several “zoom-in” simulations of individual massive halos. These representative SFHs reveal rather abrupt and quick quenching, and once a galaxy becomes quiescent, it tends to stay that way. If one of these quiescent galaxies undergoes rejuvenation, the rejuvenated remnant tends to end up in the transition region more often than the SFMS (e.g., Q0125, bottom right of Figure 6). This is a natural byproduct of the fact that mechanical AGN feedback acts not only “ejectively,” but also “preventively” as described in subsection 7.1. All of the above comes together nicely to reproduce the giant elliptical galaxies that we observe at $z \sim 0$, which are quiescent in every sense of the word (i.e., truly “red and dead”).

As we discussed in the previous subsection, the fundamental problem in the SAM is that even the fastest quenching events do not act quickly enough, so that many fast-quenching galaxies are still in the SFMS or the transition region at $z = 3$ (which corresponds to an age of only ~ 2.16 Gyr after the Big Bang). In the hydrodynamical simulations, Q0162 (bottom left of Figure 6) is the earliest quenched

galaxy: it was already nearly in the quiescent region by $z = 3$. This suggests that momentum-driven AGN feedback is one promising route for producing quiescent galaxies at such early times. However, Q0162 is in a class of its own among the sample of thirty halos that we have from Choi et al. (2016). The fastest quenching galaxies among the remaining halos resemble instead Q0380 (see Figure 6), which did not enter the quiescent region until the Universe was ~ 4 Gyr old ($z \approx 1.65$). Although such galaxies are clearly quenching very quickly, joining the transition population at early times, and not as susceptible to rejuvenation events after they become quiescent, it is still not until $z < 2$ that they enter the quiescent region.

In Figure 7, we show the CDFs of the SFMS, transition region, and quiescent region occupation timescales for the thirty galaxies from Choi et al. (2016). These galaxies tend to stay quenched longer than $z = 0$ quiescent galaxies in the SAM. They also tend to spend less time in the transition region than $z = 0$ quiescent galaxies in the SAM. However, the CDF of SFMS occupation timescales is the key diagnostic: since $z = 3$, the median time spent on the SFMS by the galaxies with momentum-driven AGN feedback is ~ 2 Gyr, which means that on average they do not join the quiescent region until $z < 2$ (see also Figure 6). This suggests that, while mechanical AGN feedback seems to be important for producing local giant elliptical galaxies, it is not yet sufficiently clear whether it alone can also solve the high redshift issues that we have pointed out in this paper. In order to produce heavily quiescent galaxies by $z \sim 3$, it might be necessary to begin the quenching process at $z \gg 3$. One possibility might involve coupling the mechanical feedback from growing SMBHs to the stronger effects expected from clustered supernovae (e.g., Gentry et al. 2016).

We note in passing that, although it is difficult to think of radiatively inefficient AGN feedback as an even more rapid quenching process than radiative mode feedback, the “genetic galaxy modification” technique of Pontzen et al. (2016) seems to be a promising way to systematically test this idea. We also again remind the reader that, despite our best efforts to ensure robust observational measurements of the sSFR (see again section 2), the sSFRs of some heavily quiescent galaxies observed at $z \sim 3$ may suffer from systematic errors that severely underestimate their true sSFRs (e.g., there might be more dust in these galaxies than is traditionally assumed; Reddy et al. 2015; Shvarei et al. 2016).

7.5 Relationship to Morphological Transitions

Given that the structural evolutionary histories of galaxies are intimately related to their SFHs, it is crucial that we at least attempt to address how morphological transitions tie into our previous theoretical discussions of SFH transitions. This is an exceptionally difficult task because the various physical processes that are thought to quench and rejuvenate star formation (e.g., AGN feedback and cooling flows) have complicated causal relationships with the physical processes thought to grow a bulge or a disk (e.g., disk instabilities and mergers). One way to proceed is to compare transition region occupation timescales to morphological change timescales. Although the implementation of morphological change timescales in the SAM is rather crude (see section 3), it is still insightful to carry out an initial exploratory analysis

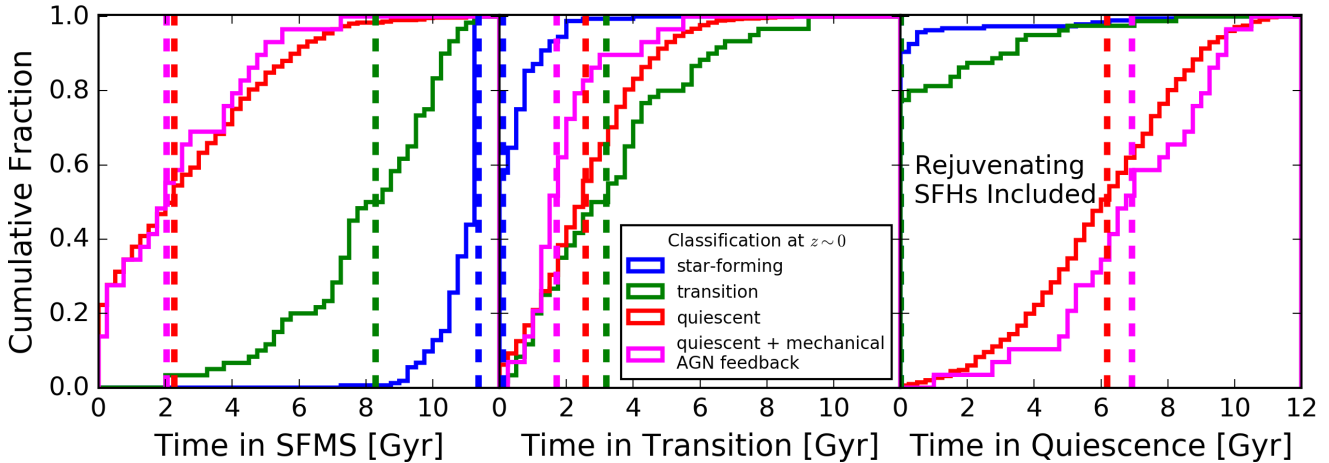


Figure 7. Normalized cumulative distribution functions for how long galaxies have spent in the SFMS, transition region, or quiescent region since $z = 3$. The CDFs are split into three separate ones for galaxies that are classified at $z = 0$ as star-forming (blue), transition (green), or quiescent (red). Also plotted are the occupation timescales for galaxies in the hydrodynamic simulations of Choi et al. (2016), which are all classified as quiescent at $z \sim 0$ (magenta). In each panel, the median corresponding to each CDF is shown by a vertical dashed line. For the SFMS and transition region occupation timescales, we only use non-rejuvenating SFHs (as described in subsection 7.3). However, for the quiescence timescale distributions, we also include rejuvenating SFHs to better appreciate how few $z = 0$ star-forming and transition galaxies have undergone a rejuvenation event since $z = 3$. Note how a non-negligible fraction of $z = 0$ quiescent and transition galaxies in the SAM have spent > 5 Gyr in the transition region since $z = 3$.

using the SAM, with the goal of motivating future hydrodynamical studies of structural evolutionary histories.

7.5.1 Bulge Formation Histories

We begin by showing representative bulge formation histories (i.e., stellar mass-weighted B/T as a function of time) in Figure 8, where the color-coding reveals whether a galaxy is classified as star-forming, transition or quiescent in each time step. These bulge formation histories correspond to and are arranged in the exact same order as the representative SFHs shown in Figure 6 (excluding the bottom row of galaxies from the hydrodynamical simulations of Choi et al. 2016). Our analysis of SAM bulge formation histories, in the context of the transition population, builds on the work presented in our first companion paper (Brennan et al. 2015, specifically the discussion in section 4.2).

The first immediately obvious feature of Figure 8 is that disk regrowth happens mostly in the SFMS, and to a lesser extent in the transition region. These disk regrowth periods occur when a galaxy is able to accrete gas and augment its stellar disk mass through star formation (see also the hydrodynamical studies by Robertson et al. 2004; Springel & Hernquist 2005; Robertson et al. 2006; Sparre & Springel 2016). In order to greatly decrease B/T (due either to mergers or disk instabilities), the disk regrowth must proceed undisturbed on rather long timescales. An extreme example is SF816 in Figure 8, which spent the last ~ 8 Gyr slowly lowering its B/T due to persistent star formation in a stellar disk. An unfortunate case is T1537 in Figure 8, which took ~ 6 Gyr to significantly decrease its high B/T, but just as it became an effectively pure disk system, it underwent a merger that swiftly grew a dominant bulge and initiated a slow quenching event. Shallower decreases in B/T can also

occur during the transition phases of some galaxies, with Q1378 and Q1941 offering two clear examples in Figure 8.

In contrast, the B/T values of quiescent galaxies either remain flat, or they increase due to mergers. The flatness is due to the fact that quiescent galaxies are not undergoing much star formation, and so they have no hope of regrowing a sufficiently massive stellar disk. While it is true that rejuvenation can raise a formerly quiescent galaxy back onto the SFMS, the most significant rejuvenation events in the SAM tend to be caused by major mergers, and these lead to star-forming bulge-dominated galaxies. Although it is possible for these star-forming bulge-dominated remnants to regrow a stellar disk, the disk regrowth period generally is not long enough to effectively overcome the pre-existing massive bulge component. Typically, these star-forming merger remnants exhaust their gas supply and descend into the transition region more quickly than “normal” galaxies on the SFMS (i.e., those that have maintained their steady-state equilibrium between gas consumption, inflows, and outflows).

In the SAM, it is unequivocally true that morphological change precedes quenching: B/T increases before the galaxy becomes quiescent (in fact, before the galaxy even enters the transition region; see again Figure 6). This is partially an artifact of the crude way in which morphological change is implemented in the SAM (e.g., after a merger or disk instability, stellar mass is moved into the spheroidal component in the next time step; see section 3 for details). But it is also a natural reflection of the way quenching is triggered in the SAM (and in many other models, both semi-analytic and hydrodynamic). The main agent for suppressing star formation in a massive central SAM galaxy is the SMBH, but the first step in activating the SMBH is sufficiently feeding it with either a merger or disk instability. Both mergers and disk instabilities should result in some degree of bulge

growth on relatively short timescales compared to the subsequent suppression of star formation by AGN feedback, which might occur on a variety of delayed timescales (see also, e.g., Ellison et al. 2013). This paradigm in which morphological transitions unequivocally precede quenching offers a natural framework for interpreting the observed correlations between quiescence, bulge mass, stellar velocity dispersion, and SMBH mass (e.g., Bell et al. 2012; Wake et al. 2012; Barro et al. 2013; Bluck et al. 2014; Bezanson et al. 2015; Whitaker et al. 2016; Bluck et al. 2016; Terrazas et al. 2016a).

On the other hand, the impact of rejuvenation on the SFHs and bulge formation histories of galaxies substantially complicates simple interpretations of the transition population as a one-time-only quenching population (see also Kaviraj et al. 2009; Fang et al. 2012; Salim et al. 2012; Salim 2014; Trayford et al. 2016). As was elucidated by McIntosh et al. (2014), observationally distinguishing newly-born ellipticals created by recent mergers from ancient ellipticals that have simply been rejuvenated is a daunting task. By carefully combining optical colors, spectroscopic signatures of star formation and AGN emission, and morphological visual classifications of galaxies at $z < 0.08$, McIntosh et al. (2014) identified compelling cases of “first generation” ellipticals, which they termed “recently quenched ellipticals.” Building on the work of McIntosh et al. (2014), Haines et al. (2015) derived spatially-resolved SFHs for a set of unusually blue spheroids with signs of morphological disturbance (i.e., blue ellipticals and post-merger systems) to test the major merger paradigm for making new ellipticals; they found that many of their galaxies were consistent with wet minor mergers rather than the gas-rich major mergers typically associated with blue elliptical remnants. These results have important ramifications for interpreting the origin and fate of relatively nearby blue spheroids, but they also raise several interesting questions. While the recently quenched ellipticals found by McIntosh et al. (2014) are consistent with being “first generation” ellipticals, it is not at all clear that they will produce “first generation” quiescent galaxies (especially in light of the results by Haines et al. 2015). Indeed, gas-rich major mergers with star-forming progenitors and blue spheroidal remnants are only one component of the overall merger paradigm; it is also important to consider mixed mergers involving a transition or quiescent progenitor with varying degrees of B/T, gas content and dissipation (see also Porter et al. 2014a; Brennan et al. 2015).

Furthermore, although there is now a general “two phase” paradigm for the formation of heavily bulge-dominated galaxies (involving the creation of a compact core whose outskirts are subsequently built up through dissipationless merging; e.g., Oser et al. 2010; Lackner et al. 2012; Naab et al. 2014), it is important to assess the potential impact of disk instabilities and massive stellar disk regrowth episodes at high redshift, both of which might give rise to galaxies with intermediate B/T (see also de la Rosa et al. 2016). In particular, if strong disk regrowth events are able to significantly decrease B/T as well as the measured global stellar velocity dispersion over a timespan of many Gyr, then this might complicate the usage of the “stellar velocity dispersion function” to connect progenitors and descendants across cosmic time (e.g., Bezanson et al. 2009, 2012; Belli et al. 2014, and references therein). Interestingly, it has been suggested that it might be better to use the central stellar

velocity dispersion, which seems to remain relatively stable over time and is a good indicator of quiescence (e.g., Loeb & Peebles 2003; Bezanson et al. 2011; Porter et al. 2014b; Bluck et al. 2016, and references therein).

In general, our work further emphasizes the need to constrain the spatially-resolved internal kinematics of high redshift galaxies, since this would open up the exciting possibility of studying kinematic transitions in addition to morphological transitions (e.g., see the recent efforts by Kassin et al. 2012; Wisnioski et al. 2015; Price et al. 2016; Simons et al. 2016; Barro et al. 2016a). Constraints on kinematic transitions as a function of redshift would allow us to directly test the universality of the “two phase” paradigm, and along with ongoing low redshift efforts (e.g., Cappellari et al. 2011; Sánchez et al. 2012; Ma et al. 2014; Brodie et al. 2014; Bundy et al. 2015), might offer important clues about the intrinsic diversity of the transition population. Our study of bulge formation histories also physically motivates the search for a more robust photometric indicator of “degree of bulge growth” compared to the often assumed Sérsic light profile parameterization – one that can also work well at high redshifts where obtaining spatially-resolved stellar velocity dispersions might be cost prohibitive (e.g., the central stellar density within 1 kpc, Σ_1 ; Cheung et al. 2012; Fang et al. 2013; Barro et al. 2015).

7.5.2 Morphological Dependence of Quenching Timescales

Building on the discussion in subsubsection 7.5.1, it is natural to ask whether there is any clear-cut dependence of transition timescales on the final morphology of a quiescent galaxy in the SAM. This question likely depends on stellar mass and halo mass (at least), but we can still carry out a general theoretical test of the two extreme morphology-dependent scenarios proposed by Schawinski et al. (2014): (1) low-redshift quiescent disk-dominated galaxies were preferentially subject to slow quenching mechanisms that preserved their stellar disks, and (2) low-redshift quiescent bulge-dominated galaxies were preferentially subject to fast quenching mechanisms that also rapidly grew their bulges. We might therefore expect that $z = 0$ disk-dominated quiescent galaxies preferentially spent much longer times in the transition region compared to $z = 0$ bulge-dominated quiescent galaxies. However, it is already obvious from Figure 8 that, in the SAM, not all slow quenching events result in a disk-dominated galaxy (e.g., Q1629 has $B/T \approx 1$), and that not all fast quenching events result in a bulge-dominated galaxy (e.g., Q1495 has $B/T \approx 0.3$). Furthermore, many of these quenching events, regardless of timescale, lead to remnants with intermediate B/T, which do not fit cleanly into the two extreme scenarios mentioned previously. This is already a hint that the connection between transition timescales and final morphology is non-trivial in the SAM.

In Figure 9, we show the fraction of time since $z = 3$ that galaxies spent in the transition region, as a function of their B/T ratio at $z = 0$. We only focus on galaxies that are quiescent at $z = 0$ because we know that they actually quenched, whereas a non-trivial fraction of $z = 0$ transition galaxies might simply be undergoing oscillations on the SFMS (see again our discussion in subsection 7.2). We further restrict this analysis only to non-rejuvenating SFHs because we want a clean estimate of the quenching timescale

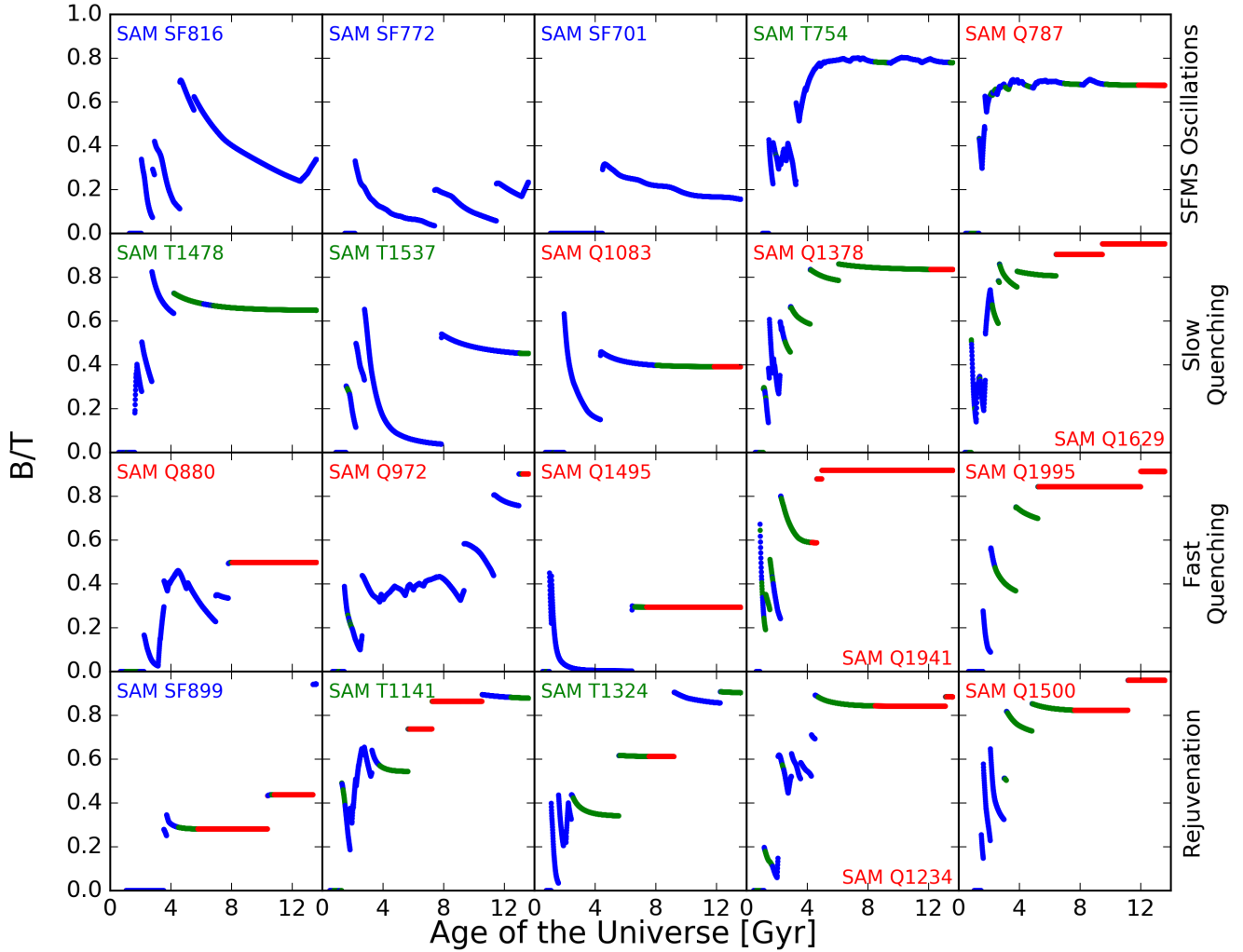


Figure 8. Representative bulge formation histories (i.e., B/T as a function of time) corresponding to and arranged in the exact same order as the representative SFHs shown in Figure 6. The color-coding reflects whether a galaxy is classified as star-forming (blue), transition (green) or quiescent (red) in each time step. The label for each galaxy is color-coded according to its classification at $z = 0$ as star-forming, transition, or quiescent. The two dashed vertical lines mark $z = 3$ (left) and $z = 2$ (right). Note how B/T can decrease due to disk regrowth while a galaxy is in the SFMS and, to a lesser extent, in the transition region. In contrast, B/T can only remain flat or increase for quiescent galaxies. Rejuvenation events in the SAM lead to star-forming remnants that have larger B/T than their quiescent progenitors.

and final morphology, whereas rejuvenation events will preferentially increase both the B/T ratio and the total time spent in the transition region. Figure 9 does not reveal the negative correlation expected from the two simple scenarios depicted above; namely, that galaxies with the highest B/T values at $z = 0$ should have spent the least amount of time in the transition region. Instead, there is significant scatter in the transition timescale for each B/T bin, and the median values are consistent with being flat.

How do we reconcile the above with our intuitive expectation that stellar disks can slowly fade and redden without undergoing significant bulge growth? In the SAM, effectively all quenching events (even very slow ones; e.g., T1478 in Figure 6) are triggered by a merger, and there is thus some degree of bulge growth, regardless of how small (disk instabilities also play a prominent role for bulge growth, but

mostly for galaxies on the SFMS and moreso at early times). Broadly considered, quiescent disk-dominated galaxies in our SAM are not the quiescent analogs of effectively pure-disk star-forming galaxies, as the former do harbor some relic bulge component, no matter how sub-dominant (see also the discussion in Brennan et al. 2015). One of the reasons that the existence of “faded” pure-disk quiescent galaxies in the real Universe would be surprising is that even a slowly-evolving, “completely isolated” disk might be expected to undergo secular processes like bar formation and disk instabilities, which may build up a pseudo-bulge component, especially on cosmological timescales (see the reviews by Kormendy & Kennicutt 2004; Fisher & Drory 2016).

In the important observational studies of Bundy et al. (2010) and Masters et al. (2010b), it was noted that “passive disk” galaxies still tend to harbor some degree of cen-

trally concentrated light (i.e., they do not preferentially have $B/T \sim 0$). Lackner & Gunn (2012) carried out astrophysically motivated bulge-disk decompositions on tens of thousands of galaxies at $z < 0.05$, with the goal of studying the relative distribution of classical and pseudo-bulges among the blue cloud, green valley, and red sequence. Among many interesting results, they found that very few red sequence galaxies have $B/T \sim 0$ (see their Figure 34), but that $\sim 17\%$ of red sequence galaxies were consistent with hosting a pseudo-bulge (see their section 5.6). They also found that red sequence galaxies that were best fit with a bulge+disk model had significantly redder disk colors than green valley galaxies that were best fit with a bulge+disk model (these galaxies were not well fit by a pure exponential profile). While this does imply that at least some fraction of red sequence galaxies with intermediate B/T underwent “disk fading” rather than bulge growth as part of their quenching process, it does not fully explain the origin of the “pre-existing” bulge component in these composite bulge+disk systems.

Our exploratory analysis spanning $0 < z < 3$ is complementary to and builds on the seminal observational studies of Schawinski et al. (2014) and Smethurst et al. (2015), which addressed the diversity of pathways through the classical green valley at $z \sim 0.1$ while also taking into account morphology. As we showed in Figure 4, transition galaxies in both the observations and the SAM (out to $z = 3$) do not seem to be preferentially extremely disk-dominated or extremely bulge-dominated (as implied by Schawinski et al. 2014); instead they tend to have intermediate Sérsic index values, which suggests that both the disk and bulge exhibit significant amounts of light (note also that composite bulge+disk galaxies dominate the green valley at $z < 0.05$ based on the work of Lackner & Gunn 2012). Interpreting the cosmological origin and evolution of these intermediate B/T systems has historically been a very difficult task (e.g., see the classic review by Dressler 1984). In the SAM, galaxies with intermediate B/T (at $z = 0$) have diverse evolutionary histories: they undergo quenching, rejuvenation, and morphological change on a variety of timescales, and their bulges can be built up through both mergers and disk instabilities. This diversity is qualitatively in agreement with the results of Smethurst et al. (2015), who found that their observational sample of $z \sim 0.1$ galaxies with intermediate B/T was consistent with a continuum of quenching timescales (albeit under the simple assumption of exponentially-declining single- τ SFHs, which do not adequately describe all SAM SFHs).

7.6 Predictions for Non-structural Properties

Throughout this paper, we have mostly focused on comparing the structural properties of galaxies between the observations and the SAM. Although the SAM does not quantitatively reproduce the observations in several respects (e.g., the quiescent fraction at high redshift), it is still worthwhile to make some predictions so that future observations can try to test the general paradigm of the transition population. In Figure 10, we present predictions from the SAM for the redshift evolution of four non-structural properties: the mean stellar age, the cold gas fraction, the SMBH mass, and the halo mass. These predictions are based on the cosmolog-

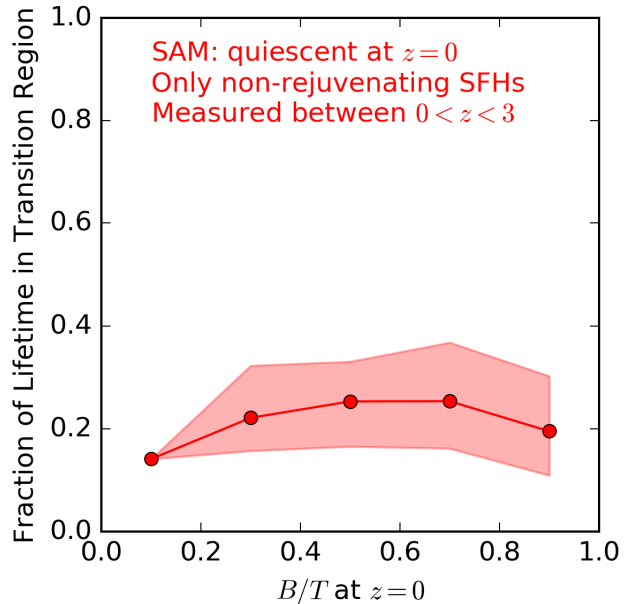


Figure 9. The fraction of time since $z = 3$ that galaxies (classified as quiescent at $z = 0$) have spent in the transition region, as a function of their $z = 0$ B/T ratio. We have restricted this analysis only to non-rejuvenating SFHs since rejuvenation events would artificially increase the B/T ratio and the total time spent in the transition region. The red circles and line show the median values in each B/T bin, and the shading reflects the 25 to 75 percentiles. The flatness of the relation does not agree with the simple expectation that the most heavily bulge-dominated galaxies at $z = 0$ should have preferentially spent the least amount of time in the transition region since $z = 3$.

ically representative SAM lightcones described in section 3, rather than our $z = 0$ grid run described in subsection 7.1. For simplicity, we have restricted this analysis only to central galaxies since satellites are subject to additional complicated physical processes that we do not consider here (e.g., tidal stripping). Furthermore, as described in subsection 4.2, the predictions are based on stellar mass-matched samples of star-forming, transition and quiescent galaxies.

The SAM predicts the mass-weighted mean stellar ages of transition galaxies to be intermediate between those of star-forming and quiescent galaxies (top-left panel of Figure 10). Deep rest-frame UV-optical spectroscopy could be used to derive non-parametric SFHs, and thus mean stellar ages of mass-matched samples of star-forming, transition and quiescent galaxies with the goal of establishing a dominant evolutionary sequence. In such an observational evolutionary sequence, transition galaxies should have older stellar populations than star-forming galaxies but younger stellar populations than quiescent galaxies. Placing robust constraints on the mean stellar age is tremendously difficult because of the dust-age-metallicity degeneracy but it is an interesting target for future infrared and spectroscopic observing campaigns (see also, e.g., Whitaker et al. 2010; Gallazzi et al. 2014; Fumagalli et al. 2016).

More directly related to the intermediate suppression of star formation in transition galaxies (relative to what we call quiescent galaxies) is the cold gas fraction ($\equiv \frac{M_{\text{cold}}}{M_{\text{cold}} + M_*}$).

Not surprisingly, our models predict that the cold gas fractions of transition galaxies are intermediate between those of star-forming and quiescent galaxies (top-right panel of Figure 10). An interesting question observationally is whether the star formation efficiency ($\equiv \frac{SFR}{M_{\text{cold}}}$) in transition galaxies exhibits a similar trend, and whether the lower amount of cold gas in transition galaxies (relative to star-forming galaxies) is due to stronger feedback or lower gas accretion rates. Modern and future facilities such as the *Atacama Large Millimeter Array* may be useful in linking the cold gas fractions and star formation efficiencies of transition galaxies to feedback events and other physical mechanisms responsible for quenching and morphological change (see also Cortese & Hughes 2009; Alatalo et al. 2014; French et al. 2015; Alatalo et al. 2016b; Barro et al. 2016b; Spilker et al. 2016).

In our SAM, as in many cosmological hydrodynamic simulations, SMBHs play a powerful and unparalleled role in quenching galaxies. We predict that transition galaxies should host SMBHs that are intermediate in mass between those of star-forming and quiescent galaxies (bottom-left panel of Figure 10). This suggests that SMBHs in transition galaxies are largely nearing the end of their growth (unlike the SMBHs that are still growing in star-forming galaxies and the SMBHs in quiescent galaxies that have minimal or no ongoing growth), thus making transition galaxies powerful observational targets to study the shutdown of common SMBH growth channels (see also, e.g., Volonteri 2010; Greene 2012; Kocevski et al. 2012; Trump et al. 2013; Terrazas et al. 2016b,a; Azadi et al. 2016).

In this paper, we have not probed the role of the environment for producing transition and quiescent galaxies because our observations do not cover the dense regions where environmental effects are thought to dominate. Nevertheless, many studies have explored possible relationships between quenching and proxies for environment. One very relevant result from the literature is the tendency of classical green valley galaxies to live in intermediate density environments (e.g., Coil et al. 2008; Peng et al. 2010; Zehavi et al. 2011; Behroozi et al. 2013; Krause et al. 2013; Woo et al. 2015). In our SAM, although transition galaxies tend to live in intermediate mass halos compared to stellar mass-matched samples of star-forming and quiescent galaxies out to $z \sim 2.5$, there is significant overlap in the halo mass distributions of transition and quiescent galaxies (bottom-right panel of Figure 10). This overlap may partially be explained by the fact that both transition and quiescent galaxies tend to be bulge-dominated, and that many of these bulges were built up through mergers, which lead to increased halo masses for the remnants.

The preference of transition galaxies to have slightly lower halo masses compared to quiescent galaxies is likely related to the fact that transition galaxies preferentially have intermediate B/T (see again Figure 4). This suggests two things: (1) transition galaxies underwent mergers that were not as major as those of quiescent galaxies, and (2) transition galaxies are more likely to have had recent disk instabilities compared to quiescent galaxies (since the former tend to have a more substantial disk component; see also Tonini et al. 2016). Note that bulges built up through secular processes like disk instabilities should presumably not be as tightly related to the growth of halo mass. In the future, it would therefore be very interesting to study the halo mass

distributions of transition and quiescent galaxies after controlling for the possibility that bulge growth may naturally be accompanied by halo mass growth. Nevertheless, our result suggests that both environmental and internal physical processes work in tandem to suppress star formation, with the environment likely playing a more significant role for the most heavily quiescent galaxies (see also Rodríguez-Puebla et al. 2015; Mandelbaum et al. 2016). Future weak lensing surveys may be able to target and constrain the halo masses of transition galaxies and stellar mass-matched samples of star-forming and quiescent galaxies to observationally test our predictions.

It is unlikely that all of our predictions for the redshift evolution of non-structural properties are exactly and quantitatively correct. However, these results still do qualitatively suggest that there are other non-morphological ways to probe the evolutionary significance of transition galaxies.

8 SUMMARY

We have carried out a comprehensive analysis of massive “transition galaxies” with $M_* > 10^{10} M_\odot$. These transition galaxies are defined in a physically and statistically motivated way to have intermediate sSFR values below the SFMS. Our investigation has been done on observations from the GAMA survey at $z \sim 0.1$ and the CANDELS survey at $0.5 < z < 3.0$, as well as on a cosmologically representative semi-analytic model of galaxy formation and a hydrodynamical simulation with state-of-the-art mechanical AGN feedback. The main results of our paper are as follows:

(i) In the observations, transition galaxies that we cleanly defined in the sSFR- M_* plane do not fall in a cleanly separated and easily identifiable part of the classical rest-frame UVJ diagram. Nevertheless, they do appear to form a non-trivial evolutionary bridge between the star-forming and quiescent subpopulations in UVJ space. A non-negligible fraction of possibly “dusty transition galaxies” are identified in the classical UVJ diagram; future studies of these objects may offer invaluable clues regarding the full diversity of transition pathways for galaxies as well as systematic errors in dust correction methods.

(ii) The transition fraction remains constant in the observations at the $\sim 20\%$ level at $0.5 < z < 3.0$. In the SAM, this is also the case and is due to the fact that galaxies are constantly moving into and out of the transition region on a variety of timescales. In contrast, the star-forming fraction decreases and the quiescent fraction increases toward low redshift, in both the observations and the SAM. The SAM has a deficit of quiescent galaxies at $z > 1$, but matches the observations very well at $z \sim 0.1$. This suggests that the overall rate at which galaxies are beginning to quench at high redshift in the SAM is correct, but that the timescales on which galaxies actually move through the transition region (i.e., quenching timescales) are too long.

(iii) In both the observations and the SAM, transition galaxies tend to have intermediate structural properties compared to star-forming and quiescent galaxies. The three structural properties that we probe in this paper are the Sérsic index, the half-light radius, and the surface stellar mass density. One possible interpretation is that morphological change accompanies or precedes quenching because

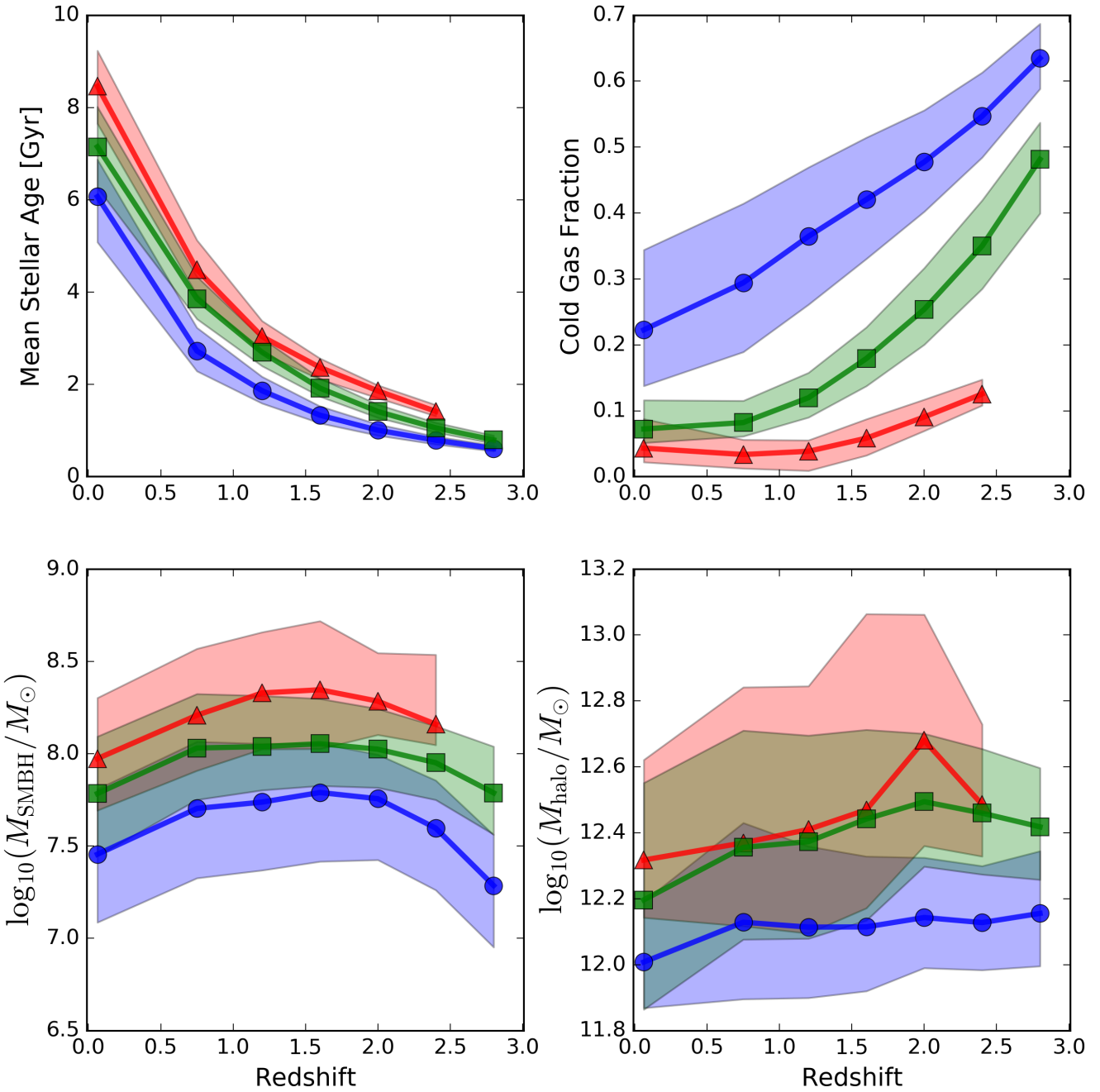


Figure 10. Predictions from the SAM for the redshift evolution of additional non-structural properties for star-forming (blue), transition (green) and quiescent (red) galaxies: mean stellar age (top-left), cold gas fraction (top-right), SMBH mass (bottom-left), and dark matter halo mass (bottom-right). These predictions are from the cosmologically representative SAM light cones (described in section 3), are restricted to central galaxies only, and are based on the stellar mass matching algorithm described in subsection 4.2. The quiescent predictions have been truncated at $z = 2.6$ due to the low number of quiescent galaxies in the highest SAM redshift slice. Note the striking separation between the predictions for the three subpopulations, and the preference that transition galaxies have for intermediate values of these non-structural properties.

transition galaxies are not yet fully quenched, but they are already substantially more compact and concentrated than star-forming galaxies (and less so than quiescent galaxies). However, the “progenitor bias” concept likely plays a non-trivial role: some transition and quiescent galaxies might be more compact than star-forming galaxies in the same epoch

simply because the former began to quench at earlier times, when all galaxies were smaller (and because star-forming galaxies continue to grow more rapidly in size compared to non-star-forming galaxies).

(iv) We explicitly use the transition population that we identified in the observations to place an observational up-

per limit on the average population transition timescale as a function of redshift. This average transition timescale is consistent with “fast track” quenching at high redshift (~ 0.8 Gyr at $z \sim 2.5$), and “slow track” quenching at low redshift (~ 7 Gyr at $z \sim 0.5$). We have made the extreme assumption that galaxies only transition once and that there are no rejuvenation events, but our measurements can also be interpreted as probing the average total time spent in the transition region (i.e., the sum of all such transits). This upper limit can be refined in the future as we obtain more observational constraints on the full distribution of possible quenching and rejuvenation timescales, and the relative frequency of these events as a function of redshift.

(v) We identify four dominant evolutionary modes for SFHs in the SAM: oscillations on the SFMS, slow quenching, fast quenching, and rejuvenation. Each of these modes is driven by different or overlapping physical processes that act on different timescales. In general, the SFHs of SAM galaxies are diverse and non-monotonic because they include the effects of stochastic events like mergers, disk instabilities, starbursts, and feedback processes.

(vi) A statistical analysis of over 1000 SAM SFHs (massive central galaxies only) reveals that many galaxies that are classified as transition or quiescent at $z = 0$ have spent several Gyr in the transition region since $z = 3$, with a median of ~ 2.5 Gyr. This is primarily due to galaxies preferentially undergoing “slow quenching” events at high or intermediate redshift in the SAM. Even the fastest quenching galaxies in the SAM generally cannot make it into the quiescent region by $z \sim 3$, suggesting that such “fast quenching” processes need to begin at even higher redshifts (or act on even faster timescales at these early epochs).

(vii) Hydrodynamical simulations with state-of-the-art implementation of mechanical AGN feedback are able to reproduce the truly “red and dead” giant ellipticals that we observe at $z \sim 0$. However, even the fastest quenching galaxies in these hydrodynamical simulations do not enter the quiescent region by $z \sim 3$, which is also the fundamental problem in the SAM. Future studies will need to address how AGN feedback might be coupled to other quenching mechanisms at these early epochs to reproduce the heavily quiescent galaxies that we observe at $z \sim 3$ (when the Universe is only ~ 2.2 Gyr old).

(viii) In the SAM, galaxies exhibit a wide diversity of bulge formation histories (i.e., stellar mass-weighted B/T as a function of time). Galaxies can decrease their B/T by regrowing a stellar disk on the SFMS and, to a lesser extent, in the transition region. In contrast, the B/T ratios of quiescent galaxies can only remain flat, or they can increase due to mergers. Rejuvenation events preferentially produce star-forming bulge-dominated remnants which typically do not stay on the SFMS for a long enough time to significantly decrease B/T through stellar disk regrowth.

(ix) For galaxies in the SAM that are classified as quiescent at $z = 0$ and which have non-rejuvenating SFHs, we do not find the negative correlation expected between their transition timescale and their morphology at $z = 0$. In other words, $z = 0$ quiescent disk-dominated galaxies in the SAM did not preferentially spend longer amounts of time in the transition region (since $z = 3$) compared to $z = 0$ heavily quiescent bulge-dominated galaxies. Furthermore, quiescent “disk-dominated” galaxies in the SAM are not the analogs of

pure-disk star-forming galaxies, as their slow or fast quenching event was initially triggered by a merger, which resulted in some degree of bulge growth. The SAM therefore predicts that even the most heavily disk-dominated quiescent galaxies in the Universe at $z = 0$ should host some relic bulge component, which might be a fossil record of an ancient slow quenching event.

(x) We use the SAM to predict the redshift evolution of the mean stellar ages, cold gas fractions, SMBH masses, and halo masses of star-forming, transition and quiescent galaxies since $z = 3$ (massive central galaxies only). Transition galaxies tend to exhibit intermediate values of these properties relative to the star-forming and quiescent subpopulations. We therefore predict that these non-structural properties might offer additional ways to observationally test the general paradigm of the transition population.

In this paper and our companion paper by [Brennan et al. \(2016\)](#), we have raised several important observational and theoretical questions about how galaxies might move below the SFMS at $0 < z < 3$. In the future, it will be important to test how different models (both semi-analytic and hydrodynamic) might reproduce the full observed spread in the “degree of quiescence” of galaxies below the SFMS as a function of redshift. This is important because it might reveal clues about the timescales on which galaxies quench and rejuvenate, and the relative frequency of such transitions. Systematically linking the structural and non-structural evolutionary histories of galaxies to their SFHs is a major goal of our future work. Many of the results, methodologies, and diagnostics that we have developed in this paper and in [Brennan et al. \(2016\)](#) are widely applicable to other observations and cosmological simulations.

ACKNOWLEDGEMENTS

We greatly thank James E. Gunn, Barry Madore, Jennifer Lotz, Romeel Dave, Phil Hopkins, Lars Hernquist, Aaron Romanowsky and Irene Shivaei for inspiring discussions. VP is grateful for the encouragement and support from Roderich Tumulka, the astronomy faculty at Rutgers (in particular Saurabh Jha, Andrew Baker and Tad Pryor), the Princeton Post-Baccalaureate Program in Astrophysics (in particular Jenny Greene, Anatoly Spitzkovsky, Michael Strauss, Jill Knapp and Jesus Hinojosa), and John Mulchaey. RB was supported in part by HST Theory grant HST-AR-13270-A. RSS thanks the Downsborough family for their generous support, and acknowledges support from the Simons Foundation through a Simons Investigator grant. PB was supported by program number HST-HF2-51353.001-A, provided by NASA through a Hubble Fellowship grant from the Space Telescope Science Institute, which is operated by the Association of Universities for Research in Astronomy, Incorporated, under NASA contract NAS5-26555. AK gratefully acknowledges support from the YCAA Prize Postdoctoral Fellowship. We acknowledge the contributions of hundreds of individuals to the planning and support of the CANDELS observations, and to the development and installation of new instruments on HST, without which this work would not have been possible. Support for Program number HST-GO-12060 was provided by NASA through a grant

from the Space Telescope Science Institute, which is operated by the Association of Universities for Research in Astronomy, Incorporated, under NASA contract NAS5-26555. This work has made use of the Rainbow Cosmological Surveys Database, which is operated by the Universidad Complutense de Madrid (UCM), partnered with the University of California Observatories at Santa Cruz (UCO/Lick, UCSC).

REFERENCES

- Abramson L. E., Morishita T., 2016, preprint, ([arXiv:1608.07577](#))
- Abramson L. E., Kelson D. D., Dressler A., Poggianti B., Gladders M. D., Oemler Jr. A., Vulcani B., 2014, *ApJ*, **785**, L36
- Alatalo K., Cales S. L., Appleton P. N., Kewley L. J., Lacy M., Lisenfeld U., Nyland K., Rich J. A., 2014, *ApJ*, **794**, L13
- Alatalo K., et al., 2016b, preprint, ([arXiv:1604.01122](#))
- Alatalo K., et al., 2016a, preprint, ([arXiv:1608.00256](#))
- Alatalo K., et al., 2016c, *ApJS*, **224**, 38
- Azadi M., et al., 2016, preprint, ([arXiv:1608.05890](#))
- Baldry et al. 2004, *ApJ*, **600**, 681
- Baldry I. K., et al., 2010, *MNRAS*, **404**, 86
- Baldry I. K., et al., 2012, *MNRAS*, **421**, 621
- Barro G., et al., 2011, *ApJS*, **193**, 30
- Barro G., et al., 2013, *ApJ*, **765**, 104
- Barro G., Faber S. M., Pérez-González P. G., Pacifici C., 2014, *ApJ*, **791**, 52
- Barro G., et al., 2015, preprint, ([arXiv:1509.00469](#))
- Barro G., et al., 2016a, *ApJ*, **820**, 120
- Barro G., et al., 2016b, *ApJ*, **827**, L32
- Behroozi P. S., Wechsler R. H., Conroy C., 2013, *ApJ*, **770**, 57
- Bell et al. 2004, *ApJ*, **608**, 752
- Bell E. F., et al., 2012, *ApJ*, **753**, 167
- Belli S., Newman A. B., Ellis R. S., 2014, *ApJ*, **783**, 117
- Belli S., Newman A. B., Ellis R. S., 2015, *ApJ*, **799**, 206
- Bertin E., Arnouts S., 1996, *A&AS*, **117**, 393
- Bezanson R., van Dokkum P. G., Tal T., Marchesini D., Kriek M., Franx M., Coppi P., 2009, *ApJ*, **697**, 1290
- Bezanson R., et al., 2011, *ApJ*, **737**, L31
- Bezanson R., van Dokkum P., Franx M., 2012, *ApJ*, **760**, 62
- Bezanson R., Franx M., van Dokkum P. G., 2015, *ApJ*, **799**, 148
- Birnboim Y., Dekel A., 2003, *MNRAS*, **345**, 349
- Bland-Hawthorn J., Gerhard O., 2016, preprint, ([arXiv:1602.07702](#))
- Blanton M. R., Moustakas J., 2009, *ARA&A*, **47**, 159
- Bluck A. F. L., Mendel J. T., Ellison S. L., Moreno J., Simard L., Patton D. R., Starkenburg E., 2014, *MNRAS*, **441**, 599
- Bluck A. F. L., et al., 2016, *MNRAS*, **462**, 2559
- Blumenthal G. R., Faber S. M., Flores R., Primack J. R., 1986, *ApJ*, **301**, 27
- Bondi H., 1952, *MNRAS*, **112**, 195
- Brammer G. B., van Dokkum P. G., Coppi P., 2008, *ApJ*, **686**, 1503
- Brammer G. B., et al., 2009, *ApJ*, **706**, L173
- Brammer G. B., et al., 2011, *ApJ*, **739**, 24
- Brennan R., et al., 2015, *MNRAS*, **451**, 2933
- Brennan R., et al., 2016, preprint, ([arXiv:1607.06075](#))
- Brinchmann J., Charlot S., White S. D. M., Tremonti C., Kauffmann G., Heckman T., Brinkmann J., 2004, *MNRAS*, **351**, 1151
- Brodie J. P., et al., 2014, *ApJ*, **796**, 52
- Bruce V. A., Dunlop J. S., McLure R. J., Cirasuolo M., Buitrago F., 2014, *MNRAS*, **444**, 1001
- Bruzual G., Charlot S., 2003, *MNRAS*, **344**, 1000
- Bundy K., et al., 2010, *ApJ*, **719**, 1969
- Bundy K., et al., 2015, *ApJ*, **798**, 7
- Butcher H., Oemler Jr. A., 1978, *ApJ*, **219**, 18
- Calzetti D., Armus L., Bohlin R. C., Kinney A. L., Koornneef J., Storchi-Bergmann T., 2000, *ApJ*, **533**, 682
- Cappellari M., et al., 2011, *MNRAS*, **413**, 813
- Cappellari M., et al., 2012, *Nature*, **484**, 485
- Cardamone C. N., Urry C. M., Schawinski K., Treister E., Brammer G., Gawiser E., 2010, *ApJ*, **721**, L38
- Cen R., 2014, *ApJ*, **781**, 38
- Chabrier G., 2003, *PASP*, **115**, 763
- Cheung E., Faber S. M., Koo D. C., Dutton A. A., Simard L., McGrath E. J., Huang J.-S., 2012, *ApJ*, **760**, 131
- Choi E., Ostriker J. P., Naab T., Oser L., Moster B. P., 2015, *MNRAS*, **449**, 4105
- Choi E., Ostriker J. P., Naab T., Somerville R. S., Hirschmann M., Núñez A., Hu C.-Y., Oser L., 2016, preprint, ([arXiv:1610.09389](#))
- Coil A. L., et al., 2008, *ApJ*, **672**, 153
- Colless M., et al., 2001, *MNRAS*, **328**, 1039
- Conroy C., 2013, *ARA&A*, **51**, 393
- Conroy C., van Dokkum P. G., 2012, *ApJ*, **760**, 71
- Conroy C., Gunn J. E., White M., 2009, *ApJ*, **699**, 486
- Conroy C., White M., Gunn J. E., 2010, *ApJ*, **708**, 58
- Conselice C. J., 2014, *ARA&A*, **52**, 291
- Cortese L., Hughes T. M., 2009, *MNRAS*, **400**, 1225
- Courteau S., Widrow L. M., McDonald M., Guhathakurta P., Gilbert K. M., Zhu Y., Beaton R. L., Majewski S. R., 2011, *ApJ*, **739**, 20
- Cowie L. L., Songaila A., Hu E. M., Cohen J. G., 1996, *AJ*, **112**, 839
- Dahlen T., Mobasher B., Faber S. M., Ferguson H. C., Barro G., Finkelstein S. L., 2013, *ApJ*, **775**, 93
- Dalcanton J. J., et al., 2012, *ApJS*, **198**, 6
- Davé R., Rafieferantsoa M. H., Thompson R. J., Hopkins P. F., 2016a, preprint, ([arXiv:1610.01626](#))
- Davé R., Thompson R., Hopkins P. F., 2016b, *MNRAS*, **462**, 3265
- Davies L. J. M., et al., 2016, *MNRAS*, **461**, 458
- Dekel A., Birnboim Y., 2006, *MNRAS*, **368**, 2
- Dekel A., Burkert A., 2014, *MNRAS*, **438**, 1870
- Domínguez Sánchez H., et al., 2016, *MNRAS*, **457**, 3743
- Dorman C. E., et al., 2013, *ApJ*, **779**, 103
- Dressler A., 1984, *ARA&A*, **22**, 185
- Dressler A., Abramson L., 2015, in Cappellari M., Courteau S., eds, IAU Symposium Vol. 311, IAU Symposium. pp 140–145, doi:[10.1017/S1743921315003555](#)
- Dressler A., Gunn J. E., 1983, *ApJ*, **270**, 7
- Dressler A., Oemler Jr. A., Poggianti B. M., Gladders M. D., Abramson L., Vulcani B., 2013, *ApJ*, **770**, 62
- Dressler A., et al., 2016, preprint, ([arXiv:1607.02143](#))
- Driver S. P., et al., 2011, *MNRAS*, **413**, 971
- Elbaz D., et al., 2011, *A&A*, **533**, A119
- Ellison S. L., Mendel J. T., Patton D. R., Scudder J. M., 2013, *MNRAS*, **435**, 3627
- Faber et al. 2007, *ApJ*, 665
- Fang J. J., 2015, PhD thesis, University of California, Santa Cruz
- Fang J. J., Faber S. M., Salim S., Graves G. J., Rich R. M., 2012, *ApJ*, **761**, 23
- Fang J. J., Faber S. M., Koo D. C., Dekel A., 2013, *ApJ*, **776**, 63
- Feldmann R., Quataert E., Hopkins P. F., Faucher-Giguère C.-A., Kereš D., 2016, preprint, ([arXiv:1610.02411](#))
- Fisher D. B., Drory N., 2016, *Galactic Bulges*, **418**, 41
- Flores R., Primack J. R., Blumenthal G. R., Faber S. M., 1993, *ApJ*, **412**, 443
- Fontanot F., De Lucia G., Monaco P., Somerville R. S., Santini P., 2009, *MNRAS*, **397**, 1776
- French K. D., Yang Y., Zabludoff A., Narayanan D., Shirley Y., Walter F., Smith J.-D., Tremonti C. A., 2015, *ApJ*, **801**, 1
- Fumagalli M., et al., 2014, *ApJ*, **796**, 35
- Fumagalli M., et al., 2016, *ApJ*, **822**, 1

- Galametz A., et al., 2013, *ApJS*, **206**, 10
- Gallazzi A., Bell E. F., Zibetti S., Brinchmann J., Kelson D. D., 2014, *ApJ*, **788**, 72
- Geha M., Blanton M. R., Yan R., Tinker J. L., 2012, *ApJ*, **757**, 85
- Genel S., et al., 2014, *MNRAS*, **445**, 175
- Gentry E. S., Krumholz M. R., Dekel A., Madau P., 2016, preprint, ([arXiv:1606.01242](#))
- Gonçalves T. S., Martin D. C., Menéndez-Delmestre K., Wyder T. K., Koekemoer A., 2012, *ApJ*, **759**, 67
- Greene J. E., 2012, *Nature Communications*, **3**, 1304
- Grogan N. A., et al., 2011, *ApJS*, **197**, 35
- Gunawardhana M. L. P., Hopkins A. M., Bland-Hawthorn J., Brough S., Sharp R., Loveday J., Taylor E., Jones D. H., 2013, *MNRAS*, **433**, 2764
- Guo Y., et al., 2013, *ApJS*, **207**, 24
- Haines T., McIntosh D. H., Sánchez S. F., Tremonti C., Rudnick G., 2015, *MNRAS*, **451**, 433
- Häußler B., et al., 2013, *MNRAS*, **430**, 330
- Hayward C. C., Hopkins P. F., 2015, preprint, ([arXiv:1510.05650](#))
- Hirschmann M., Somerville R. S., Naab T., Burkert A., 2012, *MNRAS*, **426**, 237
- Hopkins P. F., Bundy K., Hernquist L., Ellis R. S., 2007, *ApJ*, **659**, 976
- Hopkins P. F., et al., 2009, *MNRAS*, **397**, 802
- Hopkins P. F., Kereš D., Oñorbe J., Faucher-Giguère C.-A., Quataert E., Murray N., Bullock J. S., 2014, *MNRAS*, **445**, 581
- Huertas-Company M., et al., 2016, *MNRAS*, **462**, 4495
- Kang X., van den Bosch F. C., 2008, *ApJ*, **676**, L101
- Kassin S. A., et al., 2012, *ApJ*, **758**, 106
- Kauffmann G., Heckman T. M., White S. D. M., Charlot S., 2003, *MNRAS*, **341**, 54
- Kaviraj S., 2010, *MNRAS*, **408**, 170
- Kaviraj S., Peirani S., Khochfar S., Silk J., Kay S., 2009, *MNRAS*, **394**, 1713
- Kelson D. D., 2014, preprint, ([arXiv:1406.5191](#))
- Kelvin L. S., et al., 2012, *MNRAS*, **421**, 1007
- Kennicutt Jr. R. C., 1998, *ApJ*, **498**, 541
- Kirkpatrick A., et al., 2013, *ApJ*, **763**, 123
- Kirkpatrick A., Pope A., Sajina A., Roebuck E., Yan L., Armus L., Díaz-Santos T., Stierwalt S., 2015, *ApJ*, **814**, 9
- Kocevski D. D., et al., 2012, *ApJ*, **744**, 148
- Koekemoer A. M., et al., 2011, *ApJS*, **197**, 36
- Kormendy J., Kennicutt Jr. R. C., 2004, *ARA&A*, **42**, 603
- Krause E., Hirata C. M., Martin C., Neill J. D., Wyder T. K., 2013, *MNRAS*, **428**, 2548
- Kriek M., van Dokkum P. G., Labb   I., Franx M., Illingworth G. D., Marchesini D., Quadri R. F., 2009, *ApJ*, **700**, 221
- Kriek M., et al., 2015, *ApJS*, **218**, 15
- Kurczynski P., et al., 2016, *ApJ*, **820**, L1
- Labb   I., et al., 2005, *ApJ*, **624**, L81
- Lackner C. N., Gunn J. E., 2012, *MNRAS*, **421**, 2277
- Lackner C. N., Cen R., Ostriker J. P., Joung M. R., 2012, *MNRAS*, **425**, 641
- Laidler V. G., et al., 2007, *PASP*, **119**, 1325
- Lang P., et al., 2014, *ApJ*, **788**, 11
- Lee K.-S., et al., 2012, *ApJ*, **752**, 66
- Leja J., Johnson B. D., Conroy C., van Dokkum P. G., Byler N., 2016, preprint, ([arXiv:1609.09073](#))
- Lilly S. J., Carollo C. M., 2016, preprint, ([arXiv:1604.06459](#))
- Liske J., et al., 2015, *MNRAS*, **452**, 2087
- Liu F. S., et al., 2016, *ApJ*, **822**, L25
- Loeb A., Peebles P. J. E., 2003, *ApJ*, **589**, 29
- Lu Y., et al., 2014, *ApJ*, **795**, 123
- Ma C.-P., Greene J. E., McConnell N., Janish R., Blakeslee J. P., Thomas J., Murphy J. D., 2014, *ApJ*, **795**, 158
- Madau P., Dickinson M., 2014, *ARA&A*, **52**, 415
- Mandelbaum R., Wang W., Zu Y., White S., Henriques B., More S., 2016, *MNRAS*, **457**, 3200
- Maraston C., Daddi E., Renzini A., Cimatti A., Dickinson M., Papovich C., Pasquali A., Pirzkal N., 2006, *ApJ*, **652**, 85
- Margalef-Bentabol B., Conselice C. J., Mortlock A., Hartley W., Duncan K., Ferguson H. C., Dekel A., Primack J. R., 2016, *MNRAS*, **461**, 2728
- Martig M., Bournaud F., Teyssier R., Dekel A., 2009, *ApJ*, **707**, 250
- Martin D. C., Small T., Schiminovich D., Wyder T. K., Pérez-Gonz  lez P. G., 2007, *ApJS*, **173**, 415
- Masters K. L., Nichol R., Bamford S., Mosleh M., Lintott C. J., 2010a, *MNRAS*, **404**, 792
- Masters K. L., Mosleh M., Romer A. K., Nichol R. C., Bamford S. P., 2010b, *MNRAS*, **405**, 783
- McIntosh D. H., Wagner C., Cooper A., Bell E. F., Kere   D., 2014, *MNRAS*, **442**, 533
- Mendez et al. 2011, *ApJ*, **736**, 110
- Mo H. J., Mao S., White S. D. M., 1998, *MNRAS*, **295**, 319
- Mobasher B., et al., 2015, *ApJ*, **808**, 101
- Morris A. M., et al., 2015, *AJ*, **149**, 178
- Mutch S. J., Croton D. J., Poole G. B., 2011, *ApJ*, **736**, 84
- Muzzin A., Marchesini D., Stefanon M., Franx M., McCracken H. J., 2013, *ApJ*, **777**, 18
- Naab T., Johansson P. H., Ostriker J. P., Efstrathiou G., 2007, *ApJ*, **658**, 710
- Naab T., et al., 2014, *MNRAS*, **444**, 3357
- Nelson E. J., et al., 2012, *ApJ*, **747**, L28
- Nelson E. J., et al., 2016, *ApJ*, **828**, 27
- Newman A. B., Ellis R. S., Bundy K., Treu T., 2012, *ApJ*, **746**, 162
- Noeske K. G., et al., 2007a, *ApJ*, **660**, L43
- Noeske K. G., et al., 2007b, *ApJ*, **660**, L47
- Oser L., Ostriker J. P., Naab T., Johansson P. H., Burkert A., 2010, *ApJ*, **725**, 2312
- Pacifica C., Charlot S., Blaizot J., Brinchmann J., 2012, *MNRAS*, **421**, 2002
- Pacifica C., et al., 2015, *MNRAS*, **447**, 786
- Pan Z., Kong X., Fan L., 2013, *ApJ*, **776**, 14
- Pan Z., Li J., Lin W., Wang J., Kong X., 2014, *ApJ*, **792**, L4
- Patel S. G., et al., 2013, *ApJ*, **766**, 15
- Pattarakijwanich P., Strauss M. A., Ho S., Ross N. P., 2014, preprint, ([arXiv:1410.7394](#))
- Peng C. Y., Ho L. C., Impey C. D., Rix H.-W., 2002, *AJ*, **124**, 266
- Peng Y.-j., et al., 2010, *ApJ*, **721**, 193
- P  rez-Gonz  lez P. G., et al., 2010, *A&A*, **518**, L15
- Peth M. A., Lotz J. M., Freeman P. E., McPartland C., Mortazavi S. A., 2016, *MNRAS*, **458**, 963
- Planck Collaboration et al., 2014, *A&A*, **571**, A16
- Pontzen A., Tremmel M., Roth N., Peiris H. V., Saintonge A., Volonteri M., Quinn T., Governato F., 2016, preprint, ([arXiv:1607.02507](#))
- Porter L. A., Somerville R. S., Primack J. R., Johansson P. H., 2014a, *MNRAS*, **444**, 942
- Porter L. A., Somerville R. S., Primack J. R., Croton D. J., Covington M. D., Graves G. J., Faber S. M., 2014b, *MNRAS*, **445**, 3092
- Price S. H., et al., 2016, *ApJ*, **819**, 80
- Quintero A. D., et al., 2004, *ApJ*, **602**, 190
- Reddy N. A., et al., 2015, *ApJ*, **806**, 259
- Robertson B., Yoshida N., Springel V., Hernquist L., 2004, *ApJ*, **606**, 32
- Robertson B., Bullock J. S., Cox T. J., Di Matteo T., Hernquist L., Springel V., Yoshida N., 2006, *ApJ*, **645**, 986
- Rodr  guez-Puebla A., Avila-Reese V., Yang X., Foucaud S., Drory N., Jing Y. P., 2015, *ApJ*, **799**, 130

- Rodríguez-Puebla A., Behroozi P., Primack J., Klypin A., Lee C., Hellinger D., 2016a, preprint, ([arXiv:1602.04813](#))
- Rodríguez-Puebla A., Primack J. R., Behroozi P., Faber S. M., 2016b, *MNRAS*, **455**, 2592
- Rosenfield P., et al., 2014, *ApJ*, **790**, 22
- Rowlands K., Wild V., Nesvadba N., Sibthorpe B., Mortier A., Lehnert M., da Cunha E., 2015, *MNRAS*, **448**, 258
- Salim S., 2014, *Serbian Astronomical Journal*, **189**, 1
- Salim S., Rich R. M., 2010, *ApJ*, **714**, L290
- Salim S., et al., 2007, *ApJS*, **173**, 267
- Salim S., Fang J. J., Rich R. M., Faber S. M., Thilker D. A., 2012, *ApJ*, **755**, 105
- Salmon B., et al., 2016, *ApJ*, **827**, 20
- Sánchez S. F., et al., 2012, *A&A*, **538**, A8
- Santini P., et al., 2015, *ApJ*, **801**, 97
- Schawinski K., et al., 2009, *MNRAS*, **396**, 818
- Schawinski K., Urry C. M., Simmons B. D., Fortson L., Kaviraj S., 2014, *MNRAS*, **440**, 889
- Schaye J., et al., 2015, *MNRAS*, **446**, 521
- Schiminovich D., Wyder T. K., Martin D. C., Johnson B. D., Salim S., 2007, *ApJS*, **173**, 315
- Schmidt M., 1968, *ApJ*, **151**, 393
- Shapley A. E., Steidel C. C., Erb D. K., Reddy N. A., Adelberger K. L., Pettini M., Barmby P., Huang J., 2005, *ApJ*, **626**, 698
- Shivaei I., et al., 2016, preprint, ([arXiv:1609.04814](#))
- Simons R. C., et al., 2016, preprint, ([arXiv:1606.00009](#))
- Smethurst R. J., et al., 2015, *MNRAS*, **450**, 435
- Somerville R. S., Davé R., 2015, *ARA&A*, **53**, 51
- Somerville R. S., Kolatt T. S., 1999, *MNRAS*, **305**, 1
- Somerville R. S., Primack J. R., 1999, *MNRAS*, **310**, 1087
- Somerville R. S., Primack J. R., Faber S. M., 2001, *MNRAS*, **320**, 504
- Somerville R. S., Lee K., Ferguson H. C., Gardner J. P., Moustakas L. A., Giavalisco M., 2004, *ApJ*, **600**, L171
- Somerville et al. 2008a, *MNRAS*, **391**, 481
- Somerville R. S., et al., 2008b, *ApJ*, **672**, 776
- Somerville R. S., Gilmore R. C., Primack J. R., Domínguez A., 2012, *MNRAS*, **423**, 1992
- Sparre M., Springel V., 2016, preprint, ([arXiv:1610.03850](#))
- Sparre M., et al., 2015, *MNRAS*, **447**, 3548
- Spilker J. S., Bezanson R., Marrone D. P., Weiner B. J., Whitaker K. E., Williams C. C., 2016, preprint, ([arXiv:1607.01785](#))
- Springel V., Hernquist L., 2005, *ApJ*, **622**, L9
- Straatman C. M. S., et al., 2016, preprint, ([arXiv:1608.07579](#))
- Strateva I., et al., 2001, *AJ*, **122**, 1861
- Strauss M. A., et al., 2002, *AJ*, **124**, 1810
- Szomoru D., Franx M., van Dokkum P. G., Trenti M., Illingworth G. D., Labbé I., Oesch P., 2013, *ApJ*, **763**, 73
- Tacchella S., et al., 2015, *Science*, **348**, 314
- Tacchella S., Dekel A., Carollo C. M., Ceverino D., DeGraf C., Lapiner S., Mandelker N., Primack Joel R., 2016a, *MNRAS*, **457**, 2790
- Tacchella S., Dekel A., Carollo C. M., Ceverino D., DeGraf C., Lapiner S., Mandelker N., Primack J. R., 2016b, *MNRAS*, **458**, 242
- Takada et al. 2014, *PASJ*, **66**, 1
- Taylor E. N., et al., 2011, *MNRAS*, **418**, 1587
- Taylor E. N., et al., 2015, *MNRAS*, **446**, 2144
- Terrazas B. A., Bell E. F., Henriques B. M. B., White S. D. M., Cattaneo A., Woo J., 2016a, preprint, ([arXiv:1609.07141](#))
- Terrazas B. A., Bell E. F., Henriques B. M. B., White S. D. M., 2016b, *MNRAS*, **459**, 1929
- Tonini C., Mutch S. J., Croton D. J., Wyithe J. S. B., 2016, *MNRAS*, **459**, 4109
- Trayford J. W., Theuns T., Bower R. G., Crain R. A., Lagos C. d. P., Schaller M., Schaye J., 2016, preprint, ([arXiv:1601.07907](#))
- Treu T., Auger M. W., Koopmans L. V. E., Gavazzi R., Marshall P. J., Bolton A. S., 2010, *ApJ*, **709**, 1195
- Trump J. R., Hsu A. D., Fang J. J., Faber S. M., Koo D. C., Kocevski D. D., 2013, *ApJ*, **763**, 133
- Vika M., Bamford S. P., Häußler B., Rojas A. L., Borch A., Nichol R. C., 2013, *MNRAS*, **435**, 623
- Villaume A., Conroy C., Johnson B. D., 2015, *ApJ*, **806**, 82
- Vogelsberger M., et al., 2014, *MNRAS*, **444**, 1518
- Volonteri M., 2010, *A&ARv*, **18**, 279
- Vulcani B., Poggianti B. M., Fritz J., Fasano G., Moretti A., Calvi R., Paccagnella A., 2015, *ApJ*, **798**, 52
- Wake D. A., van Dokkum P. G., Franx M., 2012, *ApJ*, **751**, L44
- Wellons S., et al., 2015, *MNRAS*, **449**, 361
- Whitaker K. E., et al., 2010, *ApJ*, **719**, 1715
- Whitaker K. E., et al., 2011, *ApJ*, **735**, 86
- Whitaker K. E., Kriek M., van Dokkum P. G., Bezanson R., Brammer G., Franx M., Labbé I., 2012, *ApJ*, **745**, 179
- Whitaker K. E., et al., 2016, preprint, ([arXiv:1607.03107](#))
- Wild V., Walcher C. J., Johansson P. H., Tresse L., Charlton S., Pollo A., Le Fèvre O., de Ravel L., 2009, *MNRAS*, **395**, 144
- Wild V., Almaini O., Dunlop J., Simpson C., Rowlands K., Bowler R., Maltby D., McLure R., 2016, *MNRAS*, **463**, 832
- Williams R. J., Quadri R. F., Franx M., van Dokkum P., Labbé I., 2009, *ApJ*, **691**, 1879
- Williams B. F., et al., 2015, *ApJ*, **806**, 48
- Wisnioski E., et al., 2015, *ApJ*, **799**, 209
- Woo J., Dekel A., Faber S. M., Koo D. C., 2015, *MNRAS*, **448**, 237
- Wuyts S., et al., 2007, *ApJ*, **655**, 51
- Wuyts S., et al., 2011a, *ApJ*, **738**, 106
- Wuyts S., Förster Schreiber N. M., van der Wel A., Magnelli B., Guo Y., 2011b, *ApJ*, **742**, 96
- Wuyts S., et al., 2012, *ApJ*, **753**, 114
- Wyder T. K., Martin D. C., Schiminovich D., Seibert M., Budavári T., 2007, *ApJS*, **173**, 293
- Yano M., Kriek M., van der Wel A., Whitaker K. E., 2016, *ApJ*, **817**, L21
- Yesuf H. M., Faber S. M., Trump J. R., Koo D. C., Fang J. J., 2014, *ApJ*, **792**, 84
- Yoon I., Weinberg M. D., Katz N., 2011, *MNRAS*, **414**, 1625
- York D. G., et al., 2000, *AJ*, **120**, 1579
- Zehavi I., et al., 2011, *ApJ*, **736**, 59
- Zolotov A., et al., 2014, preprint, ([arXiv:1412.4783](#))
- de la Rosa I. G., La Barbera F., Ferreras I., Sánchez Almeida J., Dalla Vecchia C., Martínez-Valpuesta I., Stringer M., 2016, *MNRAS*, **457**, 1916
- van Dokkum P. G., Franx M., 1996, *MNRAS*, **281**, 985
- van Dokkum P. G., et al., 2015, *ApJ*, **813**, 23
- van den Bergh S., 1976, *ApJ*, **206**, 883
- van der Wel A., et al., 2012, *ApJS*, **203**, 24
- van der Wel A., et al., 2014, *ApJ*, **788**, 28
- van der Wel A., et al., 2016, *ApJS*, **223**, 29

APPENDIX A: OPTICAL ATTENUATION IN THE UVJ DIAGRAM

Here we decompose the *UVJ* diagram for each of our CANDELS redshift slices, as originally shown in [Figure 2](#), based on subpopulation classification (star-forming, transition and quiescent). We then color-code the points by their best-fit optical attenuation A_V , which is output from SED fitting as described in [section 2](#). Clearly, star-forming galaxies occupy a “dust sequence” (e.g., [Wuyts et al. 2007](#); [Williams et al. 2009](#); [Brammer et al. 2011](#)), and the quiescent galaxies tend to remain within the empirical “quiescent wedge” (boundary equations taken from [van Dokkum et al. 2015](#)).

A non-negligible number of our sSFR- M_* -defined transition galaxies extend into the classical dusty star-forming region, with high rest-frame ($U-V$) and ($V-J$) colors, even though their A_V values typically do not approach the large values found for classical dusty star-forming galaxies. Future work will be needed to determine whether this is indeed a population of “dusty transition galaxies,” and what the implications of this population are for: (1) the full diversity of transition pathways, including dusty post-starburst systems, and (2) systematic uncertainties in SED-based dust correction methods.

APPENDIX B: CUMULATIVE DISTRIBUTION FUNCTIONS OF STRUCTURAL PROPERTIES

Here we show the full cumulative distribution functions for the structural properties of galaxies in the observations and the SAM. The results presented in Figure 4 for the redshift evolution of the Sérsic index, half-light radius, and $\Sigma_{1.5}$ are based on the cumulative distribution functions shown in Figure B1, Figure B2, and Figure B3, respectively.

We also ran two-sample Kolmogorov-Smirnov tests to compare transition galaxies’ structural properties to those of mass-matched star-forming and quiescent galaxies. The resulting p -values are $\ll 0.001$ in a majority of cases, as shown in Table B1 and Table B2. This suggests that transition galaxies’ structural property distributions across a wide redshift range are drawn from different parent populations compared to those of mass-matched star-forming and quiescent galaxies.

APPENDIX C: OBSERVED GALAXY NUMBER DENSITIES

In Figure C1, we show the observed number densities of star-forming, transition and quiescent galaxies as a function of redshift. We also plot our cubic polynomial fits to these number densities; the polynomial coefficients are given in Table C1. The smooth cubic fits are used to calculate the average population transition timescale as a function of redshift using equation 3 in subsection 6.2.

AFFILIATIONS

¹Department of Astrophysical Sciences, Peyton Hall, Princeton University, Princeton, NJ 08544, USA

²Department of Physics and Astronomy, Rutgers, The State University of New Jersey, 136 Frelinghuysen Rd, Piscataway, NJ 08854, USA

³UCO/Lick Observatory, Department of Astronomy and Astrophysics, University of California, Santa Cruz, CA 95064, USA; viraj.pandya@ucsc.edu

⁴Department of Astronomy, University of California, Berkeley, CA 94720, USA

⁵Department of Physics, University of Bath, Claverton Down, Bath, BA2 7AY, UK

⁶Centre for Astrophysics and Supercomputing, Swinburne University of Technology, PO Box 218, Hawthorn 3122, Australia

⁷Hubble Fellow

⁸Yale Center for Astronomy & Astrophysics, Physics Department, P.O. Box 208120, New Haven, CT 06520, USA

⁹Department of Physics, University of California at Santa Cruz, Santa Cruz, CA 95064, USA

¹⁰Department of Physics and Astronomy, University of Missouri-Kansas City, 5110 Rockhill Road, Kansas City, MO 64110, USA

¹¹Department of Physics and Astronomy, Colby College, Waterville, ME 04901, USA

¹²Department of Astronomy, University of Michigan, 500 Church St., Ann Arbor, MI 48109, USA

¹³Center for Astrophysical and Planetary Science, Racah Institute of Physics, The Hebrew University, Jerusalem 91904, Israel

¹⁴Orange Coast College, Costa Mesa, CA 92626, USA

¹⁵Space Telescope Science Institute, 3700 San Martin Drive, Baltimore, MD 21218, USA

¹⁶The Observatories, The Carnegie Institution for Science, 813 Santa Barbara Street, Pasadena, CA 91101, USA

¹⁷University of California, Riverside, 900 University Ave, Riverside, CA 92521, USA

¹⁸Department of Physics and Astronomy, University of Pittsburgh, Pittsburgh, PA 15260, USA

¹⁹Goddard Space Flight Center, Code 665, Greenbelt, MD, USA

²⁰Department of Physics and Astronomy, Texas A&M University, College Station, TX, 77843-4242 USA

²¹Max Planck Institute for Astronomy (MPIA), Konigstuhl 17, D-69117 Heidelberg, Germany

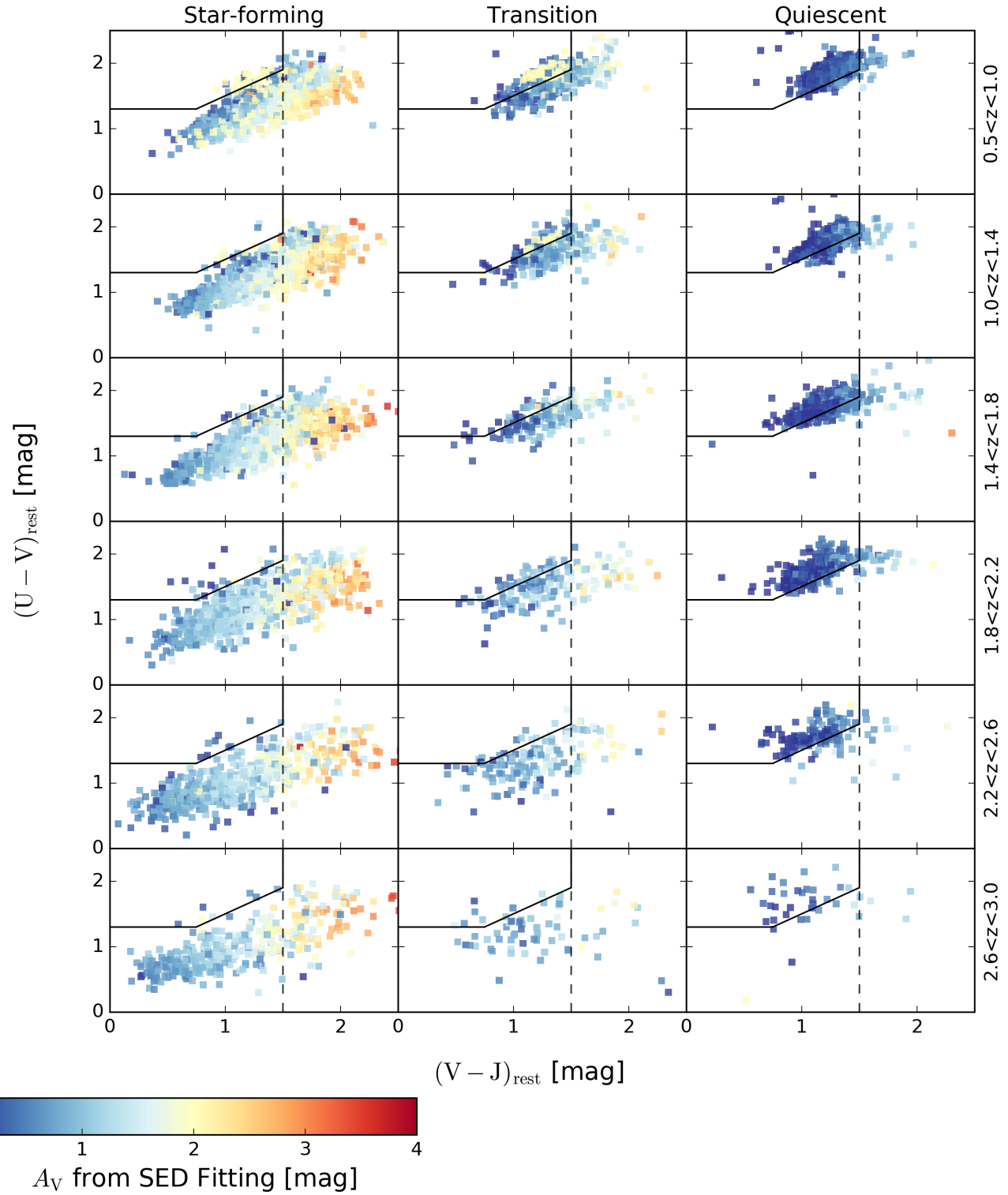


Figure A1. This is the same UVJ diagram as originally shown in Figure 2 for our CANDELS redshift slices. For clarity, here we show the UVJ distribution of sSFR- M_* -selected star-forming, transition and quiescent galaxies in each CANDELS redshift slice using different subpanels. We also color-code the points by the best-fit A_V that is output by SED fitting. The boundaries for the empirical “quiescent wedge” are taken directly from van Dokkum et al. (2015). Note how the star-forming galaxies form a “dust sequence” and tend to stay outside of the quiescent wedge, whereas the quiescent galaxies tend to stay within the empirically-defined quiescent wedge and are relatively dust-free (e.g., Wuyts et al. 2007; Williams et al. 2009; Brammer et al. 2011). In contrast, our sSFR- M_* -selected transition galaxies tends to span the region between the quiescent and star-forming galaxies, and a non-negligible fraction of transition galaxies extend into the classical dusty star-forming region, with high rest-frame ($U - V$) and ($V - J$) colors (even though their A_V do not typically approach the large values of classical dusty star-forming galaxies).

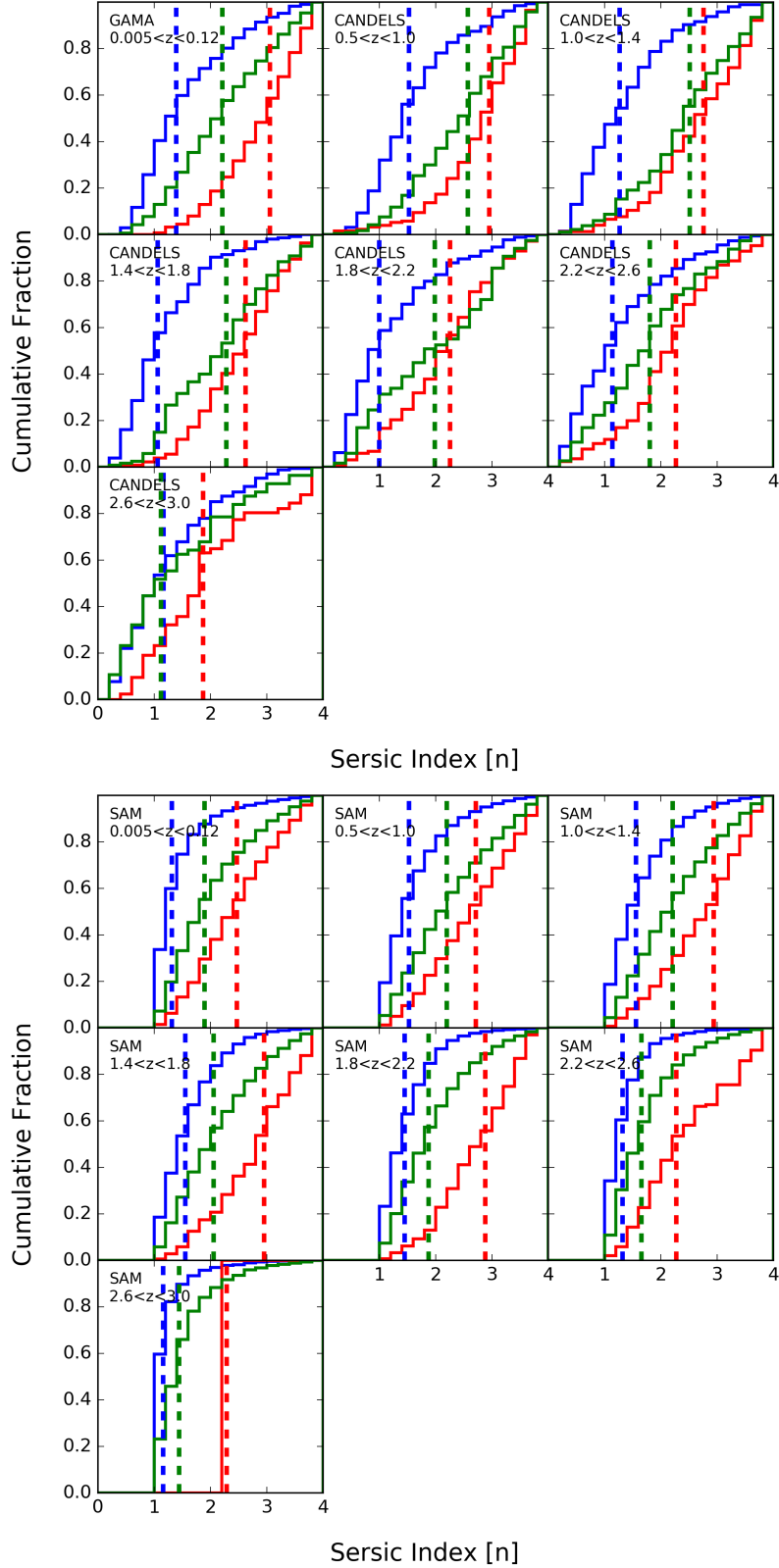


Figure B1. Normalized cumulative distribution functions for the Sérsic index of galaxies in the observations (top) and the SAM (bottom) in each of our redshift slices. The CDFs have been split into three separate ones for galaxies that are classified as star-forming (blue), transition (green), and quiescent (red). The dashed vertical lines mark the median value of each CDF in every panel.

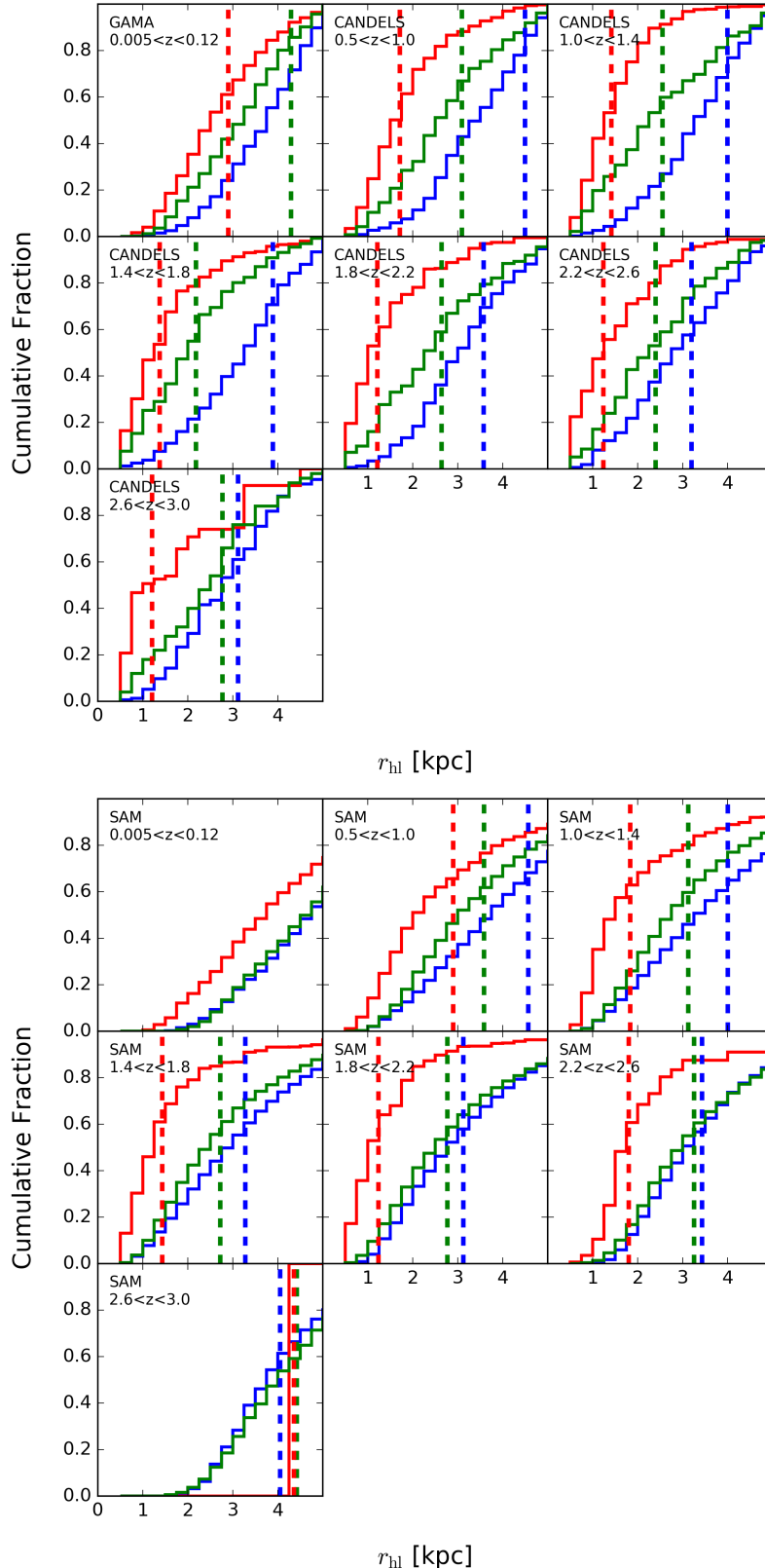


Figure B2. Normalized cumulative distribution functions for the half-light radius of galaxies in the observations (top) and the SAM (bottom) in each of our redshift slices. The CDFs have been split into three separate ones for galaxies that are classified as star-forming (blue), transition (green), and quiescent (red). The dashed vertical lines mark the median value of each CDF in every panel.

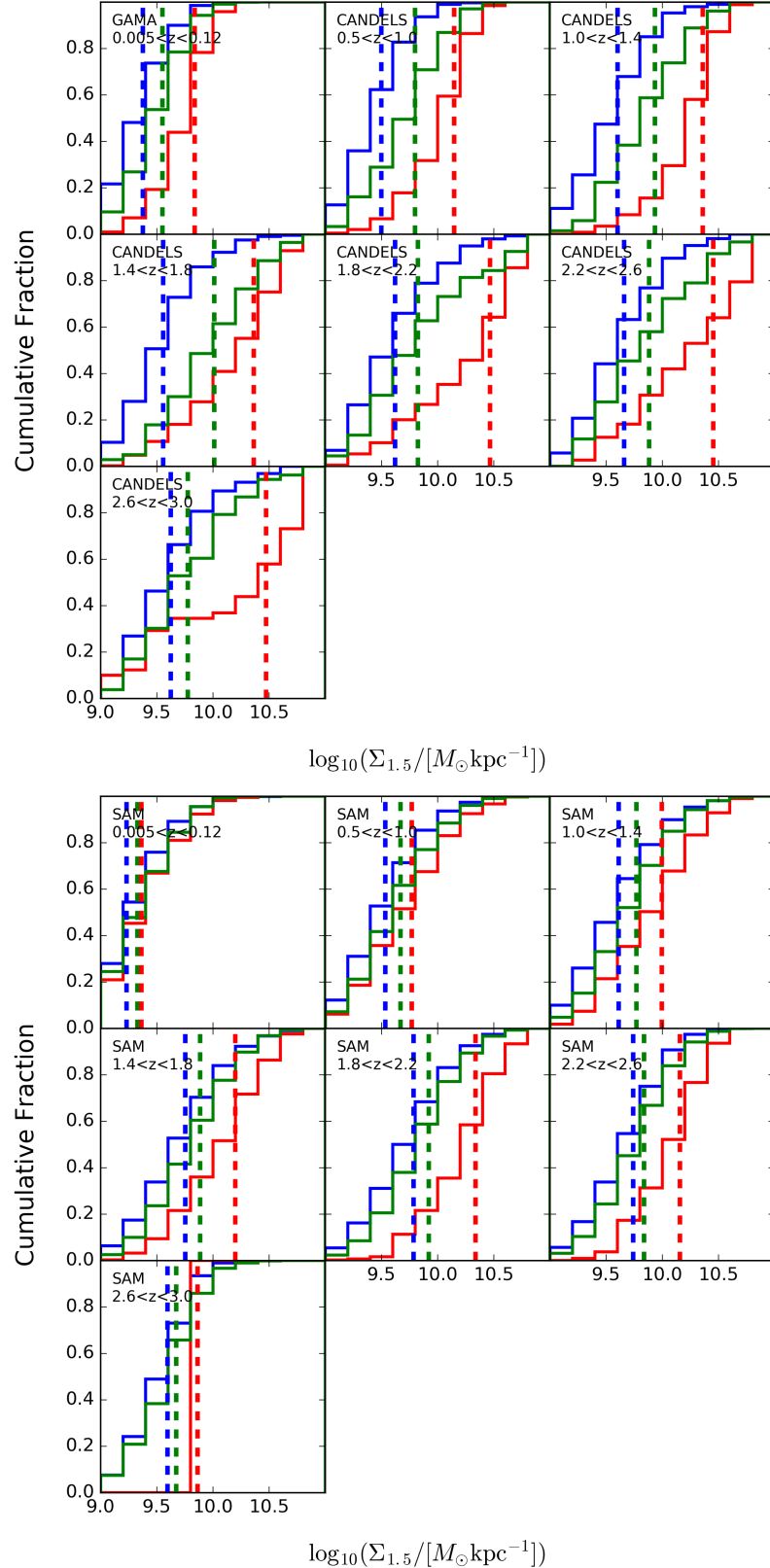


Figure B3. Normalized cumulative distribution functions for the $\Sigma_{1.5}$ parameter of galaxies in the observations (top) and the SAM (bottom) in each of our redshift slices. The CDFs have been split into three separate ones for galaxies that are classified as star-forming (blue), transition (green), and quiescent (red). The dashed vertical lines mark the median value of each CDF in every panel.

Redshift Slice (1)	$n^{\text{T,SF}}$ (2)	$n^{\text{T,Q}}$ (3)	$r_{\text{hl}}^{\text{T,SF}}$ (4)	$r_{\text{hl}}^{\text{T,Q}}$ (5)	$\Sigma_{1.5}^{\text{T,SF}}$ (6)	$\Sigma_{1.5}^{\text{T,Q}}$ (7)	Sample (8)
$0.005 < z < 0.12$	$\ll 0.001$	$\ll 0.001$	$\ll 0.001$	$\ll 0.001$	$\ll 0.001$	$\ll 0.001$	GAMA
$0.5 < z < 1.0$	$\ll 0.001$	$\ll 0.001$	$\ll 0.001$	$\ll 0.001$	$\ll 0.001$	$\ll 0.001$	CANDELS
$1.0 < z < 1.4$	$\ll 0.001$	0.008	$\ll 0.001$	$\ll 0.001$	$\ll 0.001$	$\ll 0.001$	CANDELS
$1.4 < z < 1.8$	$\ll 0.001$	$\ll 0.001$	$\ll 0.001$	$\ll 0.001$	$\ll 0.001$	$\ll 0.001$	CANDELS
$1.8 < z < 2.2$	$\ll 0.001$	0.004	$\ll 0.001$	$\ll 0.001$	$\ll 0.001$	$\ll 0.001$	CANDELS
$2.2 < z < 2.6$	$\ll 0.001$	$\ll 0.001$	$\ll 0.001$	$\ll 0.001$	$\ll 0.001$	$\ll 0.001$	CANDELS
$2.6 < z < 3.0$	0.564	$\ll 0.001$	0.191	$\ll 0.001$	0.041	$\ll 0.001$	CANDELS

Table B1. Two-sample Kolmogorov-Smirnov test p -values for structural distinctness of transition galaxies in the observations. The names of columns 2-7 indicate the structural property (Sérsic index, half-light radius or mass surface pseudodensity) and which mass-matched subpopulations are being compared (transition versus star-forming, or transition versus quiescent galaxies). The values in the table are the p -values from the two-sample Kolmogorov-Smirnov test. If a p -value is less than 10^{-3} , we show $\ll 0.001$ instead.

Redshift Slice (1)	$n^{\text{T,SF}}$ (2)	$n^{\text{T,Q}}$ (3)	$r_{\text{hl}}^{\text{T,SF}}$ (4)	$r_{\text{hl}}^{\text{T,Q}}$ (5)	$\Sigma_{1.5}^{\text{T,SF}}$ (6)	$\Sigma_{1.5}^{\text{T,Q}}$ (7)	Sample (8)
$0.005 < z < 0.12$	$\ll 0.001$	$\ll 0.001$	$\ll 0.001$	$\ll 0.001$	$\ll 0.001$	0.025	SAM
$0.5 < z < 1.0$	$\ll 0.001$	$\ll 0.001$	$\ll 0.001$	$\ll 0.001$	$\ll 0.001$	$\ll 0.001$	SAM
$1.0 < z < 1.4$	$\ll 0.001$	$\ll 0.001$	$\ll 0.001$	$\ll 0.001$	$\ll 0.001$	$\ll 0.001$	SAM
$1.4 < z < 1.8$	$\ll 0.001$	$\ll 0.001$	$\ll 0.001$	$\ll 0.001$	$\ll 0.001$	$\ll 0.001$	SAM
$1.8 < z < 2.2$	$\ll 0.001$	$\ll 0.001$	$\ll 0.001$	$\ll 0.001$	$\ll 0.001$	$\ll 0.001$	SAM
$2.2 < z < 2.6$	$\ll 0.001$	$\ll 0.001$	$\ll 0.001$	$\ll 0.001$	$\ll 0.001$	$\ll 0.001$	SAM
$2.6 < z < 3.0$	$\ll 0.001$	—	$\ll 0.001$	—	$\ll 0.001$	—	SAM

Table B2. Same as [Table B1](#) but for the SAM instead. Since there are so few quiescent galaxies in the SAM at $2.6 < z < 3.0$, we do not run the two-sample Kolmogorov-Smirnov tests comparing transition to quiescent galaxies' distributions in that redshift slice.

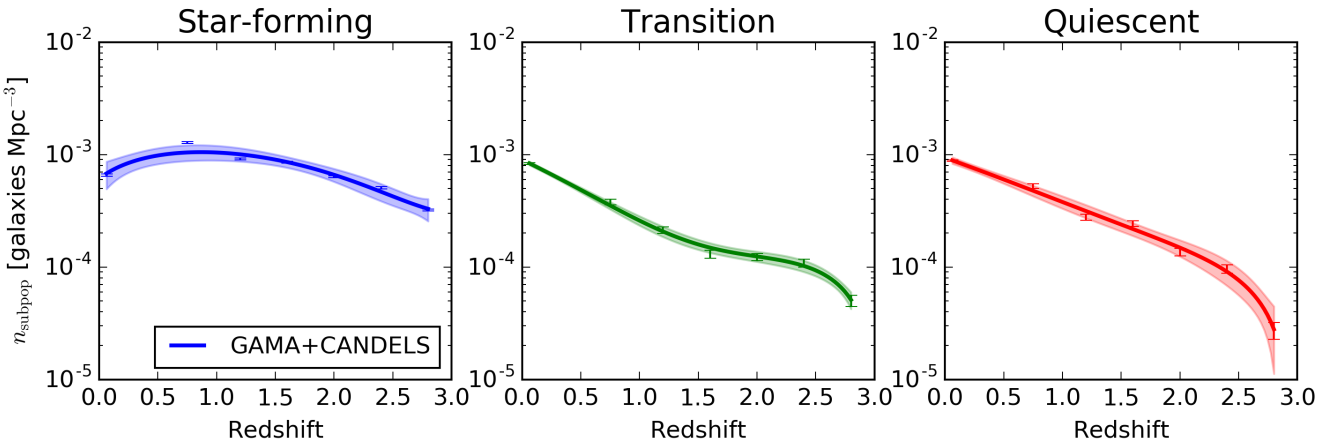


Figure C1. The observed number densities of star-forming (left), transition (middle), and quiescent (right) galaxies as a function of redshift. The scatter points show our measurements with bootstrapped errorbars, the solid lines are our cubic polynomial fits, and the shading reflects the 1σ uncertainty in the polynomial fits. The transition and quiescent galaxy polynomial fits are used to compute an observational upper limit on the average population transition timescale as a function of redshift in [subsection 6.2](#).

Table C1. Coefficients for a cubic polynomial fit to the observed number densities of star-forming, transition and quiescent galaxies as a function of redshift: $n_{\text{subpop}}(z) = a_3 z^3 + a_2 z^2 + a_1 z + a_0$, where z is the redshift. These coefficients are valid for $0.005 < z < 3.0$.

Subpopulation	a_3	a_2	a_1	a_0
Star-forming	0.0001	-0.0008	0.0011	0.0006
Transition	-0.0001	0.0005	-0.0011	0.0009
Quiescent	-0.0000	0.0003	-0.0008	0.0009